2021

FROM CANCER STEM CELLS TO BRAIN TUMOUR FORMATION: THE ROLE OF HEATR1 AND RIBOSOME BIOGENESIS

Rodriguez Diaz, Laura

http://hdl.handle.net/10026.1/17573

http://dx.doi.org/10.24382/488
University of Plymouth

UNIVERSITY OF PLYMOUTH

FROM CANCER STEM CELLS TO BRAIN TUMOUR FORMATION: THE ROLE OF HEATR1 AND RIBOSOME BIOGENESIS

by

LAURA RODRÍGUEZ DÍAZ

A thesis submitted to the University of Plymouth
in partial fulfilment for the degree of

DOCTOR OF PHILOSOPHY

Peninsula Medical School, Faculty of Health

September 2020

AUTHOR'S DECLARATION

At no time during the registration for the degree of Doctor of Philosophy has the author been registered for any other University award without prior agreement of the Doctoral College Quality Sub-Committee.

Work submitted for this research degree at the University of Plymouth has not formed part of any other degree either at the University of Plymouth or at another establishment.

The following external institutions were visited for research and consultation purposes:

Publications:

Single-cell transcriptomics reveals HeatR1-dependent ribogenesis control and growth of brain tumour initiation cells (tentative title). **Laura R. Diaz***, Jon Gil-Ranedo*, Karolina J. Jaworek, Joao Marques, Nsikan Nsek, Eleni Costa, David Hilton, C Oliver Hanemann, Matthias Futschik, Torsten Bossing and Claudia S. Barros, **manuscript *in preparation***. *Shared authorship.

Presentations at conferences:

HeatR1 and ribogenesis control of brain tumour initiation cells. **Laura R. Diaz**[1], Jon Gil-Ranedo[1], Karolina Jaworek[1,2], Joao Marques[1], Eleni Costa[1], Torsten Bossing[1] and Claudia S. Barros[1]. [1]Peninsula Medical School, University of Plymouth, U.K. [2]School of Biological Sciences, Bangor University, U.K. Brain Tumour Meeting, Berlin, Germany, May **2019**. **Oral and poster presentation.**

A translational approach to identify novel brain tumour initiation mechanisms. Jon Gil-Ranedo[1], Karolina J. Jaworek[1,2], **Laura R. Diaz[1]**, Torsten Bossing[1] and Claudia S. Barros[1]. [1]Peninsula Medical School, University of Plymouth, U.K. [2]School of Biological Sciences, Bangor University, U.K. Brain Tumour Meeting, Berlin, Germany, May **2019**. **Poster presentation.**

A single-cell screening approach to brain tumour initiation: how Neural Stem cells become tumour initiating cells. **Laura R. Diaz**[1], Jon Gil-Ranedo[1], Karolina Jaworek[1,2], Joao Marques[1,3], Eleni Costa[1,3], Torsten Bossing[1] and Claudia S. Barros[1]. [1]Peninsula Medical School, University of Plymouth, U.K.[2] School of Biological Sciences, Bangor University, U.K. BSDB/ BSCB, Warwick April **2018**. **Poster presentation.**

A single-cell screening approach to brain tumour initiation. **Laura R. Diaz**[1], Jon Gil-Ranedo[1], Karolina Jaworek[1,2], Joao Marques[1], Eleni Costa[1], Torsten Bossing[1] and Claudia S. Barros[1]. [1]Peninsula Medical School, University of Plymouth, U.K. [2]School of Biological Sciences, Bangor University, U.K. BSDB/BSCB Meeting, Warwick April **2017**. **Poster presentation**.

Word count of main body of thesis: 30,319

Signed: *Laura R. Díaz*

Date: 28.09.2020

ACKNOWLEDGEMENTS

After four years, I wrote most of this thesis during a pandemic, locked down in Plymouth, sharing a tiny desk. Now, writing the acknowledgements on the last day I think it could not have been any other way. I am incredibly grateful to everyone who made this journey even slightly easier, and for those I missed in this section, know that it is not lack of care, it is just lack of space.

Firstly, I must thank my Director of Studies, Dr Claudia Barros. You are the most inspirational scientist I have met, and I will be forever grateful for the opportunity you gave me when you invited me to be part of your lab. During the past four years you have taught me to have confidence in my own work, be resilient, work hard, and be positive (or at least try). I would be proud to become half the scientist you are. I would also like to thank my supervisor Dr Oliver Hanemann, for his support and advice during my studies, and Dr Torsten Bossing, for his incredible knowledge and for always being willing to help.

I would also like to thank the rest of my research group. I have been incredibly lucky to work with you and I could not have asked for a better team. You made going to the lab fun every single day. To Jon, on more than one occasion I have walked into your office with an “I think I messed up”, of course you always know how to fix it. I will miss our coffees and pints, and your eternal psychopathic cheerfulness, even when everyone else is in a bad mood. Hearing your whistling always made me smile. To Jamie and Nsikan, for all the office talks and lab disasters. But especially for fitting in so easily. Honestly, I cannot remember what we did when you two were not yet around. I wish you the best of luck with your projects.

Besides my lab group, I need to thank a lot of people who have made my journey so much easier. Liyam, Bora, Jemma, Trish, Ollie, Caterina, Foram, Laurien… You have become my friends. Without you, it would just be work. Thank you for all the laughs, day trips, night outs, night ins, yoga, beach days, and even pub quizzes. I cannot wait to see you again.

Outside the lab I would like to thank my family. You accept that I am always away and meet me with open arms. Especially both my nans, who still ask if my exams went well every time I see them. And to my second family, the girls, because you are home. I can assure you that without you all I would not have finished this thesis, maybe I would not have even started it. To Raqui, for staying with me since the first day of Uni, thank you for making going for a drink and adventure. To Roci, because you have always been with me and always will be. Thank you for being the kind of friend who jumps on a plane like a life-saver landing in England in mid-January. To Lauri, for always being just a phone call away, and for being so like me that our conversations are just re-enforcements

of what has been said. To Sari because te quiero mazo neno (translating Coruño is harder than writing a thesis). And because I love going back to Coruña and having endless coffees with oat milk with you while we speak about our dramas. To Luquis, for coping with me during the last stages of this thesis, and for always being there when I go home. To Ivan, thank you for always being there, in the good and the bad times.

To my girls from 1 Maple Grove. That place will never be the same without us. You made me feel at home from the start, and you made a party of my Plymouth years. To Gotzo, because there is only goodness in you, with a bit of sassiness, obviously. To Eri, because you are positivity, glitter, and good vibes. To Lour, who sees life through a pint glass. I cannot believe how lucky I was to land in that house.

To Riordan, because somehow you ended up spending the lock-down with me, that is something that I would not wish on anyone. Thank you for being prouder of my achievements than myself.

Lastly, I would like to thank my parents and my sister, Olga. By now you will be laughing about how lame this section is, but I think deep inside you like it. Anything I say will sound like a cliché, so I will simply say, thank you for all the years of unconditional support.

To all of you, near or far, thank you.

AGRADECIMIENTOS

Después de cuatro años, he escrito la mayor parte de esta tesis durante una pandemia, confinada en Plymouth compartiendo un escritorio minúsculo. Ahora, escribiendo los agradecimientos el último día, creo que no podía haber sido de otra forma. Le estoy increíblemente agradecida a todo el que ha hecho este camino un poquito más fácil, y los que no nombro en esta sección, no es por falta de cariño, es falta de espacio.

Primero, debo darle las gracias a mi directora de estudios, Dr Claudia Barros. Eres la científica más inspiradora que conozco, y te estaré siempre agradecida por la oportunidad que me diste cuando me invitaste a formar parte de tu laboratorio. Durante estos cuatro años me has enseñado a tener confianza en mi propio trabajo, a ser resiliente, trabajar duro y ser positiva (o por lo menos intentarlo). Si llego a ser la mitad de lo buena científica que tu eres, estaré orgullosa. Me gustaría agradecérselo también a mi supervisor Dr Oliver Hanemann, por su apoyo y consejo durante mis estudios, y a Dr Torsten Bossing, por su increíble sabiduría y por estar siempre dispuesto a ayudar.

También me gustaría agradecérselo al resto de mi grupo de investigación. He tenido la increíble suerte de trabajar con vosotros, y no podría haber pedido un equipo mejor. Vosotros hicisteis que ir al laboratorio fuese divertido todos los días. A Jon, al que he tenido que ir a buscar en más de una ocasión con un “creo que la he liado”, por su puesto tú siempre sabes como arreglarlo. Echaré de menos nuestros cafés y nuestras pintas, y ese eterno optimismo de psicópata que tienes hasta cuando todo el mundo está de mal humor. Escucharte silbar por el pasillo siempre me ha hecho sonreír. A Jamie y a Nsikan por las conversaciones en el despacho y los desastres en el laboratorio. Pero sobre todo por encajar tan fácilmente en el grupo. Sinceramente no recuerdo lo que hacíamos cuando no estabais vosotros. A los dos os deseo la mejor suerte en vuestros proyectos.

Además de mi grupo, necesito agradecérselo a un montón de gente que ha sido muy importante para mí durante esta etapa. Liyam, Bora, Jemma, Trish, Ollie, Caterina, Foram, Laurien… Os habéis convertido en mis amigos. Sin vosotros, solo sería trabajo. Gracias por todas las risas, excursiones, noches de fiesta, noches de quedarse en casa, yoga, días de playa e incluso pub quizzes. Espero veros pronto.

Fuera del laboratorio me gustaría agradecérselo a mi familia. Por aceptar que siempre esté lejos, y recibirme con los brazos abiertos. Sobre todo a mis abuelas, que todavía preguntan si me salieron bien los exámenes cada vez que las veo. Y a mi segunda familia, las niñas, por ser casa. Os puedo asegurar que sin vosotras yo no habría acabado esta tesis. Igual ni la habría empezado. A Raqui, por quedarse conmigo desde el primer día de universidad, gracias por convertir ir a tomar una caña en una

aventura. A Roci, porque siempre has estado, y siempre estarás. Gracias por ser la clase de amiga que se sube a un avión en plan salvavidas y se planta en Inglaterra en pleno enero. A Lauri, por estar siempre a una llamada de distancia, y por ser tan como yo, que nuestras conversaciones a veces solo son para reforzar lo dicho. A Sari, porque te quiero mazo neno y me encanta volver a Coruña y que me invites a cafés con leche de avena mientras hablamos de nuestras penas. A Luquis, por aguantarme al final de la tesis y por estar siempre ahí cuando vuelvo a casa. A Iván, gracias por estar siempre ahí, en las buenas y en las malas.

A mis chicas de 1 Maple Grove. Ese lugar no volverá a ser lo mismo sin nosotras. Me hicisteis sentir en casa desde el minuto uno e hicisteis de mis años en Plymouth una fiesta. A Gotzo, porque dentro de ti solo hay cosas buenas, y un poquito de carácter. A Eri, que es positividad, purpurina y buenrollismo. A Lour, que ve la vida a través de una cerveza. Aún no me creo la suerte que tuve al aterrizar en esa casa.

A Riordan, porque de alguna forma acabaste pasando un confinamiento conmigo, y eso es algo que no le deseo a nadie. Gracias por estar más orgulloso de todos mis logros que yo misma.

Por último, a mis padres y mi hermana, Olga. A estas alturas ya estaréis riéndoos de lo cursi que es esta sección, pero en el fondo yo creo que os gusta. Cualquier cosa que os diga va a sonar como un cliché, así que simplemente diré, gracias por todos los años de apoyo incondicional.

A todos, cerca o lejos, muchas gracias.

ABSTRACT

Laura Rodríguez Díaz

From cancer stem cells to brain tumour formation: The role of HEATR1 and ribosome biogenesis

Brain tumours are initiated by neoplastic transformation of brain cells followed by uncontrolled proliferation, and are driven by genetic mutations. Despite years of study towards increasing our understanding of their origin and development, the high recurrence rate and poor prognosis of brain tumours in general, and specially of glioblastoma multiforme (GBM), the most aggressive type, highlight the need for more efficient therapeutic approaches[1,2]. According to the Cancer Stem Cell (CSC) hypothesis, tumour initiation and relapse might be caused by a subpopulation of cells with stem cell characteristics[3–5]. Loss of the *Drosophila melanogaster* tumour suppressor Brat or its human orthologue, TRIM3, promotes brain tumour growth in the *Drosophila* brain and in GBM, respectively[6,7]. To investigate molecular characteristics of brain CSCs, single-cell transcriptome data from *brat* brain tumour-initiating cells was obtained by the C. Barros laboratory (Diaz *et al*., *in preparation*), and is the foundation of this thesis' studies. *L(2)K09022,* the conserved orthologue of human *Heat Repeat Containing 1* (*HEATR1*) was identified as upregulated in *brat* tumour initiation cells, and selected for further investigation with the main aim of exposing its potential role in brain tumour development. I show here that HEATR1 is overexpressed in GBM and low-grade glioma, and in both GBM immortalised cells and patient-derived GBM stem cells (GSCs). Using the *Drosophila brat* model, GBM cell lines, and GSCs, I demonstrated that although L(2)K09022/HEATR1 is not required for malignant transformation of brain tumour initiating cells, it is necessary for their enlargement, proliferation and tumour growth. HEATR1 acts in brain CSCs to promote ribosome biogenesis and thus contributing to protein synthesis, tumour cell growth and proliferation. Its action is, at least in part,

mediated by recruiting and enhancing the activity of the oncogene c-Myc in nucleoli, the sites of ribogenesis. These findings reveal HEATR1 as a novel brain tumourigenesis player and suggest that it may be as a potential future therapeutic target for GBM and possibly other brain tumours.

TABLE OF CONTENTS

LIST OF FIGURES

LIST OF TABLES

LIST OF ABBREVIATIONS

Abbreviation	Full name
aPKC	Protein kinase C
Ase	Asense
BAX	BCL2 associated X protein
Baz	Bazooka
BDNF	Brain-derived neurotrophic factor
Brat	Brain tumour
Casp3	Caspase 3
cDNA	complementary DNA
CSC	Cancer Stem Cell
DA	Diffuse Astrocytomas
DFC	Dense Fibrillar Component
dHEATR1	Drosophila HEATR1
DNA	Deoxyribonucleic Acid
Dpn	Deadpan
EdU	5-ethynyl-2´-deoxyuridine
EGF	Epidermal growth factor
EMT	Epithelial-Mesenchymal transition
EGFR	Epidermal growth factor receptor
Erm	Earmuff
ETS	External transcribed spacers
EU	5-ethynyl uridine
FACS	Fluorescent activated cell sorting
FBL	Fibrillarin
FBS	Foetal Bovine Serum
FC	Fibrillar Centre
FGF	Fibroblast growth factor
GBM	Glioblastoma Multiforme
GC	Granular Component
GFP	Green Fluorescence Protein
GMC	Ganglion Mother Cell
GSC	Glioma Stem Cell
HEATR1	HEAT Repeat containing 1
Hh	Hedgehog
HPH	Hours post hatching
IDH	Isocitrate dehydrogenase
iINP	immature Intermediate Neural Progenitor
INP	Intermediate Neural Progenitor
Insc	Inscuteable
IRBC	Impaired Ribosome Biogenesis Checkpoint
ITS	Internal transcribed spacers
Klu	Klumpfuss

Lola	Longitudinals lacking
L(2)gl	Lethal (2) giant larvae
Mdlc	Midlife crisis
Mira	Miranda
mRNA	messenger RNA
NADPH	Nicotinamide adenine dinucleotide phosphate
NB	Neuroblast
Nerfin-1	Nervous fingers 1
NICD	Notch Intracellular Domain
NOR	Nucleolar Organizer Region
NPM	Nucleophosmin
ns	Non significant
NSC	Neural Stem Cell
OL	Optic lobe
OPP	O-propargyl-puromycin
Ptch1	Patched 1
PBS	Phosphate-Buffered Saline
PCR	Polymerase Chain Reaction
PDGFR	Platelet-derived growth factor receptor
PH3	Phospho-Histone 3
PINS	Partner of Inscuteable
pnt	Pointed
Pol I	Polymerase I
Pol II	Polymerase II
PON	Partner of Numb
PP2A	Protein phosphatase 2A
pre-rRNA	precursor ribosomal RNA
Pros	Prospero
Pum	Pumillo
rDNA	Ribosomal DNA
RNA	Ribonucleic Acid
RNAi	RNA interference
ROS	Reactive Oxygen Species
RP	Ribosomal Protein
rRNA	ribosomal RNA
RT-qPCR	Real time-quantitative PCR
SGZ	Subgranular Zone
shRNA	short hairpin RNA
siRNa	silencing RNA
Smo	Smoothened
snoRNPs	Small nucleolar ribonucleoprotein particles
SSU	Small Subunit
SVZ	Subventricular Zone
TCGA	The cancer genome atlas
TMZ	Temozolamide

TUNEL	Terminal deoxynucleotidyl transferase-mediated dUTP nick end labeling
UAS	Upstream Activating Sequence
UBF	Upstream Binding Factor
UTP10	U3 small nucleolar RNA-associated protein 10
VNC	Ventral nerve cord
WHO	World Health Organization
WT	wild-type
YFP	Yellow fluorescence protein
Zld	Zelda

1 INTRODUCTION

1.1 Preface

Cancer is an umbrella term used to describe a set of diseases characterised by uncontrolled cell proliferation driven by the sequential acquisition of mutations[8]. It is the second most frequent cause of death world-wide, being responsible for an estimated figure of 9.6 million deaths in 2018 according to the World Health Organization (WHO). Moreover, its incidence is expected to increase by more than 50% over the coming decades due to the aging and growth of the world's population[9].

Different therapies have been developed in the past years that have proven to be effective to some extent for several common cancers such as lung, breast or prostate malignancies. However, these therapies have little or no effect against tumours located in the central nervous system (CNS), including those found in the brain. CNS tumours are relatively rare, having an average incidence of 28.57 per 100,000 population[10], nevertheless, their poor prognosis situates them among the top 10 most lethal cancers in Europe[11]. Moreover, due to the scarcity of these tumours and/or difficulties to study them, in 2017 the investment on brain tumour research in the UK was only 1.5% of the total cancer investment from funding bodies, according to the Brain Tumour Research Manifesto (2019).

This dissertation which sprouted from transcriptomic data of brain tumour initiating cells obtained in the Barros laboratory using a brain tumour *Drosophila melanogaster* model, aims at shedding more light on the initiation of brain tumours towards providing new potential targets for enhanced clinical intervention.

1.2 Cancer stem cells and tumour development

Individual tumours contain varying proportions of differentiated cell types together with anaplastic cells, which are undifferentiated cancer cells that lose their morphological characteristics and have an enhanced proliferative capacity[1]. To explain this heterogeneity, two different models have been proposed: the stochastic and the

hierarchical model[12]. The stochastic model predicts that all the cells in a tumour have similar tumourigenic potential, which is activated randomly by cumulative mutations or adaptation of the cells to their microenvironment[12]. Therefore, tumours are formed by a pool of heterogenous cells that all can act as tumour-founding cells, although this might happen only rarely[12–14] **(Figure *1.1* A)**. The hierarchical model holds that only a rare subset of cells presents extensive cell renewal properties and maintain and sustain the growth of the tumour[12–14] **(Figure *1.1* B)**. The main difference is the prediction according to the hierarchical model, that whatever the environment or mutational status, only a small group of cancer cells have the ability to form a new tumour and all its different cell types. These cells are known as Cancer Stem cells (CSCs) and are defined as cells with capacity to self-renew and to originate the various lineages of cancer cells that drive the formation, growth and recurrence of the tumour[15]. CSCs are also thought to be often relatively quiescent[16]. The CSC hypothesis suggests that tumour heterogeneity arises from these cells[5,17,18]. However, the two models are not mutually exclusive and other factors like the tumour microenvironment add yet another level of complexity to tumour heterogeneity[19].

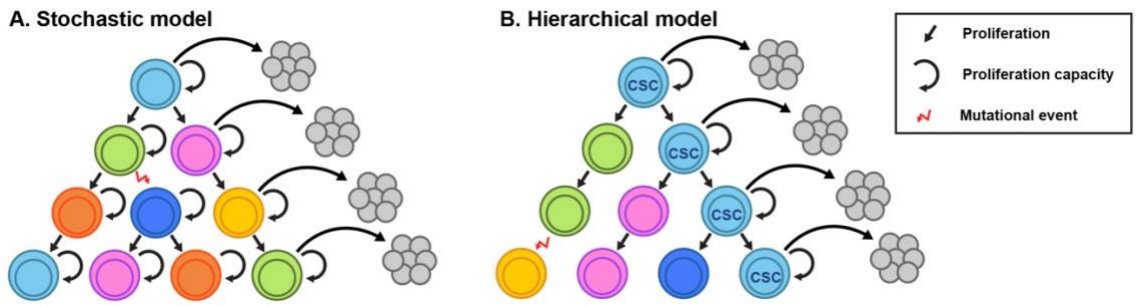

Figure 1.1 Two classic models explaining cell heterogeneity and tumour development. (A) Stochastic model: tumour cells are heterogeneous but most of them can proliferate extensively and have tumour formation capacity. **(B)** Hierarchical model: tumour cells are heterogeneous, but most have limited proliferation potential and only CSCs can self-renew and form tumours. Adapted from Reya *et al*., 2001[14].

1.2.1 Isolation and identification of CSCs

In order to study CSCs, it is essential to differentiate them from the bulk of the tumour. The gold standard to define CSCs has been serial i*n vivo* transplantation, pioneered by Bonnet and Dicks in 1997[20]. Transplantation assays typically consist of isolating tumour cell populations using fluorescent activated cell sorting (FACS) based on their surface-markers and inoculating them into immunodeficient mice in numbers sufficiently low to limit the formation of a xenograft by the bulk tumour cell population[19–21]. The ability of a given cell population to initiate a tumour over serial passages is then interpreted as evidence for the presence of CSCs. CSCs were first found in human acute leukaemia myeloid in 1994, when Lapidot *et al*., isolated a population of $CD34^+/CD38^-$ tumour cells, a phenotype that defines immature haematopoietic cells, and demonstrated that they were the only cells capable of extensive proliferation and reforming the tumour when transplanted into immunodeficient mice[21]. Since then, this experimental design has been widely replicated in a variety of tumour types using different CSC surface markers **(Table 1)** and CSC-like cells have been found in many solid tumours such as breast cancer[22], medulloblastoma, glioblastoma multiforme (GBM)[5], prostate cancer[23], renal cancer[24], melanoma[25] and many more.

Cancer	Cell surface phenotype	Reference
Acute myeloid leukaemia	$CD34^+$ $CD38^-$	Lapidot *et al.* 1994
Breast	$CD44^+$ $CD24^-$ ESA^+ $ALDH^+$	Al-Hajj *et al.* 2003 Ginestier *et al.* 2007
Medulloblastoma	$CD133^+$	Hemmati *et al.* 2003
Glioblastoma	$CD133^+$ $CD15^+$ $A2B5^+$ Sox2	Hemmati *et al.* 2003 Son *et al.* 2009 Tchoghandjian *et al.* 2009 De la Rocha *et al.* 2014
Prostate	$CD44^+$ $\alpha_2\beta_1{}^+$ $CD133^+$ Sca-1	Collins *et al.* 2005 Xin *et al.* 2005
Renal	Prominin-1^+ $CD133^+$	Florek *et al.* 2005
Melanoma	$CD271^+$ $ALDH^+$	Boiko *et al.* 2010 Luo *et al.* 2012
Lung	$CD133^+$ $CD44^+$ $ALDH^+$	Eramo *et al.* 2008 Leung *et al.* 2010 Jiang *et al.* 2009
Ovarian	CD44+ CD117+ CD133+ ALDH+ CD133+ CXCR4+	Zhang *et al.* 2008 Silva *et al.* 2011 Cioffi *et al.* 2015

Pancreas	CD44+ CD24+ ESA+ CD44+ CD133+ ESA+	Li, Lee and Simeone 2009 Bao *et al.* 2014

Table 1: Cell surface phenotypes to identify CSCs in different tumours. References included in table.

Whilst xenotransplantation assays are effective for assessing the tumour initiation potential of a population of cells, they carry intrinsic technical and conceptual limitations, as they do not provide information on the fate of the implanted cells and involve heavy manipulation that can affect their behaviour[19]. To overcome these difficulties, *in vivo* lineage tracing experiments, in which individual cells are permanently marked with a reporter in their native environment, have been developed. Driessens *et al*. were the first ones to use this approach in a chemically induced tumour model for squamous skin cancer in mice, although this had been achieved in *Drosophila* melanogaster before[26]. Using the Cre-Lox recombination system the team was able to induce yellow fluorescence protein (YFP) expression in keratin-14 expressing cells within the tumour[26]. They found that the majority of the labelled tumour cells were lost after terminal differentiation, however, some survived long term and generated large clones within the growing tumours, indicating the existence of CSCs[26]. However, the complex genetic modifications required for this approach have limited lineage-tracing techniques to animal models.

In recent years, CRISPR/Cas9 (clustered regularly interspaced short palindromic repeats/caspase 9) technology has been used to edit the genome of patient derived organoids and insert reporter cassettes at marker genes enabling cancer lineage tracing. Organoids are 3D structures grown from stem cells and consisting of organ-specific cell types that self-organise through cell sorting and spatially restricted lineage commitment, resembling *in vivo* organ development[27,28]. Two different research groups simultaneously engineered human colorectal cancer organoids to insert reporter cassettes knocked into the Leucine-rich repeat containing G protein coupled receptor 5 (Lgr5) locus, which codes for a protein expressed in adult intestinal stem cells[29,30]. Study of the xenografts

generated from these organoids in mice, revealed that Lgr5^{+} cells behave similarly to normal intestinal stem cells and propagate disease in healthy mice very efficiently[29,30]. Lgr5^{+} cells self-renew and produce progeny during long-term periods, which progressively undergo differentiation, confirming a hierarchical organization similar to that seen in colonic epithelium[29,30]. These studies provide a strategy for analysing CSCs in human organoids and xenografts that so far had only been available in animal models.

1.2.2 Therapeutic implications of CSCs

The CSC hypothesis has tremendous therapeutic implications that in many cases could explain the failure of traditional therapies. It is well established that CSCs have acquired different mechanisms that make them resistant to ionizing radiation and conventional chemotherapy[31,32]. Furthermore, most cancer treatments target rapidly dividing cells[12,15,18,33], efficiently eliminating bulk cells but not CSCs, leaving a residual population enriched on stem-like cells that can drive the recurrence of an even more aggressive tumour[3,34]. Below, I summarise some of the known major mechanisms that CSCs use to resist conventional cancer treatments.

Increased efflux of cytotoxic agents

Normal stem cells have developed multiple mechanisms to protect themselves from toxins and mutations, CSCs share many molecular traits with their healthy counterparts that help them resist cancer chemotherapies. For example, stem cells have a higher expression of ATP-binding cassette (ABC) transporters, a family of transmembrane proteins that allow active transport of a wide spectrum of substrates through the cell membrane, helping them clear a wide range of nonspecific toxic agents[3]. CSCs have hijacked this property, increasing their drug efflux capacity and becoming less sensitive to chemotherapy[3,34]. Additionally, the ABC transport family is essential for normal physiological functions like maintaining the blood brain barrier, gastrointestinal tract and the blood testis barrier, therefore, inhibitors of the ABC transporters can result in severe side effects which limits their clinical potential[32].

Enhanced DNA damage repair and resistance to redox stress

Like normal stem cells, CSCs seem to be protected from DNA damage-induced cell death, which makes them resistant to radiation and certain chemotherapy agents such as platinum based drugs, one of the most common kind of anticancer drugs[13]. This has been well studied in GBM, in which radiotherapy is the standard procedure. In these solid tumours most patients relapse after treatment even following full remission[35]. It has been shown that in treated patients' mouse xenografts and *in vitro* cell culture models, the surviving population of cancer cells is enriched in $CD133^+$ cells, a widely used CSC marker[3]. This enrichment appears to be driven by the enhanced ability of CSCs to repair DNA damage, as pharmacological inhibition of the DNA damage checkpoint kinases (Chk) 1 and 2 sensitizes CSCs to radiotherapy[3]. In addition, DNA damage can be caused by accumulation of Reactive Oxygen Species (ROS) derived from molecular oxygen. ROS are highly reactive unstable molecules produced naturally as a product of reduction-oxidation (redox) cellular reactions but can also result from chemotherapy and radiation and easily result in peroxidation of nucleic acids, lipids, amino acids and carbohydrates[32]. Although high levels of ROS are normally found in tumour cells due to elevated metabolism, the relatively quiescence of CSCs is thought to make them intrinsically resistant to oxidative stress-based therapies[32]. Furthermore, hypoxic regions within solid tumours attract CSCs and promote acquisition of stem-like features[36–38]. The scarcity of molecular oxygen in these niches minimizes ROS accumulation and oxidative DNA damage[32,36].

Slow cell cycle

The majority of chemotherapy agents only work on highly proliferative cells. Some populations of CSCs reside in a state of reversible growth arrest, known as quiescence, for long periods of time, which makes them inherently resistant to cell cycle targeting drugs[32]. For example, using a genetically engineered mouse model of glioma, Chen *et al.* labelled quiescent subventricular zone adult neural stem cells and a subset of

endogenous glioma tumour cells with CSC properties with green fluorescence protein (GFP)[39]. After administration of the chemotherapy agent temozolomide (TMZ), pulse-chase experiments using BrdU analogues demonstrated that tumour regrowth originated from the quiescent GFP^+ subpopulation, which re-entered the cell cycle[39]. Ablation of the GFP^+ cells with ganciclovir significantly arrested tumour growth, and the combination of ganciclovir and TMZ completely stopped tumour development[39]. This and other studies demonstrate that the relatively quiescent subset of glioma CSCs is responsible for sustaining long-term tumour growth after chemotherapy treatment through the production of transient populations of proliferative cells[39–41].

CSCs and epithelial-mesenchymal transition (EMT)

The conventional paradigm for metastasis, states that cancer cells within most primary tumours, must undergo epithelial-mesenchymal transition (EMT) to enter circulation and transit to secondary sites[3]. EMT is a biological process through which epithelial cells undergo multiple biochemical changes that enable them to assume a mesenchymal cell phenotype[42]. This includes enhanced migratory capacity, invasiveness, elevated resistance to apoptosis and increased production of extra-cellular matrix components[42]. Over the past years, the connection between CSCs and EMT has become evident. Numerous publications support a gradient of tumour cells expressing both epithelial and mesenchymal characteristics within the primary tumour, circulation, and at the secondary site[3]. Most disseminated tumour cells express stem cell markers and conversely, CSCs are enriched in EMT markers[43]. A genome-wide analysis of cells undergoing EMT and circulating tumour cells revealed remarkably similar transcriptomic profile between these cells and CSCs[3]. Moreover, tumour cells that express stem cell markers have a higher capacity to form metastasis[44], and overexpression of EMT transcription factors, like Twist or Snail, promotes tumour-initiating potential of CSCs[19,43,45]. These data strongly suggest that CSC properties rely on EMT mechanisms.

Immune system evasion

In the past few decades, immunotherapy has emerged as a promising treatment exploiting the innate ability of the immune system to track and neutralise cancer cells. However, recent publications suggest CSCs can alter the tumour microenvironment by modulating tumour infiltrating cells, evading the immune response[19,46,47]. A machine learning algorithm, used to identify epigenetic and transcriptomic signatures from human non-transformed pluripotent stem cells and their differentiated progeny, revealed that undifferentiated tumour landscape, high in stem cell markers, correlates with a lower immune infiltration and downregulation of programmed cell death 1 ligand 1 (PD-L1), a ligand protein involved in immune checkpoint signalling[46]. This is supported by studies in melanoma in mouse models, in which activation of the Wnt/β–catenin signalling pathway results in T-cell exclusion and resistance to PD-L1 immunotherapy, suggesting that specific oncogenic signals produced by CSCs can mediate immune evasion[47]. Bladder CSCs also modulate tumour infiltrating lymphocytes by producing inflammatory mediators like interleukin-6 (IL-6) and IL-8 which attract pro-tumourigenic myeloid cells[48]. These studies exemplify the interplay between CSCs and the immune system, highlighting the need for a better understanding of these processes.

1.2.3 Developing approaches to target CSCs

CSC specific therapies have been proposed in conjunction with traditional cancer treatments to target both differentiated and stem-like tumour cells simultaneously and prevent subsequent tumour relapse[4]. One major issue in the development of CSC targeting drugs is the similarity between CSCs and normal stem cells, as they share numerous markers and signalling pathways involved in regulating differentiation and self-renewal[49]. On the other hand, the redundancy of regulatory pathways within CSCs and their varied protective mechanisms, such as the described above, can limit therapeutic efficiency[49]. Nevertheless, current efforts targeting CSC populations in different cancer

types have demonstrated some success in early phase clinical trials, and promising results are expected in the years to come[4].

Targeting surface markers expressed by CSCs

Specific surface markers used for identification and isolation of CSCs, like the ones mentioned in **Table 1**, are becoming important targets for therapy. The major challenge of this approach is that the majority of stem cell markers cannot distinguish normal stem cells from CSCs and therefore, are not suitable for antibody therapies which specifically target these proteins[32]. Another limitation is that cell-surface phenotypes can vary from patient to patient, and even between different CSC populations within the same tumour, which can additionally diverge or evolve acquiring distinct phenotypes upon relapse[4]. Examples of this approach are therapies targeting CD44, one of the most common CSC markers[50]. A new recombinant humanized monoclonal anti-CD44 antibody was tolerated in a phase 1 clinical trial on 44 patients with acute myeloid leukaemia, with the majority of adverse effects being mild to moderate[50]. The treatment resulted in increased macrophage recruitment and decreased stem-like tumour cells, alongside with a higher presence of differentiated tumour cells[50].

Other immunologic approaches to targeting CSCs

In addition to the antibody-based CSC targeting therapies described above, new immunotherapy approaches are being developed. These include the use of CSC lysates as a source of antigen to prime immune cells, inhibition of components of the immune checkpoint system, *in vitro* generation of CSC-specific T cells with subsequent injection into host, or the production of CSC-dendritic vaccines[4]. Targeting the immune checkpoint molecules, programmed cell death-1 (PD-1) and cytotoxic T-lymphocyte antigen 4 (CTLA-4,) with blocking antibodies that inhibit their interaction with their ligands, allows cytotoxic T-cells to attack cancer cells despite them expressing inhibitory ligands[49]. This has proven to be effective in a small set of cancer types such as lung cancer and

melanoma[49]. These therapies are in early development, but they represent a promising future direction.

Targeting the tumour microenvironment

The tumour mass consists of heterogeneous populations of cancer cells, a variety of resident and infiltrating cells, secreted proteins, and extracellular matrix proteins, altogether known as microenvironment[51]. Within the tumour microenvironment, CSCs reside in specialized regions known as niches, which provide necessary signals for their maintenance, self-renewal and regulation, that have proven to be critical for their resistance to therapy[3,19,51]. Targeting the niche to deprive tumour cells of these factors holds great therapeutic potential, especially for multi-CSC/tumour targeting purposes, as some niche elements are shared by most tumours independently of their origin and type[4].

One of the best known forms of interaction between CSCs and tumour stroma is mediated by the C-X-C chemokine ligand (CXCL) 12 - C-X-C chemokine receptor (CXCR) 4 axis[4]. This is well studied in acute myeloid leukaemia, where leukaemic stem cells overexpress the receptor CXCR4, which binds to CXCL12 expressed by cells in the niche of the bone marrow stroma, maintaining their protective quiescence[4,52]. Blocking of CXCR4 results in a severe reduction on number of stem cells, although it does not impair expansion of the more mature progenitors[52]. Several early phase clinical trials are currently exploring this possibility using the CXCR4 antagonist, plerixafor, in combination with chemotherapy in acute myeloid leukaemia, obtaining encouraging rates of remissions[4,53].

CXCR1 is another target being explored for breast cancer treatment[54]. It is almost exclusively expressed by breast CSCs and functions as a receptor for CXC ligand 8 (IL-8) promoting self-renewal, tumour progression, and metastasis[54]. Reparixin is an inhibitor of CXCR1/2 that when used in combination with chemotherapy has demonstrated a 30% response rate in metastatic breast cancer in a phase 1b study[55].

Targeting CSC signalling pathways

Several CSC signalling pathways are currently being pursued as potential clinical targets. These include mainly Hedgehog (Hh), Notch and Wnt signalling, and most of the significant advances have been achieved by targeting the first two.

The Hh signalling pathway was first identified in *D. melanogaster* as essential for the development of dorso-ventral body pattering[56]. In vertebrates, three Hh protein family members with similar functions to *Drosophila* Hh have been identified: Sonic Hedgehog (SHh), Indian Hedgehog (IHh) and Desert Hedgehog (DHh). The Hh family is involved in an evolutionary conserved pathway of signal transmission that plays a critical role in normal embryonic development, maintenance of tissue polarity, pattering and stemness[57–59]. In adult organisms, the pathway remains functional in stem and progenitor cells to promote maintenance and regeneration, being of particular importance in cancer[59].

In Hh canonical signalling, binding of Hh to its receptor, the tumour suppressor Patched 1 (Ptch1), results in activation of the pathway by preventing Ptch1-dependent inhibition of Smoothened (Smo)[57]. Accumulation and activation of Smo leads to the translocation of the Glioma-associated oncogene family (Gli) transcription factors to the nucleus and the transcription of target genes[57]. Activation of this pathway has been detected in a variety of cancers and linked to CSCs[32,60]. For example, Hh-Gli signalling regulates the expression of stemness genes of $CD133^+$ glioma stem cells and is required for sustained glioma growth and cell survival[60]. GBM tumours of patients who received vismodegib, a Hh pathway antagonist, for seven days before surgical intervention, had reduced ex-vivo $CD133^+$ neurosphere formation[61]. However, the treatment did not prolong progression-free and overall patient survival[61]. Despite the promising preclinical activity and number of trials with Hh inhibitors, the clinical efficacy of these drugs has been limited to a subset of tumours with active Hh signalling[4]. This suggests that the inhibition of this pathway might be compensated by other CSC-driving mechanisms[4].

Notch signalling is a cell-cell communication system, initiated when a membrane-bound Notch ligand interacts with a transmembrane Notch receptor on juxtaposed

cells[62]. This results in the translocation of the intracellular part of the Notch receptor to the nucleus, where it acts as a transcription factor and promotes the expression of target genes[62]. The Notch pathway regulates a wide set of cell fate decisions during both development and homeostasis, including lineage commitment, differentiation, cell cycle progression and maintenance, and self-renewal of stem cells[62]. The first evidence of Notch's oncogenic effect in solid tumours came from mouse studies, which demonstrated that the integration of the mouse mammary tumour virus into Notch 4 leads to the formation of a truncated dominant active form of Notch that causes mammary tumours[63]. Since then, several studies have shown the important role of the pathway in carcinogenesis, tumour angiogenesis and EMT[62]. Clinical studies targeting Notch have taken two main approaches: γ-secretase inhibition and antibodies against the Notch receptor or ligand. Yet, these therapies have shown minimal response as single-agent therapies in patients with metastatic or recurrent tumours[4].

In summary, the studies mentioned above suggest that effective tumour eradication requires that we rethink the way we diagnose and treat tumours, targeting CSCs and the signals critical to sustaining this population while sparing normal stem cells.

1.3 Brain tumours and CSCs

Brain tumours are among the most challenging cancers to treat[64]. Firstly, their location in one of the most crucial organs of the body often hampers surgical options, as access to the tumour mass is limited[1,64]. Additionally, these tumours are located behind the blood-brain barrier, a semipermeable system of endothelial cells that protects the brain from exposure to factors in the circulating blood, but also limiting exposure to chemotherapy[1]. Furthermore, the unique developmental, genetic, epigenetic and microenvironmental features of the brain make these cancers resistant to most treatments[1].

1.3.1 Glioblastoma multiforme (GBM)

Grade IV glioma, glioblastoma multiforme (GBM), is the most aggressive and common type of brain tumour in adults[65] with an estimated incidence of 3:100,000 that increases with age, and more than 10,000 cases being diagnosed annually[10]. Moreover, over the past 20 years, a sustained rise in the incidence of glioblastoma across of all age groups has been reported in the UK, while the incidence of lower grade brain tumours has decreased, which is thought to be caused by environmental or lifestyle factors[11]. Current treatments involve surgical removal of the main tumour mass followed by radiotherapy and chemotherapy, but despite all efforts it remains untreatable, with a dismal prognosis of 10 to 15 months[17,64–66].

The most recent WHO guidelines (2016) distinguish GBMs that are isocitrate dehydrogenase (IDH)-mutant from those that are not[64,65]. These mutations occur early in gliomagenesis and consist in a change of function of the IDH enzyme, which causes it to produce 2-hydroxyglutarate instead of nicotinamide adenine dinucleotide phosphate (NADPH)[67]. IDH-wild-type GBMs arise *de novo* as primary brain tumours, whereas IDH-mutant develop as the result of malignant progression from a lower-grade diffuse astrocytoma or anaplastic astrocytoma and are, therefore, secondary tumours[64,65]. Primary GBMs account for about 90% of the cases and predominate in patients over 55 years of age, whereas secondary GBMs are only about 10% and preferentially develop in younger patients[65]. Primary GBMs are molecularly distinct from secondary GBMs[64,65] and genetic properties of GBM recurrences were shown to differ from those of primary tumours, suggesting that one reason for treatment failure is likely the result of current inefficiency in controlling these tumours right at their original site[66].

1.3.2 Mammalian adult neural stem cells and glioma stem cells (GSCs)

Traditionally it was believed that the adult nervous system had no regenerative capacity, however, it is well established now that Neural Stem Cells (NSCs), at least in mammalian brain models such as adult mice, contribute to brain plasticity and integrity

through life[68,69]. NSCs cells share fundamental properties to CSCs such as the ability to self-renew through symmetric divisions as well as undergoing asymmetric cell division, relative quiescence and differentiation capacity into different neural lineages[68].

Studies mainly using mouse models demonstrate that there are two major neurogenic niches in mammals where NSCs reside, the subventricular zone (SVZ) of the forebrain lateral ventricles and the subgranular zone (SGZ) in the dentate gyrus of the hippocampus. Smaller populations of NSCs have also been isolated from the subcortical white matter[70] and the hypothalamus[71]. The SVZ is composed of three main cell types; NSCs, also known as type B cells, extend a basal process to terminate on blood vessels and an apical process that contacts the cerebrospinal fluid through a layer of ependymal cells. Type B NSCs give rise to transiently proliferating precursor cells known as type C which, in turn, generate mitotically active type A neuroblasts that divide while forming a chain and migrating tangentially towards the olfactory bulbs, where they integrate as new interneurons **(Figure *1.2* A)**. In the SGZ the cellular hierarchy is similar to that in the SVZ, radial glia-like NSCs give rise to intermediate progenitor cells, which after limited rounds of proliferation generate neuroblasts that migrate tangentially along the SGZ and develop immature neurons. These neurons migrate radially into the granule cell layer and differentiate into dentate granule neurons **(Figure *1.2* B)**[12,72].

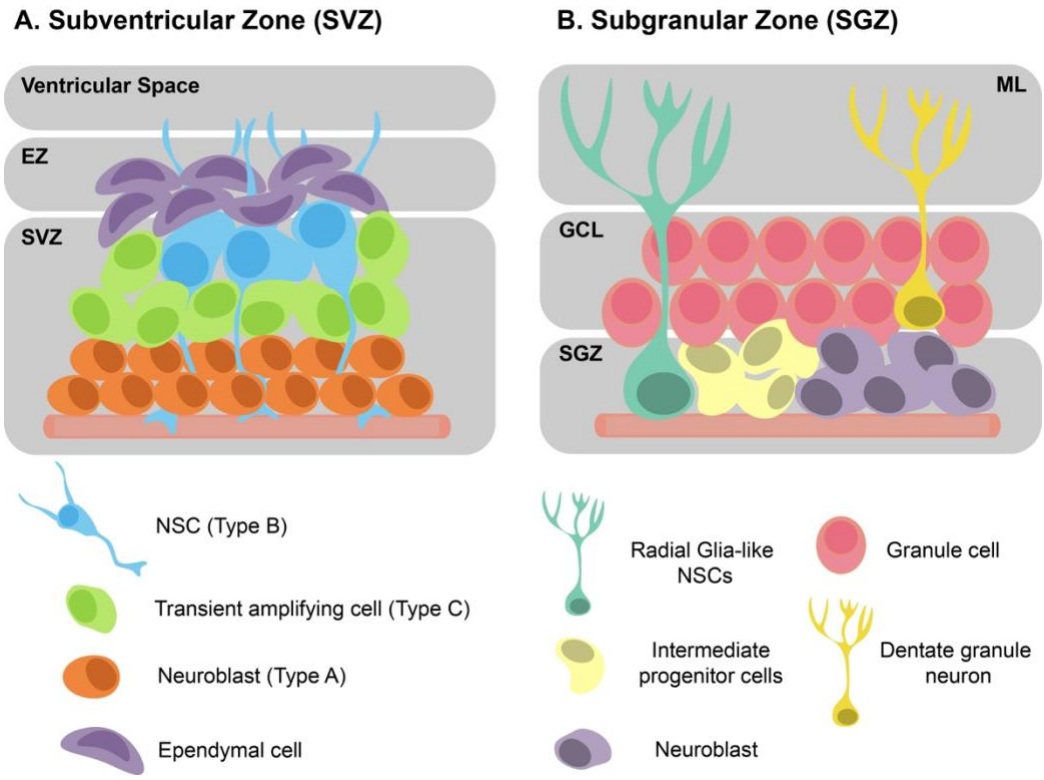

Figure 1.2 Major adult NSC niches in the brain. (A) Schematic diagram depicting the SVZ. NSCs (B cells) reside along the ependymal zone in the SVZ and contact the ventricular space and blood vessels. They generate transient amplifying cells (C cells) which generate neuroblasts (A cells). **(B)** Schematic diagram depicting the SGZ. Radial glia-like NSCs reside in the SGZ and extend radial processes through the granular cell layer contacting the molecular layer. They generate intermediate progenitor cells which generate neuroblasts which will differentiate into dentate granule neurons that migrate into the granular cell layer[12,72]. EZ, Ependymal Zone; ML, Molecular Layer; GCL, Granular Cell Layer.

In the adult human brain, whether or not neurogenesis exists remains a controversial matter. In recent years two prominently published studies have arrived at opposite conclusions; Sorrells *et al*. reported that neurogenesis in the dentate gyrus of primates and humans is undetectable beyond adolescence[73], in contrast, Boldrini *et al*. reported lifelong neurogenesis in humans[74]. However, several publications in agreement with Boldrini *et al.* have led to the general belief that the hippocampus continues to generate new neurons through life[75–77].

Although GBMs were presumed to originate from malignant transformation of differentiated glia, recent evidence shows that NSCs and progenitor cells might function as a more likely source of tumour initiating glioma stem cells (GSCs)[18,78,79]. Experiments

performed in rat models exposing the brain to avian sarcoma retrovirus, that carries the oncogene *src,* or drugs like N-ethyl-N-nitrosourea, that lead to carcinogenesis, demonstrate that gliomas preferentially develop in germinal regions of the brain as opposed to the non-proliferative brain parenchyma, suggesting that tumours are more likely to arise from less differentiated cells[79,80]. Another study in mice, showed that activation of the oncogenes *Ras* and *Akt* in neural progenitors, results in a higher frequency of tumour formation than such alterations in GFAP-expressing differentiated astrocytes[78]. These studies suggest that the state of differentiation is an important feature of the cell of origin in gliomas.

Evidence of the existence of GSCs and a proliferative hierarchy in GBM has been derived from xenotransplantation of specific populations defined by surface marker expression[5,81–83], genetic lineage tracing in mouse models[84] and single cell RNA sequencing[85]. Moreover, lineage tracing assays based on genetic mouse models and xenotransplantation have demonstrated that GSCs are responsible for brain tumour recurrence following chemotherapy[17,39].

Recent comprehensive genomic, transcriptomic and epigenomic studies have shed new light onto tumour-driving events and cellular heterogeneity in GBM. Common genetic alterations include loss of heterozygosity of the chromosome arm 10q, occurring in 60-90% of cases, deletions that affect the p53 gene, as high as 85.3-87% in secondary GBM, and mutations in the epidermal growth factor receptor (EGFR) and in the platelet-derived growth factor receptor (PDGFR), that occurred in 57% and 60% of the studied cases respectively[86]. A genomic analysis from The Cancer Genome Atlas (TCGA) database indicates that the main signalling pathways involved in GBM tumourigenesis are the receptor tyrosine kinase/Ras/Phosphoinositide 3-kinases (RTK/Ras/PI3K) and retinoblastoma protein (pRb) signalling pathways[87]. The RTK/Ras/PI3K signalling pathway is involved in the regulation of cell proliferation, survival, differentiation and angiogenesis and was found altered in 86-90% of the GBM cases analysed[86]. pRb is a tumour suppressor involved in the regulation of cell cycle entry and progression. The pRb pathway is altered in 77-78.9% of GBM cases[86].

Despite the breakthroughs achieved during the last decades, GBMs remain untreatable. In this thesis, I use different approaches combining *in vitro* and *in vivo* models to study GSCs and brain tumour initiation biology.

1.4 *Drosophila* as a model for brain cancer research

The model organism *Drosophila melanogaster*, also known as fruit fly, has been extensively used in many research areas, including developmental neurobiology, and more recently, in brain cancer research. Indeed, the first ever tumour suppressor, *lethal (2) giant larvae (l(2)gl)*, was described in *Drosophila* in the 1960s by Elizabeth Gateff, who found that *l(2)gl* mutations result in the formation of invasive and lethal tumours in the larval brain and the epithelia of the imaginal discs[88]. Gateff then continued describing new tumour suppressors in flies and propelled tumour biology in this model. Moreover, *Drosophila* studies were also the foundation link between cell polarity deficiencies and asymmetric cell division, oncogenic signalling, and cancer[88].

The numerous benefits of using *Drosophila* as a model include short life cycle of approximately 11 days at 25ºC, cost-effectiveness compared to other models such as mice or rats, highly fecund and easy to breed and most importantly, a high (70%) orthology level of disease gene sequences with humans[89]. Additionally, fruit flies count with a vast genetic toolkit available for easier gene manipulation[90]. One of the key gene editing techniques used in *Drosophila* is the UAS-GAL4 system, a genetic tool adapted from yeast allowing targeted gene expression[91], which I have used extensively in this work.

In its simplest form, the system is based on a cross between a driver and a responder fly line. The driver line will contain a desired promoter gene region fused to the transcriptional activator GAL4, which will selectively activate any gene region fused to an Upstream Activation Sequence (UAS) in the responder line. GAL4 will only activate transcription when bound to its UAS responder. In the absence of GAL4 the target gene is silent, allowing to work with potentially lethal traits[92]. For example, an NSC gene-GAL4 driver-line will only drive the expression of transgenes under the control of an UAS

sequence, such as UAS-GFP. Thus, when the transgenic driver and responder flies are crossed, their progeny will express the gene sequence of interest (GFP) in the tissue pattern dictated by the desired promoter (NSCs) **(Figure *1.3*)**.

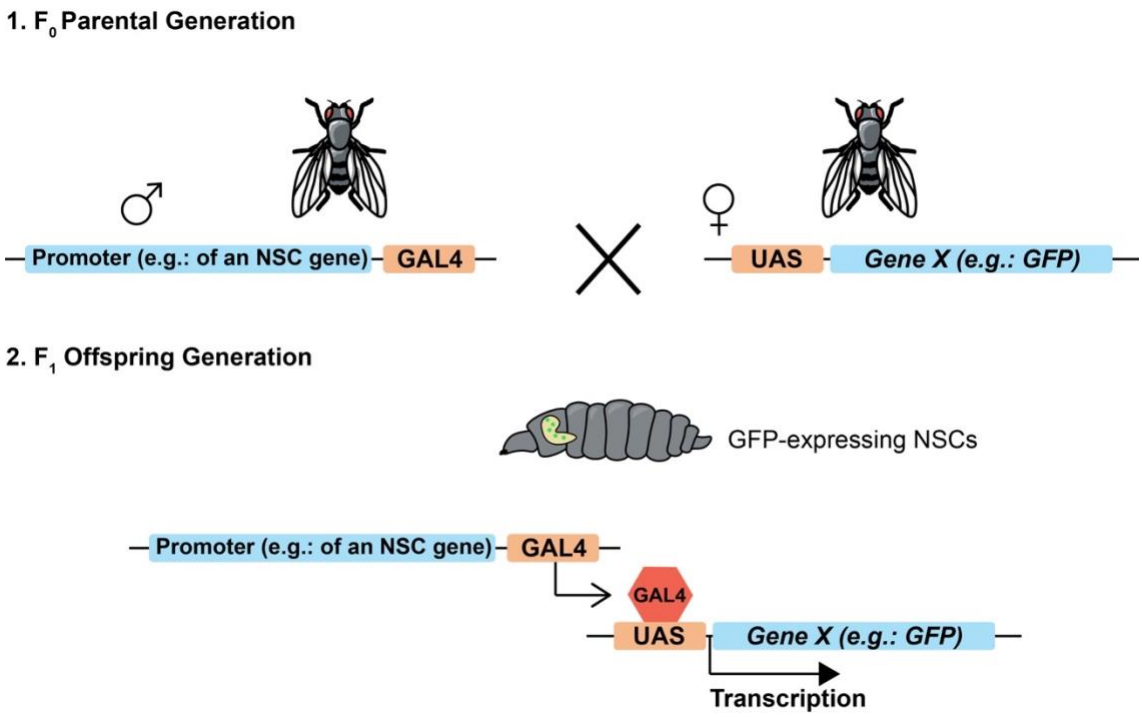

Figure 1.3 Schematic representation of the *Drosophila* GAL4/UAS system. When one fly strain carrying a GAL4 promoter is mated to another carrying a UAS responder, progeny will express the gene of interest fused to the UAS sequence in the pattern dictated by GAL4. In the case depicted, the NSC gene promoter drives the expression of the responder, therefore, the progeny will express GFP in all NSCs.

Since its establishment, the UAS/GAL4 system has been widely used, modified, and expanded to allow for more specific temporal and spatial control of targeted gene expression. For instance, it can be used for a variety of loss and gain of function assays, and simultaneously with other independent expression systems such as LexA/LexAop allowing additional manipulation, and using different reporters. It can inform on a variety of parameters including visualization of cells and their organelles, cell metabolic status and behavior[92].

1.4.1 *Drosophila* NSCs

Drosophila NSCs, also known as neuroblasts (NBs), recapitulate many of the key features of mammalian NSCs in the developing brain, acting as a simpler, well-characterised system, that is also amenable to sophisticated genetic manipulation[93,94].

Drosophila neurogenesis takes place in two waves; during the first one, embryonic NSCs are formed by delamination from the neuroectoderm and start dividing to generate neurons and glia[93,94]. Acquisition of NSC identity depends on a process called lateral inhibition, in which Notch/Delta signalling interactions between adjacent neuroectodermal cells lead to stem-cell specific expression of pro-neural genes[93,94]. During this specification, the *Sox* genes, *soxN* and *dichaete*, and members of the *Snail* family, act redundantly promoting pro-neural gene expression[24]. Neural diversity is achieved by spatial determination, which is established along the anterior-posterior axis by *Hox* genes, and temporal transcription factors like *hunchback* (*hb*), *kruppel* (*kr*), and *castor* (*cas*), which are sequentially expressed in NBs and their progeny[94,95]. Embryonic NSCs become smaller after every division until they enter apoptosis, in most cases, or a quiescent state that marks the end of the first neurogenic wave[93]. 8-10 hours post-larval hatching (HPH), the second wave of neurogenesis begins as the NSCs exist quiescence, enlarge, and start entering mitosis[93]. Larval NSCs re-grow to their original size after each division and are capable of dividing hundreds of times, being responsible for 90% of the neurons in the adult CNS[93].

NSCs divide asymmetrically along the apical-basal axis following their delamination from the neuroectoderm, from which they inherit their polarity[96]. At the apical pole, the adaptor protein Inscuteable (Insc) links the Par protein complex, consisting of Bazooka (Baz), Protein Kinase C (aPKC), Par3 and Par6, to a second complex containing heterodimeric G protein α-subunit (Gα) and the adaptor protein Partner of Insc (PINS), which binds to the microtubule-associated dynein-binding protein Mud[96]. These proteins determine the spindle orientation and regulate the asymmetric localization of cell-fate determinants[96]. The endocytic protein Numb, which inhibits Notch-Delta signalling, the translation inhibitor Brain tumour (Brat), and the homeodomain transcription factor

Prospero (Pros), accumulate at the basal membrane during metaphase mitosis due to two adaptor proteins known as Partner of Numb (Pon) that binds to Pros and Numb, and Miranda (Mira) that binds to Brat[96] **(Figure *1.4* A)**. The basal accumulation of these so-called cell fate determinant proteins means they will be segregated only to the daughter cells upon division and confer a different identity to the progeny. After mitosis, Brat and Pros act to prevent self-renewal and induce cell cycle exit and differentiation[6,97–99].

During post-embryonic development, the *Drosophila* CNS consists of two brain lobes, each comprising an optic lobe at the lateral surface and the central brain located medially, and a ventral nerve cord (VNC). There are two main types of NSCs in the larval central brain that can be distinguished based on their position and lineage characteristics: type I and type II[93] **(Figure *1.4* B)**. Type I constitute the majority of NSCs, approximately 90 per lobe, and are located both in the anterior and posterior sides of each brain lobe and in the VNC. Type I NSCs divide asymmetrically to self-renew and bud off a ganglion mother cell (GMC) that divides once more to generate two differentiated neural cells[6,93,100,101]. All type I NSCs express the neural precursor gene and maturation marker Asense (Ase) and the self-renewal transcription factor Deadpan (Dpn)[93,94]. As they divide and differentiate into GMCs, they stop Dpn expression but maintain Ase[93,94] **(Figure *1.4* C)**. There are only eight type II NSCs per brain lobe, which localize to the posterior brain region and are also called Dorsomedial (DM) NSCs one (1) to eight (8)[102]. There are no type II NSCs in the VNC. In contrast to type I, type II NSCs express Dpn, but not Ase[93]. They divide asymmetrically to self-renew and generate immature intermediate neural progenitors (iINPs), which do not express any of these markers. Within a few hours, iINPs acquire Ase and Dpn expression to become mature transit amplifying intermediate neural progenitors (INPs)[93]. Each INP divides asymmetrically between three to five times generating another INP and a GMC that divides once more into two neurons or glia[93,100,101] **(Figure *1.4* D).** Due to their transient-amplifying capacity, Type II NSC lineages give rise to most of the neural cells in the adult brain[103].

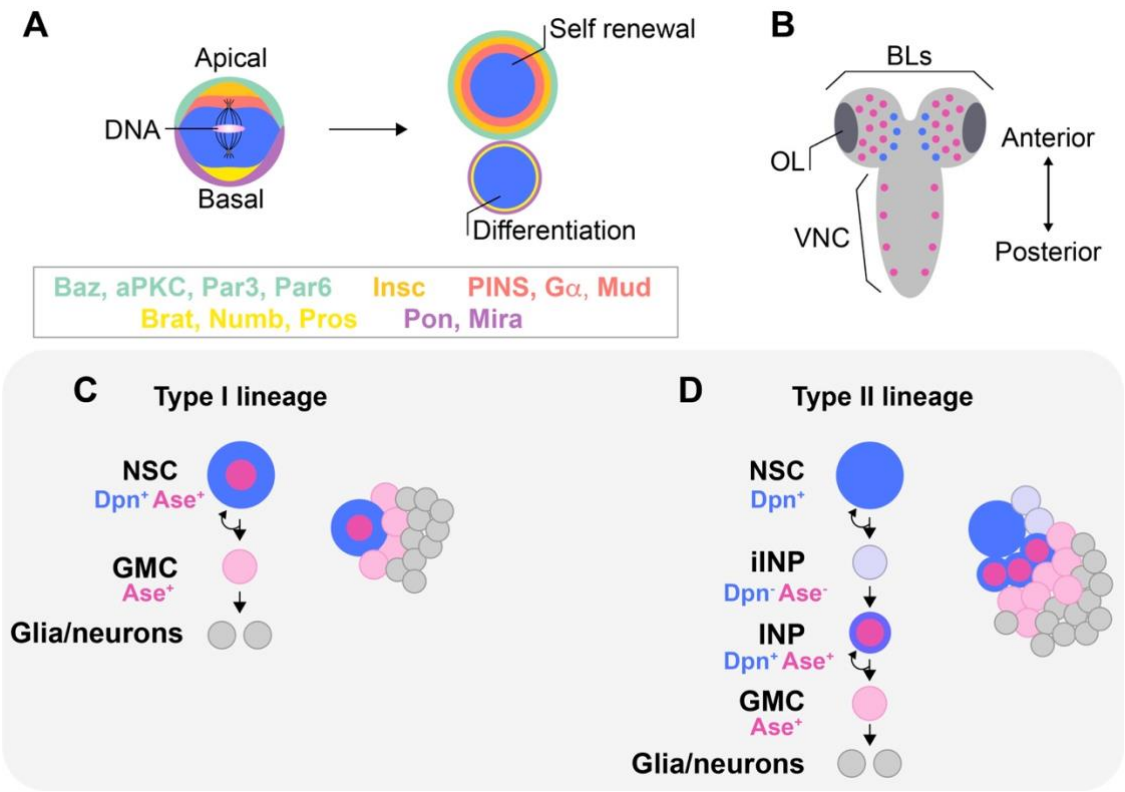

Figure 1.4 ***Drosophila*** **central nervous system and asymmetric division of type I and type II NSCs. (A)** In dividing NSCs, the adaptor Insc links the protein complexes Baz, aPKC, Par3, Par6 with PINS, Gα and Mud at the apical pole of NSCs. Brat binds to Mira and Numb and Pros bind to Pon and localise to the basal pole. After asymmetric division, the apical components remain at the mother NSC which keeps self-renewal capacity, and the basal components segregate to the daughter cell promoting differentiation. Adapted from Knoblich (2010)[96]. **(B)** *Drosophila* larval brain composed of two brain lobes (BLs) with their respective optic lobes (OLs) and central brain region (BL excluding OL), and a ventral nerve cord (VNC), depicting the two major post-embryonic NSC populations: type I (pink) and type II (blue). **(C)** Type I NSCs (blue/pink) generate GMCs (pink) that differentiate into glia or neurons (grey). **(D)** Type II NSCs (blue) divide asymmetrically to self-renew and generate an immature intermediate neural progenitor (iINP) (light blue), which matures into an INP (pink/blue). INPs divide asymmetrically to self-renew and generate GMCs (pink) that divide only once more to generate glia or neurons (grey)[93,100,101]. Adapted from Homem and Knoblich (2012)[93].

1.4.2 *Drosophila* brain tumour models

Defects in NSC asymmetric cell division and cell fate determination can lead to tumour formation in the brain[97–99,101,104,105]. Loss of polarity in NSCs impairs the mechanisms that specify the fate of the daughter cells, which lose their ability to respond to proliferation control, forming NSC-like tumour cells that resemble human CSCs[104].

In one of the seminal studies investigating the effect of disrupted asymmetric NSC division and tumourigenesis using *Drosophila* as a model, Caussinus and Gonzalez generated larval NSCs with mutations in different proteins that are known to segregate asymmetrically during NSC mitosis: *aPKC, PINS, mira, pros* and *numb*[104]. The authors transplanted the mutated NSCs into healthy hosts demonstrating that loss of function of any of the mentioned proteins, except for aPKC, leads to tumour formation[104]. Furthermore, the team was able to maintain the tumours *in vitro*, showing that the transformed cells become immortal and have unlimited proliferation potential, and that many of the regulators of asymmetric division behave as tumour suppressors[104].

Since those initial studies, publications that use fruit flies to study cancer have exponentially increased as several brain tumour developmental models have been characterized. A brief overview of some of them is given below.

Pros is a homeodomain transcription factor[106]. After cell division, it enters the nucleus of GMCs where it regulates over 700 genes[106]. In the absence of Pros, GMCs fail to differentiate and revert to a stem cell-like fate, over-proliferate, and form a brain tumour[97]. Similarly, its vertebrate ortholog, Prox1, is critical for organ development during embryogenesis, it is expressed in newly differentiated neurons and inhibits neural progenitor proliferation[107]. Alterations in its expression and function are associated with a number of human cancers including brain tumours[108].

As previously mentioned, Notch signalling is a central node that directs self-renewing proliferation of NSCs and is considered an important pro-tumourigenic protein in numerous cancers[109]. In *Drosophila* larval NSCs, the Notch inhibitor, Numb, accumulates at the basal membrane upon mitosis, where it binds to Pon, and is asymmetrically segregated to the GMC to repress activation of Notch targets in progeny cells[105]. Type I NSC *numb* mutant clones show only mild defects: almost all clones contain at least one ectopic neuroblast in addition to differentiated cells[105]. However, in type II lineages, the loss of *numb* impairs INP maturation and triggers their overproliferation as type II NSC-like cells, generating clones that contribute to a dramatic enlargement of the larval brain[6,105]. Loss of Notch, results in the transformation of type II NSCs into type I-like

NSCs[110]. Interestingly, Notch inhibition does not affect identity and self-renewal of type I NSCs although it is similarly activated in type I and type II[111].

Like *pros* and *numb, brat* is a tumour suppressor that acts as a cell fate determinant[98,99,101]. Its loss leads to uncontrolled proliferation of transformed immature INPs, which are unable to commit to maturation and act as brain tumour initiating NSC-like cells[98,99,101]. A detailed description of the *brat* model is provided in the next section, as I extensively use it as a brain tumour model in my studies.

Earmuff (*erm*) is another transcription factor that maintains restricted developmental potential of INPs in type II lineages, limiting proliferation by promoting nuclear localization of Pros and suppressing de-differentiation by antagonizing Notch signaling[112]. Interestingly, loss of *erm* leads to de-differentiation and overproliferation in type II lineage cells but does not affect type I, which suggests that type II lineages are more susceptible to mutations in cell fate determinants[6].

All of the above, are examples of how defects in asymmetric cell division and/or cell fate determination can impair the differentiation of immature cells. In contrast, a different class of mutants in which de-differentiation of *bona fide* neurons leads to tumour formation has also been identified.

Longitudinals lacking (Lola) is a transcription factor required to maintain neurons in a differentiated state by repressing NSC and cell-cycle genes in post-mitotic neurons[113]. In *lola* mutants, neurons revert to a pluripotent state and proliferate forming brain tumours[113]. Similarly, loss of *Nervous fingers 1* (*Nerfin-1*), a zinc finger transcription factor previously implicated in embryonic axon guidance in *Drosophila*[114], causes reversion of neurons into multipotent NSCs[115]. Nerfin-1 mutant lineages are dependent on the oncogene Myc and target of rapamycin (Tor)-mediated cell growth[115]. *Midlife crisis* (*Mdlc*) is another zinc finger-containing protein required for the maintenance of neuronal differentiation and NSC proliferation through the regulation of *pros* splicing. *Mdlc* mutant neurons initiate but fail to complete differentiation and instead acquire NSC marker expression[116]. These three examples demonstrate that differentiated cells can also become tumourigenic cells.

These studies add further evidence of the link between asymmetric cell divisions, cell determination and cancer and provide an excellent toolbox to study tumour formation *in vivo*, highlighting the power of *Drosophila* as a model system.

1.4.3 The *brain tumour* (*brat*) model

Among the models described above, probably one of the better characterised, is the *brat* brain tumour model, which I have used in my project to study the initiation and development of brain tumours.

Brat is a tumour suppressor and cell fate determinant that belongs to the tripartite motif (TRIM)-NHL protein family[6]. It consists of 1031 amino acids and contains two B-Box zinc finger motifs, a coiled-coil domain at the N-terminus and a C-terminal NHL domain[117]. These motifs are reported to be involved in protein-protein interactions[117]. Brat is encoded by a gene located in chromosome II which consists of five exons and four introns, although only exon 5 contains the coding region[117].

Brat is known to act as translational repressor and plays an important role in post-transcriptional regulation, an essential process during development and metabolism[118]. One well studied example of this function is the regulation of *hb* during *Drosophila* embryogenesis. *Hb* mRNA is uniformly distributed across the embryo and translationally repressed from the posterior pole, creating an anterior-to-posterior gradient which is necessary for the correct segmentation of the specimen[118]. The NHL domain of Brat mediates *hb* mRNA recruitment to repress its translation through the interaction with Pumilio (Pum) and Nanos (Nos), two conserved RNA-binding proteins[118]. In the imaginal discs of the larval brain, Brat overexpression results in growth suppression, caused by a reduction in the number of cells in the wing through a mechanism thought to be similar to *hb* regulation[118]. Additionally, Brat and its *C.elegans* orthologue, *ncl-1*, have been shown to regulate cell growth through the regulation of ribosome synthesis, as their loss results in larger cells with larger nucleoli and increased amounts of ribosomal RNA[119].

In the larval brain, Brat is expressed in both type I and type II NSCs. During asymmetric division it binds to the scaffolding protein Mira, which segregates Brat

exclusively into the daughter cells[99]. Komori *et al.*, performed several experiments mutating specific regions of the Brat protein and demonstrated that the B-boxes are dispensable for unequal partition of Brat during asymmetric cell division, whereas the NHL and coiled-coil domains are crucial for its segregation into the daughter cell[120].

Loss of *brat* leads to dramatic overproduction of NSC-like cells, but not all NSC lineages are affected[6]. Indeed, type I NSCs seem not affected by its loss. Bowman *et al*., (2008) showed that ectopic expression of the maturation factor *ase* in all NSCs eliminates type II lineages, that become type I-like[6], and that simultaneous overexpression of *ase* and downregulation of *brat* does not induce either overgrowth or NSC-like transformation, indicating that type I lineages are not affected by *brat* loss[6]. In contrast, loss of *brat* in type II NSC lineages has a massive effect. Its loss hampers the maturation of iINPs, which enter a brief cell cycle delay during which the cells grow in size and acquire NSC-like features, transforming into brain tumour initiation cells and leading to neoplastic overgrowth[6,98,99,101] **(Figure *1.5* A, B)**. These transformed iINPs never express the mature INP marker Ase and all acquire the self-renewal marker Dpn[6]. In *brat* mutant brains, normal brain structure and organization are disrupted, and the expression levels of the neuronal marker, Elav, and the glial marker, Repo, are reduced[121]. Similar to mammalian CSCs, if *brat* larval tumour initiating cells are transplanted into healthy adult hosts, they re-form the whole tumour mass and metastasize[93,104,121]. These metastases are mainly formed by undifferentiated cells that do not express either Elav or Repo, can be sequentially passaged into new hosts without losing their proliferation ability, and have a uniform expression pattern, indicating that they derivate from a clonal origin[121].

Brat is essential for the maturation of INPs. It specifies their identity by attenuating the function of the self-renewal transcription factor Klumpfuss (Klu) and promoting the Adenomatous polyposis coli 2 (Apc2) destruction complex, which negatively regulates β-catenin/Armadillo (Arm) activity and Wnt targets[122] **(Figure *1.5* C)**. In the absence of Brat, the increased activity of Klu and Arm cooperatively induce reversion of the iINP into an NSC-like state[122]. Expression of *brat* mutant constructs without the coiled-coil or NHL

domains in *brat* null brains, suppresses the supernumerary NSC-like cell phenotype, proving that these two domains are not necessary for INP specification[122]. Yet, expression of a *brat* form without its B-boxes failed to suppress the phenotype, demonstrating that they are essential for this process[122]. Interestingly, high β-catenin levels are a hallmark of many cancers including brain tumours[123,124]. Particularly in GBMs, growing evidence suggests that Wnt/β-catenin signalling is aberrantly activated and that it promotes GBM growth and invasion through the maintenance of stem cell properties[125].

Recently, Brat has also been shown to repress self-renewal of transit amplifying INP cells by inhibiting Zelda (Zld), a protein required to allow re-expression of the transcriptional repressor Dpn in iINPs to resume transient self-renewal[126]. Brat's NHL domain binds the 3'UTR of *dpn* and *zld* mRNA to mediate their degradation[126]. Upon Brat loss, Dpn and Zld continue to be expressed in the tumour initiating iINPs and inhibition of either of them stops tumourigenesis, indicating that they are required for the malignant transformation of brain tumour initiating cells[126]. Thus, in type II NSC lineages, Brat prevents newly born iINPs reversion to NSC-like cells by repressing the expression of Dpn, Zld and Klu **(Figure *1.5* C)**.

For a long time, it has been known that brain tumour phenotypes developed by *numb*, an inhibitor of Notch signalling, and *brat* mutants in type II NSC lineages are similar, suggesting common shared pathways between the two. However, a link between Brat and Notch was not proven until recently, when Mukherjee *et al.* demonstrated that inhibition of *brat* results in upregulation of Notch signalling and increased nuclear transport of Notch intracellular domain (NICD) in brain tumour cells[127].

Brat has also been shown to be required for repression of *Drosophila* Myc (dMyc) in NSC progeny. In the larval brain, dMyc is expressed in all NSCs but not in their daughter cells[98]. In *brat* mutants, however, dMyc can be found in all the cells of the lineage[98]. Like the human (proto)-oncogene c-Myc, dMyc is a known regulator of ribosomal RNA (rRNA) synthesis, a limiting step in ribosome biogenesis that controls protein synthesis and cellular growth[128,129]. Upon loss of Brat, NSC lineage cells present enlarged nucleoli (the

sites of ribogenesis), a consequence of enhanced rRNA synthesis, as well as increased cell size[98] **(Figure *1.5* C)**. Of note, c-Myc upregulation has been described in many cancers and its expression modulation shown to be critical in tumourigenesis[130].

To summarize, upon loss of *brat*, immature INPs behave like brain CSCs and initiate brain tumour growth.

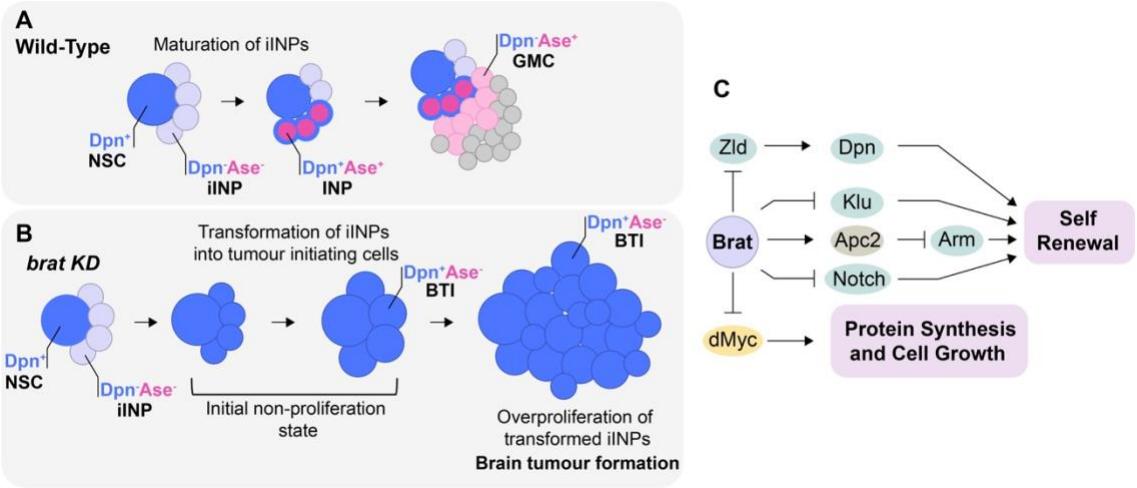

Figure 1.5 The *brat* model of brain tumour initiation and growth. (A) Schematic representations of normal (wild-type) development of type II NSC lineages. Neural stem cells (NSC, blue) divide asymmetrically generating immature Intermediate neural progenitors (iINP, light blue) that mature (pink/blue) and form ganglion mother cells (GMC, pink), which differentiate into neurons and/or glia (grey). **(B)** In a *brat* mutant or inhibition, type II NSCs divide asymmetrically but iINPs never mature. Instead, *brat* iINPs go through a brief non-proliferative stage in which they transform, acquiring self-renewal characteristics of NSCs and becoming brain tumour initiating cells (BTI, blue) that overproliferate forming a tumour[6,98,99]. Adapted from Homem and Knoblich (2012). **(C)** Brat specifies INP identity in iINPs by inhibiting the self-renewal factors Zelda[126], Deadpan[126], Notch[127] and Klu, and antagonizing Arm function via an Apc2-dependent mechanism[120]. Brat also inhibits dMyc, which regulates ribosome biogenesis and cell growth[98].

1.4.4 TRIM3, the *brat* human orthologue, is a GBM tumour suppressor

The *brat* tumour suppressor function is conserved in human brain tumours by its orthologue *TRIM3*, a gene located in chromosome 11p15.5[131,132]. TRIM3 was identified as Brat closest human orthologue based on its high degree of amino-acid sequence identity (25%) and similarity (41%), and conserved functional domains[131].

TRIM3 is part of the TRIM-NHL protein family; its members have an evolutionary conserved role as neural cell fate determinants in *C.elegans, Drosophila* and mammals[133]. Most TRIM proteins function as E3 ubiquitin ligases and are known to be involved in cellular processes such as proliferation, apoptosis and transcription regulation[133]. Interestingly, impairment of their function has been previously associated with diverse pathological conditions, such as developmental disorders, neurodegenerative diseases and cancer[133,134]. For example, TRIM13 and TRIM19 inhibit tumour development by interacting with murine double minute 2 (MDM2), a regulator of the tumour suppressor p53[134], while TRIM24 and TRIM28 suppress p53 stability and expression[134].

In the past decade, *TRIM3* has been linked to numerous cancer types (e.g. gastric cancer, liver cancer, colorectal cancer, and brain tumours) where it has been shown to act as a tumour suppressor, inhibiting tumour growth and metastasis[7,135,136]. Significantly for my research project, *TRIM3* is reported to be deleted (homo- or hemizygous deletions) in 20-35% of gliomas of all grades, including 25% of GBMs, where its function has been extensively studied[127,131,132]. TRIM3 expression is found downregulated in human GBM tumours[137], cell lines and neurospheres derived from GBM patients[131]. Moreover, TRIM3 expression is lower in the population of normal human neuroprogenitor cells that express the stem cell marker CD133 compared to those that do not, and is also enriched in their differentiated state compared to undifferentiated, indicating that TRIM3 expression is inversely correlated to stemness[127]. TRIM3 reconstitution in GBM primary cell lines impairs neurosphere formation and inhibits expression of stem cell markers such as CD133, Nestin and Nanog[131]. TRIM3 overexpression in these cells also leads to a switch from predominantly symmetric to asymmetric cell division[131]. Altogether, these studies indicate that, like *Drosophila* Brat, human TRIM3 is a brain tumour suppressor. TRIM3 has also been suggested to be a tumour suppressor in mice, where its loss facilitates the formation of gliomas upon platelet derived growth factor (PDGF) upregulation, a common signalling pathway upregulated in brain tumours[132].

Again similar to Brat, in GBM neurospheres TRIM3 inhibits Notch activity through the regulation of Musashi, an RNA binding protein that activates Notch by inhibiting Numb[127,131]. In addition, *TRIM3* expression has been found to negatively correlate with *c-Myc* in GBM samples from the TCGA database, and overexpression of TRIM3 in GBM immortalised cells results in reduced nuclear c-Myc expression[131]. Moreover, analysis of c-Myc targets upon TRIM3 overexpression in human astrocytes revealed a suppressive effect on c-Myc transcriptional activity[131]. Together, the above described studies indicate existent common mechanisms of action between *Drosophila* Brat and it human orthologue TRIM3[98,127,131], supporting the use of the *brat* model for the identification of potential mechanisms underlying the formation of human brain tumours, and specifically GBM.

1.5 HEATR1: a candidate player in brain tumourigenesis

Prior to my studies in the Barros laboratory, the team conducted a single-cell transcriptome analysis of *brat* brain tumour initiation cells with the aim to identify molecular changes potentially leading to brain tumour initiation and development (C. Barros, *unpublished*). The group generated via genetic recombination and combinations *Drosophila* strains carrying GAL4 fused to the promoter of the *pointed* gene, expressed in type II NSC lineages[138], and a *UAS-mcd8-GFP* genetic construct, to achieve the expression of membrane-tagged GFP in type II NSC lineages of *brat* mutants (*UAS-mCD8-GFP,brat^{k6028};pointed-GAL4*) and controls (*UAS-mCD8-GFP;pointed-GAL4*). The *brat* mutant allele used (*brat^{k6028})* is a null mutant resulting from a P-element insertion in exon 4 after nucleotide 32500[117]. Using micro-manipulation techniques and an established single-cell transcriptome analysis protocol[139,140], single iINPs were harvested from *brat* and control live brains at a time-point when *brat* iINPs start to express molecular properties indicating their conversion into tumour-initiating cells (24 HPH)[6,101]. Single-cell RNA was immediately reverse transcribed and amplified into complementary DNA (cDNA), and samples from both genotypes were compared on whole-genome microarrays. Analysis of results revealed a large set of genes differentially expressed in

the tumour initiating cells, a majority with high orthology to human genes. Functional analysis of KEGG pathways revealed ribogenesis as one of the most overrepresented in the data, and among the identified genes was *l(2)k093422,* the *Drosophila* orthologue of human *HEAT Repeat containing 1 (HEATR1)* (Diaz *et al., in preparation*). Herein, I will refer to *l(2)k09022* as *Drosophila HEATR1 (dHEATR1).*

dHEATR1 was detected upregulated in *brat* tumour initiating cells and the result validated via RT-qPCRs. Additionally, preliminary data using the *Drosophila brat* model revealed a strong reduction on cell proliferation upon *dHEATR1* knockdown, preventing tumour growth. Previous research in our group further showed that human HEATR1 is overexpressed in GBM samples and GBM immortalised cell lines (U87MG and U251MG) (Diaz *et al., in preparation)*. Based on these encouraging preliminary data, my proposed PhD project focuses on further characterizing the role of HEATR1 as a potential novel candidate player in brain tumour formation and growth.

1.5.1 HEATR1 features and known functions

The human *HEATR1* gene is located at chromosome 1q43 and encodes a large protein consisting on 2144 amino acids, corresponding to 236 kDa. It contains only one HEAT repeat on its C-terminal end, which is its only known domain[141].

HEATR1 has been associated with ribosome biogenesis, the process of generating and assembling ribosomes, key for the regulation of proliferation and cell growth and one of the major energetic processes of the cell[142]. Ribogenesis occurs in the nucleoli of cells and starts with the transcription of the ribosomal DNA (rDNA) by RNA polymerase I (RNA Pol I) to synthesize the precursor rRNA (pre-rRNA), which is rapidly processed and assembled on pre-ribosomal particles[143–145]. Each rDNA gene produces a 47S rRNA transcript that contains one copy of the 18S, 5.8S and 28S rRNAs, separated by the internal transcribed spacers 1 (ITS1) and 2 (ITS2), and flanked by the 5' and 3' external transcribed spacers (5'ETS and 3'ETS)[143–145]. The gene encoding 5S rRNA is transcribed by RNA polymerase III (Pol III) in the nucleus and imported to the nucleolus[143–145]. The nascent primary transcripts associate with ribosomal proteins (RPs), pre-ribosomal

factors and small nucleolar ribonucleoprotein particles (snoRNPs)[143–145], which together enable rRNA processing. Finally, the ribosomal subunits are assembled and exported to the cytoplasm; the small 40S subunit contains the 18S rRNA and 33 RPs, and its main function is to bind and scan mRNAs[143–145], whereas the large 60S subunit comprises the 5S, 5.8S and 28S rRNAs, associated with 47 RPs, and is responsible for peptide bond formation and quality control of nascent peptides[143–145]. Together they compose the mature 80S ribosome **(Figure *1.6*)**.

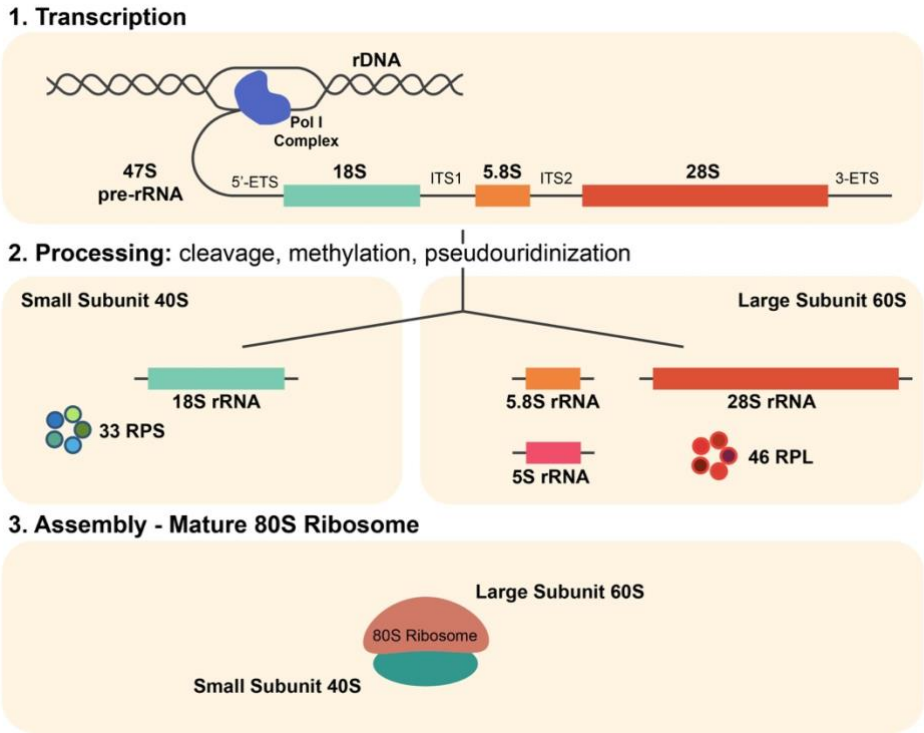

Figure 1.6 Schematic representation of ribosome biogenesis. Ribosome biogenesis starts with the **(1)** transcription of the rDNA genes by the RNA Pol I complex into the 47S pre-rRNA. Then, **(2)** the 47S pre-rRNA is processed through cleavage, methylations, and pseudouridinization to yield the 18S, 5.8S, and 28S rRNAs. The processed fragments are packed with other ribosomal proteins into the small subunit (40S) composed of 18S rRNA and 33 RPS, and the large subunit (60S) composed of the 5.8S, 28S and 5S rRNAs, the latter being transcribed by Pol III in the nucleus, and 46 RPLs. **(3)** Both subunits are then assembled into the 80S ribosome and exported to the cytoplasm[146–148].

HEATR1's best known orthologue is yeast U3 small nucleolar RNA-associated protein 10 (UTP10), originally identified as a protein required for the processing of 18S rRNA precursors, acting in association with other nucleolar proteins in a protein complex termed small subunit processome[149]. UTP10 also plays a role in pre-rRNA transcription

together with other UTPs, which lead to their classification as transcription-UTP (t-UTP) proteins[149,150]. Similarly, HEATR1's zebrafish orthologue, bap28, has been shown to be required for transcription of rDNA and processing of the 18S and 28S rRNAs[151]. Its knockout was shown to induce cell apoptosis in early nervous system development, a phenotype that was recovered by overexpressing the tumour suppressor p53[151]. While I was conducting my studies, a report using human osteosarcoma cells further showed that HEATR1 regulated p53-dependent cell cycle arrest through the impaired ribosome biogenesis checkpoint (IRBC), a mechanism related to the nucleolar stress response[152]. Additionally, very recently, in human non-small lung cancer cell lines, HEATR1 was shown to regulate cell death through the p53/PUMA pathway, affecting mouse xenograft growth[153]. Interestingly, while to date there are no reports on *dHEATR1,* it was identified in a genome-wide RNAi screen aiming at identifying regulators of NSC proliferation as leading to reduced divisions[154].

Of particular note, HEATR1 has been reported to be overexpressed in GBMs in one study, in agreement with the preliminary data obtained by our team, and in the A2B5^{+} population of a GBM cell line, a marker for immature glial-committed progenitors[155]. The same authors show that HEATR1 peptides can induce functional cytotoxic T lymphocytes response in glioma patient samples[155]. In contrast, HEATR1 was reported to be down-regulated in pancreatic cancer by two independent groups, and to correlate with poor prognosis[156,157]. In these studies, *HEATR1* knockdown was shown to enhance xenograft tumour growth, as well as increased resistance to gemcitabine chemotherapy in pancreatic cell lines through the negative regulation of Akt, which is a central node in the regulation of cell proliferation, survival, angiogenesis and glucose metabolism, through the phosphorylation of substrates[156]. Mechanistically, it was proposed that HEATR1 acts as a scaffold to facilitate the interaction between Akt and Protein Phosphatase 2A (PP2A), thereby promoting Akt dephosphorylation and consequent inactivation[156]. In addition, HEATR1 is also thought to increases resistance through regulating nuclear factor erythroid 2-related factor 2 (Nrf2) signalling, which is involved in electrophilic and oxidative stress protection through regulating expression of

cytoprotective and antioxidant genes[157]. In normal conditions, HEATR1 was shown to bind p61 competing with Kelch-like ECH-associated protein 1 (Keap1), which is bound to Nrf2 in the cytoplasm, where it is degraded by E3 ubiquitin-proteasome maintaining Nrf2 levels low. In pancreatic cells, the absence of HEATR1 leads to the binding of p61 with Keap1, which in turn is released from Nrf2 causing it to accumulate in the nucleus, where it promotes transcription of downstream genes, contributing to gentamicine resistance[157].

To summarize, in the recent years several groups have made efforts to elucidate the functions of HEATR1 in both normal development and health, and in some cancer types, implicating it to some extent in varied processes such as ribogenesis and cell survival. Yet, a role for HEATR1 in NSC lineages and brain tumour initiation or growth remains currently unknown.

1.6 Hypothesis and objectives of proposed PhD study

The hypothesis underlying my proposed PhD project is that *dHEATR1*, identified in a transcriptome analysis performed in our laboratory as upregulated in *Drosophila brat* brain tumour initiating cells versus control counterparts, plays a role in brain tumour initiation and development, and that this role may be conserved in GBM cells contributing to tumourigenesis in humans. The main objectives of the studies are:

1. Characterise the expression of HEATR1 in GBM cancer stem cells and further its analysis using GBM tissues.
2. Elucidate the function and mechanism of action of dHEATR1/ HEATR1 in brain tumour initiation and growth *in vivo* using *Drosophila* as a model, and *in vitro* using GBM cell lines and patient-derived GSCs.

2.1 dHEATR1 is required for brain tumour growth *in vivo*

As detailed in the Introduction, *dHEATR1* was found upregulated in brain tumour initiating INPs from the *brat* brain tumour model versus control INPs in a single cell transcriptome analysis performed in our laboratory, and the result was confirmed by RT-qPCR (Diaz *et al., in preparation*). To begin examining the function of dHEATR1 in brain tumour development, the *Drosophila* UAS/GAL4 genetic binary system[91] was used to knock down *dHEATR1* and/or *brat* specifically in type II NSC lineages, by crossing the corresponding *UAS-RNAi* fly lines[126,154] with a *pointed-GAL4* (*pnt-G4*) driver line[158]. Simultaneous expression of *UAS-mCD8-GFP*[159] outlined cell membranes of all type II NSC lineage cells.

Overproliferation of transformed INPs acting as brain tumour initiating cells is one of the main characteristics of *brat* brain tumours, thus, it was the first parameter to be analysed. Larval brains of control (*pntG4>mcd8GFP*), *dHEATR1* knockdown (*pntG4>mcd8GFP,dHEATR1-RNAi*), *brat* knockdown (*pntG4>mcd8GFP,brat-RNAi*) and *dHEATR1,brat* double knockdown (*pntG4>mcd8GFP,dHEATR1-RNAi;brat-RNAi*) were dissected at 48 and 93 hours post hatching (HPH, second and third instar larval stages) and immunostained with antibodies against the mitotic marker phospho-histone H3 (PH3), Dpn, a basic transcriptional repressor expressed by all self-renewing cells, and GFP to delineate cell membranes in the type II NSC lineages. Divisions were measured by scoring $GFP^+/PH3^+/Dpn^+$ cells within the type II NSC lineages in all genotypes. At 48 HPH, there is an average of 10 $GFP^+/PH3^+/Dpn^+$ cells per brain lobe proliferating in control brains **(Figure *2.1* A, I)** and *dHEATR1* knockdown in this background does not have a significant effect **(Figure *2.1* B, I)**. In the *brat* tumour model, however, overproliferation is evident with an average of 25 $GFP^+/PH3^+$/Dpn cells found **(Figure *2.1* C, I)**. Strikingly, *dHEATR1* knockdown in this tumour background prevents to some extent the overproliferation of the brain tumour cells, and levels of divisions are closer to those in found in control brains **(Figure *2.1* D, I)**. At 93 HPH, the last stage before larval

pupation, *dHEATR1* knockdown in control brains induces a strong reduction in proliferation, from an average of 20 in controls to 10 $GFP^+/PH3^+/Dpn^+$ cells per brain lobe in *dHEATR1-RNAi* brains **(Figure *2.1* E, F, J)**. At this late developmental stage, there is a major cell overproliferation in *brat-RNAi* brains, around 800 $GFP^+/PH3^+/Dpn^+$ cells per brain lobe, which leads to the characteristic aberrantly overgrown brain lobes of the *brat* model[98,99,101] **(Figure *2.1* G, J).** Knockdown of *dHEATR1* in *brat-RNAi* brains prevents this proliferation, with approximately half the number of dividing cells per brain lobe detected, and a resulting comparatively reduced size tumour **(Figure *2.1* H, J)**. This assay (93 HPH) was initially performed and scored by Joao Marques, a former member of our team, and was repeated and confirmed by my findings depicted on **Figure *2.1* E-H**. Collectively, the above assays show that *dHEATR1* knockdown can inhibit the growth of brain tumours in *brat* deficient *Drosophila* larval brains, suggesting an important role of the protein in tumour development.

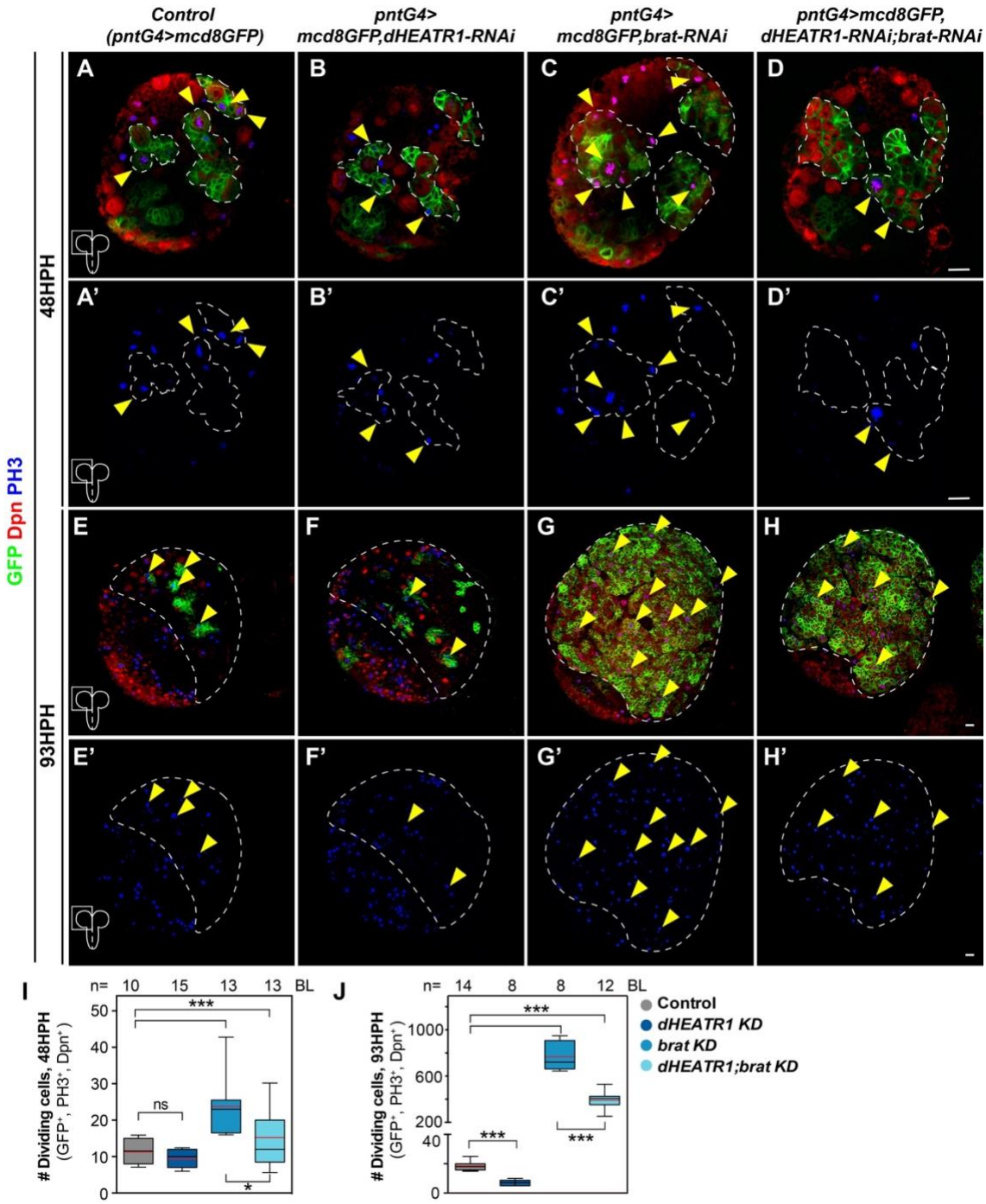

Figure 2.1 *dHEATR1* knockdown inhibits the proliferation of *brat* brain tumour cells. Larval brain lobes from **(A, A', E, E')** control (*pntG4>mcd8GFP*), **(B, B', F, F')** *dHEATR1* knockdown (*pntG4>mcd8GFP,dHEATR1-RNAi*), **(C, C', G, G')** *brat* knockdown (*pntG4> mcd8GFP,brat-RNAi),* and **(D, D', H, H')** *dHEATR1, brat* double knockdown (*pntG4> mcd8GFP,dHEATR1*-RNAi*;brat*-RNAi) at specified developmental stages, immunostained for GFP (type II NSC lineages, green), Deadpan (Dpn, red) and Phospho-Histone H3 (PH3, blue). **(I)** 48 HPH (Student's t-test used for all comparisons except for control vs *brat* knockdown, in which Mann-Whitney was used; ***p<0.001; *p<0.05; p≥0.05, ns: non-significant) and **(J)** 93 HPH quantification of proliferating cells (GFP^+, Dpn^+, $PH3^+$) shows a strong decrease upon *dHEATR1* downregulation in the *brat* background. A decrease is also observed at the later developmental stage in a control background. N numbers (Brain lobes, BL, analysed) indicated in figure. Median

is represented by a black line and mean by a red line (Student's t-test; ***p<0.001). Yellow arrowheads indicate proliferating cells. Dotted lines delineate type II lineages (48 HPH) and central brain region (93 HPH). Anterior is up. Scale bar, 10μm.

2.2 dHEATR1 does not affect cell death of *brat* brain tumour cells

To determine whether the reduced *brat* tumour size observed upon *dHEATR1* inhibition may also result from increased cell death, I performed a TUNEL assay at 93 HPH to detect apoptotic cells in type II NSC lineages of the previously described phenotypes. A minor number of GFP^+/$TUNEL^+$ cells could be observed in the central brain region of control brain lobes, which was not affected by *dHEATR1* knockdown **(Figure 2.2 A, B, E)**. Interestingly, in *brat-RNAi* brains there is a significant increase in the total number of apoptotic cells compared to controls, which is reduced when *dHEATR1* is knocked down simultaneously **(Figure 2.2 C, D, E)**. However, when the number of $TUNEL^+$ cells was measured per area in the bulk of the tumour, knockdown of *dHEATR1* shows no effect **(Figure 2.2 F)**, implying that the tumour size reduction caused by *dHEATR1* loss is not due to increased apoptosis.

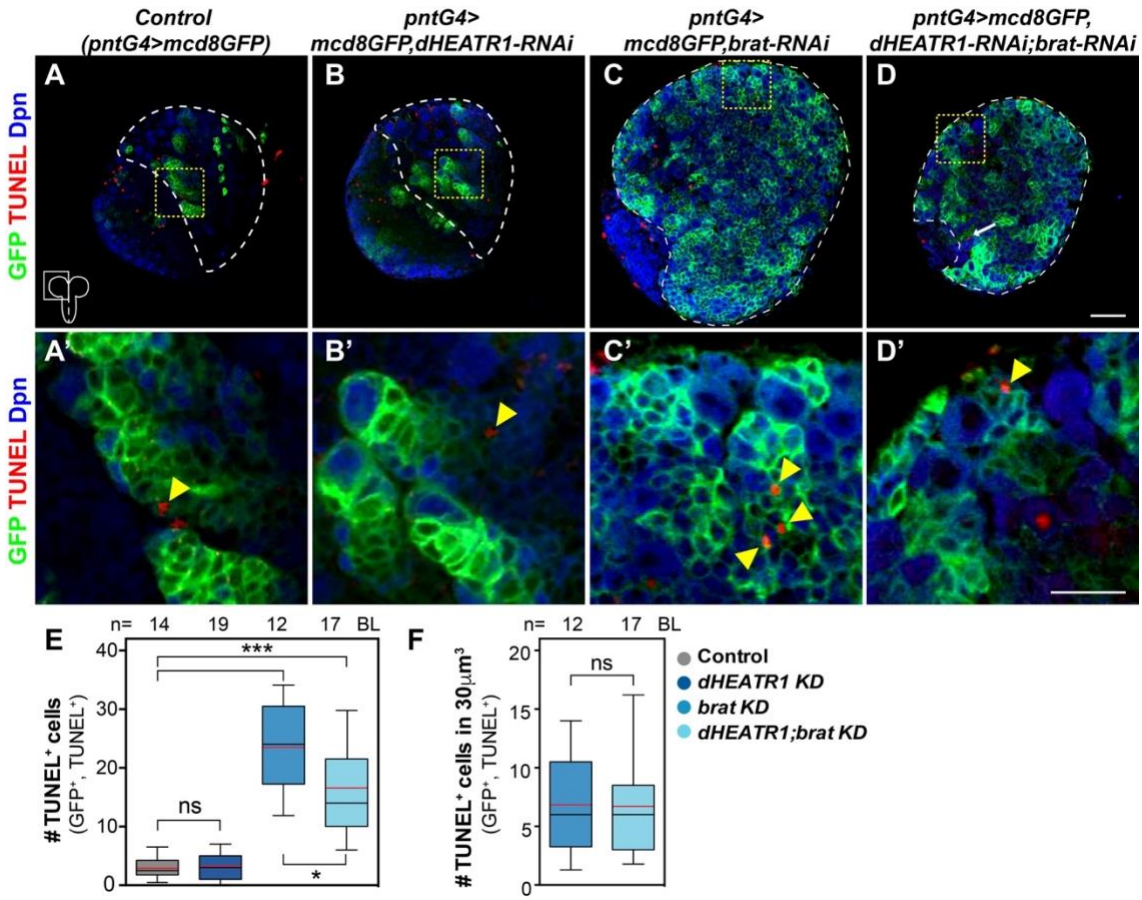

Figure 2.2 *dHEATR1* knockdown does not affect cell death in control or *brat* brains. Larval brain lobes at 93 HPH from **(A)** control (*pntG4>mcd8GFP*), **(B)** *dHEATR1* knockdown (*pntG4>mcd8GFP,dHEATR1-RNAi*), **(C)** *brat* knockdown (*pntG4>mcd8GFP,brat-RNAi*), and **(D)** d*HEATR1*, *brat* double knockdown (*pntG4>mcd8GFP,dHEATR1-RNAi;brat-RNAi*) immunostained for GFP (type II NSC lineages, green), TUNEL (cell death; red) and Dpn (blue). Scale bar 50μm. **(A'-D')** Insets depicting magnified area marked by yellow dotted squares. Scale bar, 15μm **(E)** Quantification of the number of TUNEL$^+$ cells within type II NSC lineages (GFP$^+$) shows a decrease upon *dHEATR1* knockdown in the *brat* background. Student's t-test used for all comparisons. **(F)** Number of TUNEL$^+$ cells in 30 μm^3 in *brat* and *dHEATR1*-RNAi;*brat*-RNAi shows no difference in cell death. Mann-Whitney test. N numbers (Brain lobes, BL, analysed) indicated in figure. Median is represented by a black line and mean by a red line. ***p<0.001; *p<0.05; p≥0.05, ns: non-significant. Yellow arrowheads indicate TUNEL$^+$ cells. Dotted lines delineate central brain region. Anterior is up.

2.3 dHEATR1 is required for *brat* tumour initiating cells proliferation and growth

To investigate the role of *dHEATR1* in brain tumour initiation, brains were dissected at 24 HPH; the developmental time point when transformation of *brat* INPs into brain tumour initiation cells is already observed, but the characteristic overproliferation has not

yet started[6,98,99,101]. Three key characteristics were analysed: proliferation, transformation, and size growth of brain tumour initiating cells.

Proliferating cells were measured by scoring GFP$^{+/}$Ph3^{+}/Dpn^{+} cells in all type II NSC lineages. At this stage, only an average of two dividing cells per brain lobe in control larvae were detected **(Figure 2.3 A, E)**. Proliferation was not affected by knockdown of either *dHEATR1* or *brat* independently **(Figure 2.3 B, C, E)**, as expected for the latter[99]. Interestingly, simultaneous knockdown of *dHEATR1* and *brat* reduces cell proliferation by half **(Figure 2.3 D, E)**. This suggests that downregulation of *dHEATR1* in the tumour background triggers a delay in the proliferation of brain tumour initiating INPs, slowing down the formation of the brain tumour.

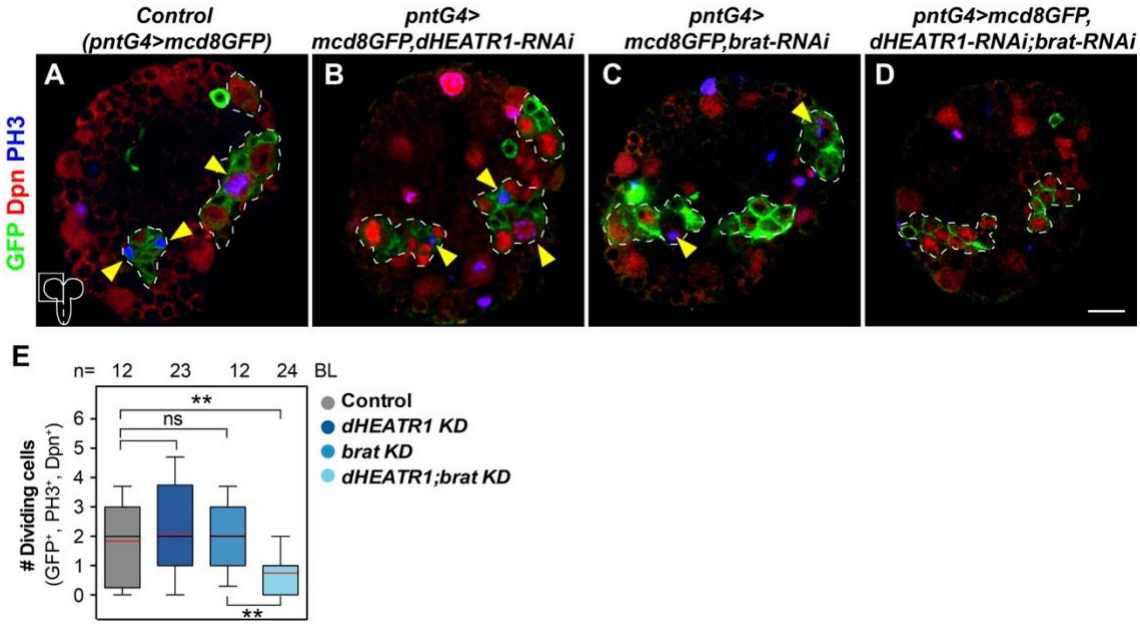

Figure 2.3 *dHEATR1* knockdown impairs proliferation of *brat* brain tumour initiation cells. Brain lobes from **(A)** control (*pntG4>mcd8GFP*), **(B)** *dHEATR1* knockdown (*pntG4>mcd8GFP,dHEATR1-RNAi*), **(C)** *brat* knockdown (*pntG4>mcd8GFP,brat-RNAi*), and **(D)** d*HEATR1*, *brat* double knockdown (*pntG4>mcd8GFP,dHEATR1-RNAi;brat-RNAi*) at 24 HPH immunostained with GFP (type II NSC lineages, green), Dpn (red) and PH3 (blue). **(E)** Quantification of proliferating cells shows a reduction upon *dHEATR1* knockdown in the *brat* background. N numbers indicated in figure. Median is represented by a black line and mean by a red line (Student's t-test used for all comparisons; $^{**}p<0.01$; $p\geq0.05$, ns: non-significant). Yellow arrowheads indicate proliferating cells. Dotted lines delineate type II NSC lineages. Anterior is up. Scale bar, 10μm.

To analyse effects on type II NSC lineage cell fate, immunostainings were performed against Dpn, expressed by NSCs and mature INPs, and Ase, a transcription factor expressed by mature INPs and GMCs[93]. The number of total type II NSC lineage cells and each cell type per brain lobe were scored: Type II NSCs (Dpn^+/Ase^-), *brat* INP tumour initiating cells (Dpn^+/Ase^-), iINPs (immature INPs; Dpn^-/Ase^-) and INPs (Ase^+ or Dpn^+/Ase^+).

In control brains, all Type II NSCs express Dpn but not Ase (Dpn^+, Ase^-) while iINPs show no Dpn or Ase expression (Dpn^-/Ase^-). Upon maturation, INPs turn on Ase followed by Dpn expression (Ase^+/Dpn^+) and resume asymmetric cell division generating more INPs, and GMCs which are Ase positive but Dpn negative[6,98,100] **(Figure *2.4* A)**. At 24 HPH, I consistently found approximately 80 type II NSC lineage cells per brain lobe, of which 8 are NSCs, around 18 are iINPs and 22 are INPs **(Figure *2.4* E)**. Upon *brat* knockdown, iINPs fail to initiate Ase expression and start expressing Dpn, reverting to NSC-like cells, but at this early stage, the total number of cells remains the same, as previously reported, and consistently with the proliferation results[99] **(Figure *2.4* C, E)**. Knockdown of *dHEATR1* alone has no effect at this stage in type II NSC lineage cell numbers or marker expression **(Figure *2.4* B, E)**. However, simultaneous knockdown of *brat* and *dHEATR1* leads to a significantly lower total number of cells (around 60) compared to the other genotypes, matching my earlier result **(Figure 2.3)**, and all cells are NSC-like Dpn^+ cells **(Figure *2.4* D, E)**. Thus, dHEATR1 does not affect the transformation of normal iINPs into tumour initiating cells but it is necessary for their proliferation.

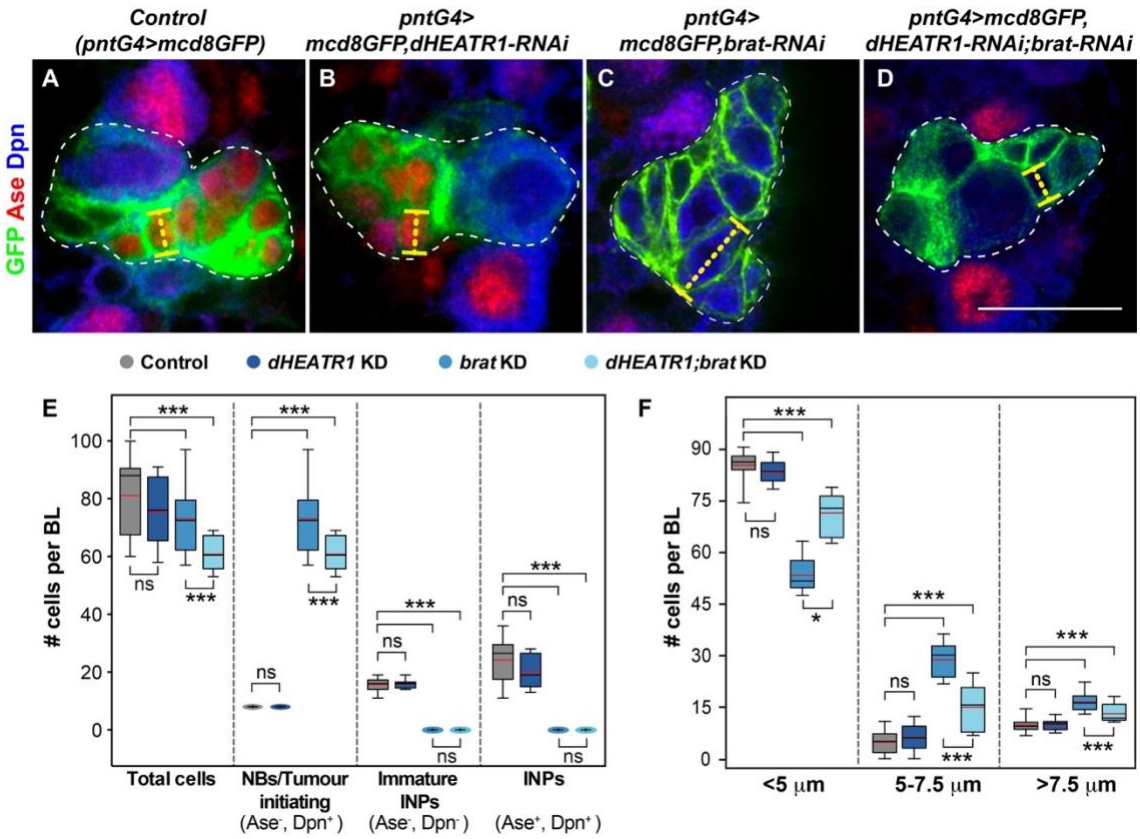

Figure 2.4 *dHEATR1* loss does not affect transformation of iINP into tumour initiating cells but it impairs their proliferation and cell size growth. Type II NSC lineages from **(A)** control (*pntG4>mcd8GFP*), **(B)** *dHEATR1* knockdown (*pntG4>mcd8GFP,dHEATR1-RNAi*), **(C)** *brat* knockdown (*pntG4>mcd8GFP,brat-RNAi),* and **(D)** dHEATR1*, brat* double knockdown (*pntG4>mcd8GFP,dHEATR1-RNAi;brat-RNAi*) brains at 24 HPH, immunostained with antibodies against GFP (type II NSC lineages, green), Ase (red) and Dpn (blue). NSC: Neural Stem Cell, iINP: immature Intermediate Neural Progenitor, INP: Intermediate Neural Progenitor. **(E)** Quantification of the different cell types and **(F)** cell size, measured as maximum diameter of each cell (yellow line) (control n=10, *dHEATR1*-RNAi n=10, *brat*-RNAi n=10, *dHEATR1-RNAi; brat*-RNAi n=10 brain lobes). Median is represented by a black line and average by a red line. Student's t-test used for all comparisons; ***p<0.001; **p<0.01; p>0.05, ns: non-significant. Scale bar, 10μm.

Enlarged nucleus and cytoplasm are common characteristics of tumour cells[160]. Similarly, it is known that tumorous cells in the *brat* model (*brat* INPs) are larger than control INP cells[119]. To analyse if dHEATR1 has an effect on size of *brat* tumour initiating cells, Z-stacks comprising the whole type II NSC lineages in brain lobes of control, *brat* knockdown, *dHEATR1* knockdown and *dHEATR1, brat* double knockdown were obtained at 24 HPH. At this stage, the average reported maximum diameter in control

brains of NSCs is approximately 7-8μm whereas INPs are around 4-6μm[161,162]. To examine cell size, the maximum diameter of each cell in the lineage was measured[162,163] and the results were grouped in three categories: cells smaller than 5μm, cells between 5 and 7.5μm and cells bigger than 7.5μm **(Figure *2.4* F)**. The comparison between the percentage of cells that fall in each category revealed that *HEATR1* depletion alone has no effect in cell size distribution compared to controls at this stage. In *brat-RNAi* brains, an increase in the percentage of cells between 5 and 7.5μm and bigger than 7.5μm is observed compared to any other genotype, at the expenses of the smaller cells, as expected[6,164]. Interestingly, *dHEATR1* knockdown in the *brat* tumour background results in an increase in the percentage of cells smaller than 5μm and decrease of those bigger than 5μm, indicating that inhibition of *dHEATR1* impairs the growth of *brat* tumour cells **(Figure *2.4* F)**. I concluded that *HEATR1* is necessary for the enlargement of *brat* brain tumour initiating cells.

So far, these assays have shown that dHEATR1 is not required for the malignant transformation of iINPs into tumour initiating cells, but it is necessary for their enlargement and proliferation. Additionally, dHEATR1 is not involved in cell death.

2.4 HEATR1 is overexpressed in glioma

Human HEATR1 has been previously linked in one publication to brain tumours, specifically GBM, in which it was shown to be overexpressed[155]. The transcriptome screen performed in our team revealed its fly orthologue, *dHEATR1,* to be also overexpressed in *brat* tumour initiating cells compared to controls, a result validated by previous members of the team by quantitative RT-qPCR (Diaz *et al., in preparation*). To begin the translation of these findings into human based systems, an initial analysis of HEATR1 expression performed in our laboratory also confirmed its upregulation in nine human GBM samples compared to three controls from non-tumourous brain samples. In order to expand this dataset and compare HEATR1 expression in high- and low-grade gliomas, I additionally examined protein lysates for five other GBM samples (samples

IDs: 65, 68, 70, 71 and 73), five grade II diffuse astrocytomas (DA) (IDs 55, 56, 57, 61 and 63), and three control (IDs 78, 79, 77) brain tissue samples, provided by the Brain UK biobank (Licence 14/004) via Derriford Plymouth Hospital (Plymouth, UK). Western blot analysis shows that HEATR1 is overexpressed in GBMs compared to grade II DA and to control non-tumorous brain, corroborating and strengthening the previous findings in our group and literature. HEATR1 seems also to be overexpressed in DA compared to controls **(Figure 2.5)**.

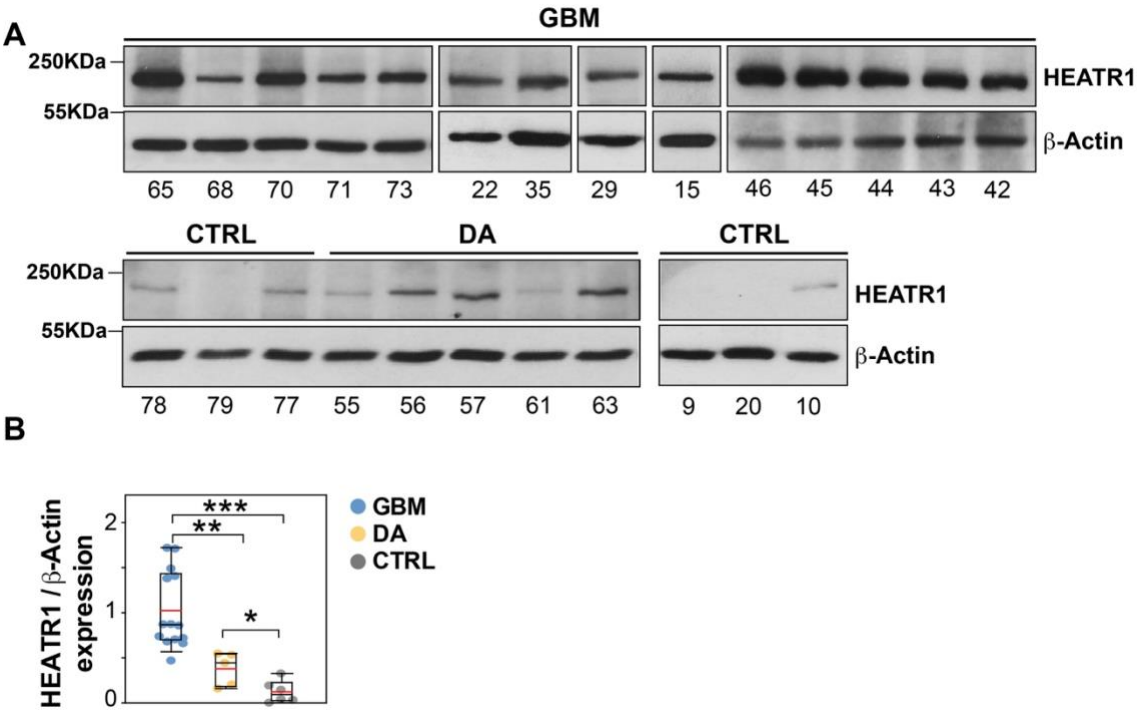

Figure 2.5 HEATR1 is overexpressed in human GBMs compared to DAs and control brains. (A) Western blots showing HEATR1 expression in 14 GBMs, 5 DA and 6 controls. GBM: glioblastoma multiforme, DA: diffuse astrocytoma. **(B)** Quantification of HEATR1 normalised against β-Actin levels functioning as loading control. The graph was made using the following numbers of samples; N_{GBM}=14, N_{DA}=5, N_{CTRL}=6. Student's t-test used for all comparisons, **p<0.01; *p<0.05; p>0.05, ns: non-significant.

2.5 HEATR1 is overexpressed in GBM cell lines and can be efficiently knocked down

In order to investigate the role of HEATR1 in a human-based system, I have used different *in vitro* models. Two immortalised GBM cell lines, U87MG and U251MG, and two different patient-derived GBM stem cells (GSCs), GSC-5 and GSC-8[83]. The latter, were derived from GBM specimens and initially characterized by Dr. Gil-Ranedo[83], a

postdoctoral fellow currently in Dr. Barros laboratory. Briefly, both cell lines grow exponentially forming neurospheres in cell culture media supplemented with EGF and FGF-2 and express different neural stem cell markers like CD133, Nestin and Sox2 in 70-90% of cultured cells[83]. They effectively initiate tumours that recapitulate the cellular heterogeneity present in the parental GBM upon orthotopic xenografts in immunocompromised mice, and are able to differentiate into neurons, astrocytes and oligodendrocytes[83]. In order to establish these cultures in the laboratory, some of these characteristics were replicated. As shown in **Figure 2.6 A**, GSC-5 cells grow forming free floating neurospheres when cultured in the appropriate medium and, as expected, can be differentiated into the three neural lineages, as demonstrated by the Olig-2 (oligodendrocytes), GFAP (astrocytes) and β-III-Tubulin (neurons) immunostainings **(Figure 2.6 B)**, providing a valuable model to study tumour initiation and stem cell potential *in vitro.*

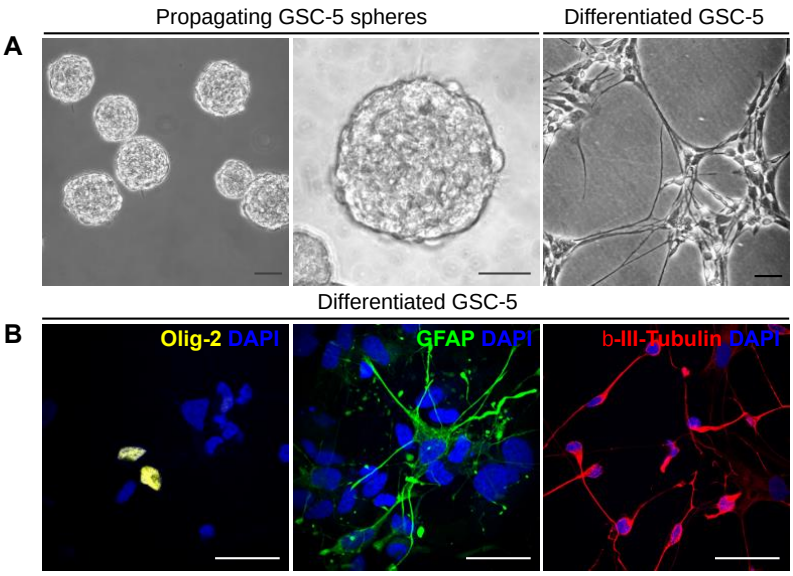

Figure 2.6 Establishment of the patient-derived GBM derived GSCs. (A) Propagating free floating neurospheres versus differentiated GSC-5 line (transmitted light). **(B)** Differentiated GSC-5 express glia markers as shown by the immunostainings against Olig-2 (oligodendrocytes, yellow) and GFAP (astrocytes, green), and the neuronal marker β-III-Tubulin (red). Nuclei are counterstained with DAPI (blue). Scale bar 50μm.

Previous experiments demonstrate that HEATR1 is overexpressed in U87MG and U251MG cells compared to control brain tissues (Diaz *et al.*, *in preparation*). As

dHEATR1 is overexpressed in *Drosophila brat* INP tumour initiating cells, I hypothesised that HEATR1 is likely to also be overexpressed in human GSCs. I compared HEATR1 expression in the patient-derived line GSC-5, to a human foetal NSC line obtained from the Glioma Cellular Genetic Resource (MRC Institute of Genetics and Molecular Medicine, The University of Edinburgh, Cancer Research, UK). The results show a relative increase in HEATR1 levels by 72.8% in GSC-5 **(Figure *2.7* A)**.

To study the role of HEATR1 using the above brain tumour cell lines, loss of function assays were performed using silencing RNA (siRNA) transfection and lentivirus-mediated *HEATR1* short hairpin RNA (shRNA) infections. *HEATR1* siRNA knocked down approximately 71.2% and 71.3% of the protein 48 hours post transfection (hpt) in U87MG and U251MG cells, respectively, compared to that of control cells transfected with *GFP* siRNA **(Figure *2.7* B)**. As GSCs were not easily transfected, and for experiments that required a long-term inhibition of the protein, I produced lentiviral particles containing five different *HEATR1* shRNA constructs that I named 22, 37, 50, 62, and 97 (for the last digits of their respective serial numbers, see Materials and Methods section) and an empty vector termed shControl. Preliminary tests performed 48 hours post infection (hpi) pointed at *shHEATR1* #22 and #97 as the most effective ones **(Figure *2.7* C)**, therefore, they were selected for further assays. After a longer infection period (168 hpi), *shHEATR1* #22 and #97 efficiently knocked down HEATR1 protein in U87MG, by 78.8% (#22) and 81.0% (#97), GSC-5, by 86.6% (#22) and 86.0% (#97), and GSC-8 by 87.4% (#22) and 88.2% (#97) **(Figure *2.7* D)**.

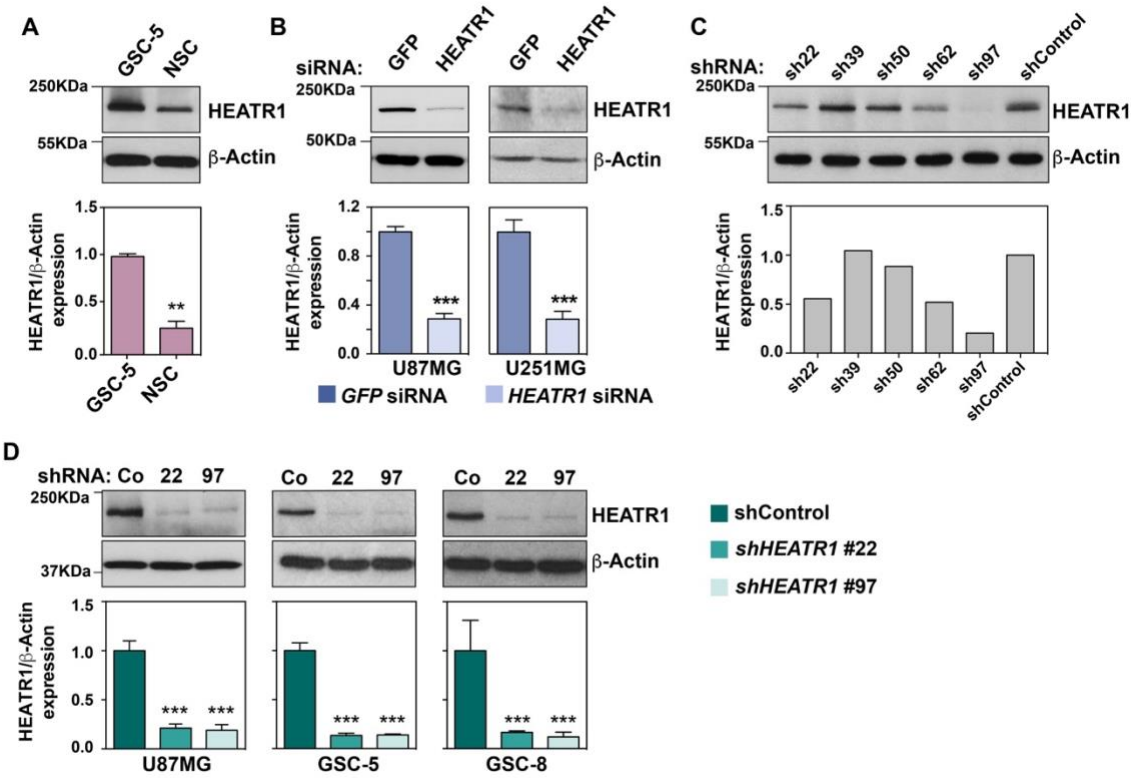

Figure 2.7 HEATR1 is overexpressed in GSCs and can be efficiently knocked down by siRNAs and shRNAs in GBM cell lines and GSCs. (A) Western blot showing upregulation of HEATR1 in GSC-5 compared to NSCs and respective quantification. **(B)** *HEATR1* siRNA knockdown compared to *GFP* siRNA control in U87MG and U251MG cells 48 hours post transfection. **(C)** *HEATR1* knockdown effect of *HEATR1* shRNAs 22, 39, 50, 62, and 97 compared to control shRNA in U87MG cells 48 hours post infection. **(D)** *HEATR1* knockdown by *shHEATR1* RNAs 22 and 97 in U87MG, GSC-5, and GSC-8 and respective quantifications (n=3, biological repeats, i.e., independent experiments) (Student's t-test used for all comparisons; ***$p<0.001$; **$p<0.01$).

2.6 HEATR1 promotes proliferation but not survival of immortalised GBM cells

To test whether HEATR1 has a significant role in the proliferation of GBM cells, *HEATR1* siRNA knockdown was performed in U87MG and U251MG cells. Cells were fixed and immunostained 48 hpt with the proliferation markers Ki67 and EdU. Ki67 labels the S, G_2 and M phase of the cell cycle, while a one-hour pulse of EdU labels specifically the S phase. Both markers show that depletion of HEATR1 leads to a decrease in proliferation in both cell lines by 16.5% (Ki68) and 8.4% (EdU) in U87MG **(Figure 2.8 A, B, E)** and by 24.8% (Ki67) and 19.3% (EdU) in U251MG **(Figure 2.8 C, D, F)**. The effect

is stronger when using Ki67, probably due to the broader specificity of the marker, capturing more cells in different stages of the cycle.

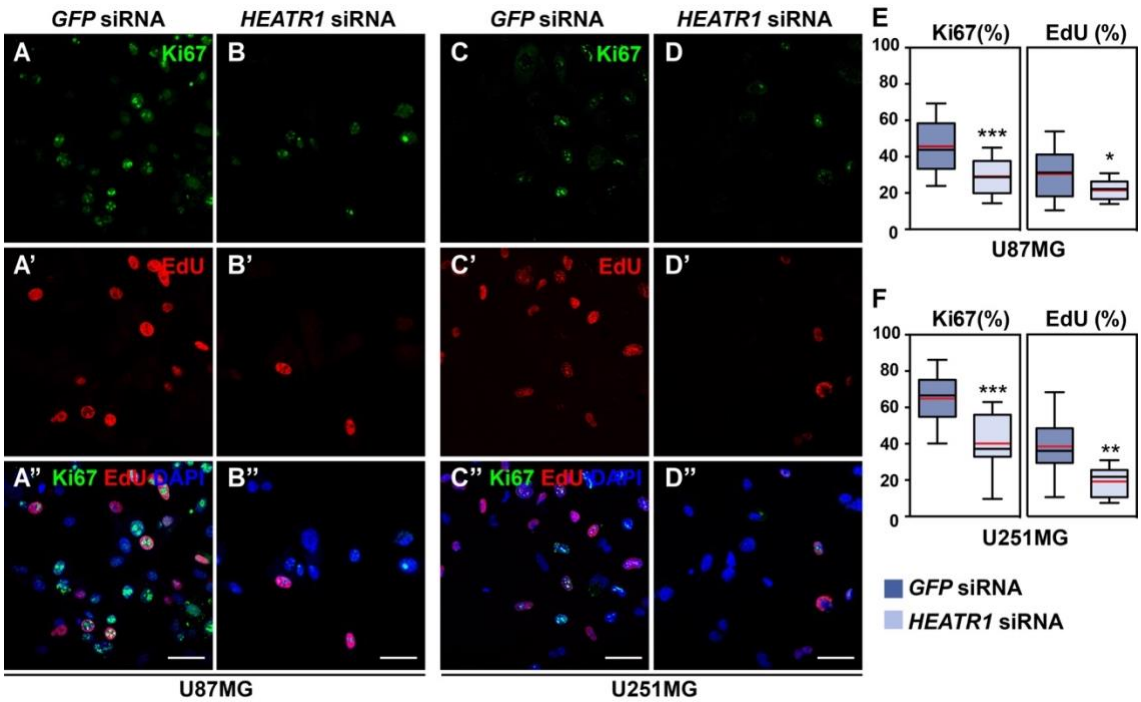

Figure 2.8 ***HEATR1* downregulation impairs proliferation of GBM cell lines. (A, B)** U87MG and **(C, D)** U251MG cells transfected with either *GFP* or *HEATR1* siRNAs and immunostained 48 hours post transfection against Ki67 (green), EdU (1 h pulse, red) and DAPI (nuclei; blue). **(E, F)** Quantification of the number of positive Ki67 and EdU positive cells normalised to total cell numbers identified by nuclei staining in both cell lines, showing that *HEATR1* knockdown reduces cell proliferation. Median is represented by a black line and mean by a red line. N=3, biological repeats, *i.e., independent experiments*. Student's t-test used for all comparisons; ***$p<0.001$; **$p<0.01$; *$p<0.05$; $p>0.05$, ns: non-significant. Scale bar 50μm.

To test whether HEATR1 also affects survival of GBM cells, a TUNEL assay was performed in both GBM cell lines to detect apoptotic cells, finding no significant difference between controls and *HEATR1* knocked-down cells, which is consistent with the *in vivo* results in *brat* model **(Figure 2.9 A-E)**. However, *HEATR1* knockdown has been reported to induce cell death during zebrafish development[151] and in two non-small lung cancer cell lines, where it increased cell death and was linked to the p53/BAX/PUMA apoptotic pathway[153]. It is worth noting that the increase in cell death reported is of approximately 5%[153]. To make sure HEATR1 was not affecting the same processes in our models, BCL2 associated X protein (BAX) apoptosis regulator and Caspase 3 (Casp3)

expression levels were evaluated in U87MG and GSC-5 upon *HEATR1* knockdown, but again, no difference could be observed between the conditions **(Figure 2.8 F-I)**. Together, these data indicate that HEATR1 promotes proliferation of GBM cells but does not affect cell death.

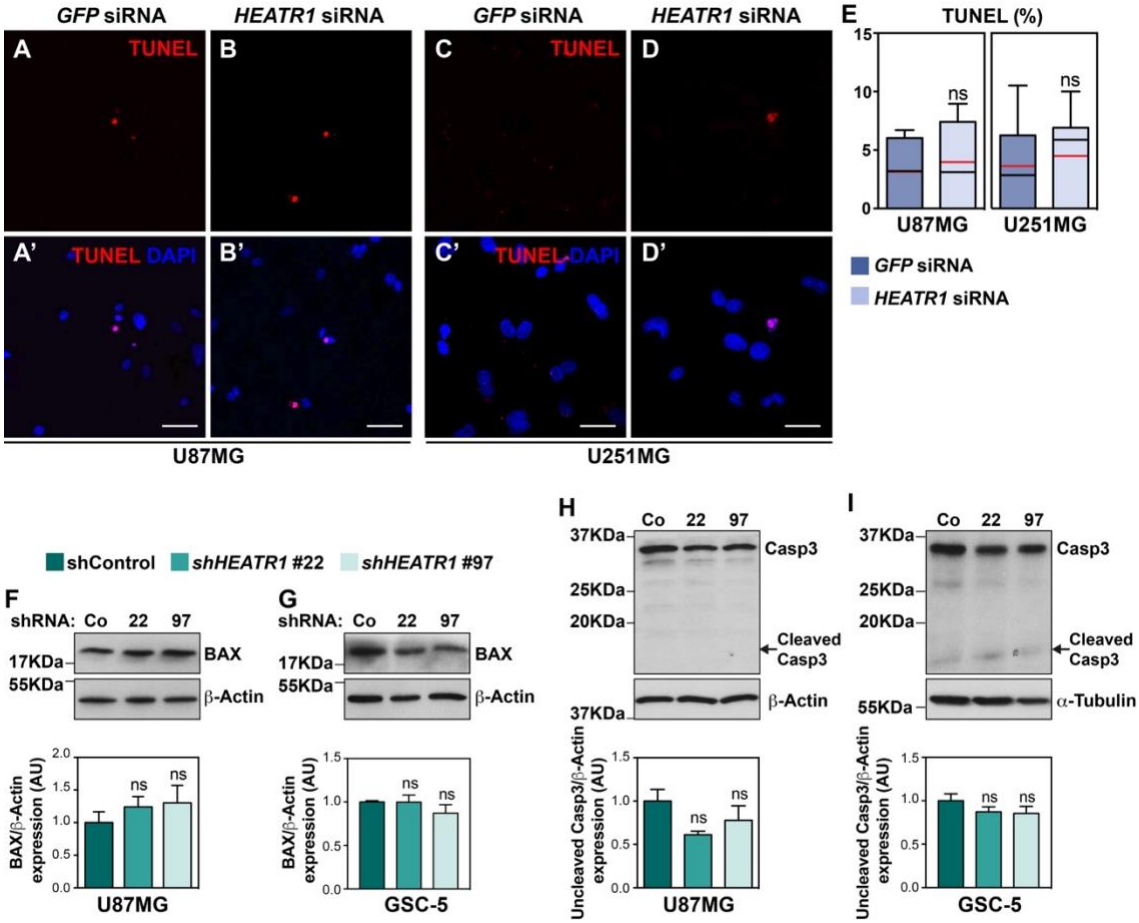

Figure 2.9 *HEATR1* knockdown does not affect cell death in GBM. (A, B) U87MG and **(C, D)** U251MG cells 48 hours post transfection with *GFP* and *HEATR1* siRNAs incubated with TUNEL assay (red) for 30 min to detect apoptotic cells. Nuclei are counterstained with DAPI (blue). **(E)** Quantification of TUNEL positive cells shows that HEATR1 does not affect cell death. Median is represented by a black line and mean by a red line. BAX, Casp3, and cleaved Casp3 expression levels are unaffected 168 hours post infection with sh*HEATR1* #22 and #97 in **(F, H)** U87MG and **(G, I)** GSC-5. N=3, biological repeats*, i.e., independent experiments*. (Student's t-test used for all comparisons; ***p<0.001; **p<0.01; *p<0.05; p>0.05, ns: non-significant). Scale bar 50μm.

2.7 HEATR1 is essential for the tumourigenic potential of GSCs

To examine if HEATR1 contributes to the tumourigenic potential of GSCs, I used the soft agar colony formation assay, to our knowledge, the most stringent assay to assess carcinogenesis *in vitro*[165]. This was done together with Dr. Jon Gil-Ranedo (C. Barros Laboratory) and the work was performed in parallel.

GSC-5 and GSC-8 lines were infected with *HEATR1* shRNA #22 and #97. Next, the cells were selected in puromycin containing NSC medium for a week, dissociated, and grown in a layer of soft agar mixed with cell culture media on top of a base layer containing a higher percentage of agar so they could not adhere to the culture plate (see Materials and Methods for details). Normal cells depend on cell to extracellular matrix contact to be able to grow and divide, while tumourigenic cells have the ability to do so more independently of their surrounding environment[165]. It has been shown that the GSC ability to grow in soft agar conditions correlates with their *in vivo* tumour potential, as it resembles their 3D environment and prevents spontaneous cell aggregation[165]. After seven days in NSC-agar medium, both cell lines show a striking reduction on their ability to form colonies, with this reduction being slightly more pronounced using the *shHEATR1* #22 **(Figure 2.10 A, B)**. As the level of *HEATR1* knockdown using both shRNAs is almost identical, a possible explanation for this difference is that it is related to off-target effects[166]. In addition, I measured the size of the colonies formed, showing that they are significantly smaller upon *HEATR1* knockdown compared to the control **(Figure 2.10 C, D)**.

Taken together, these findings suggest that HEATR1 is necessary to maintain the tumourigenic potential of GBM tumour initiating cells.

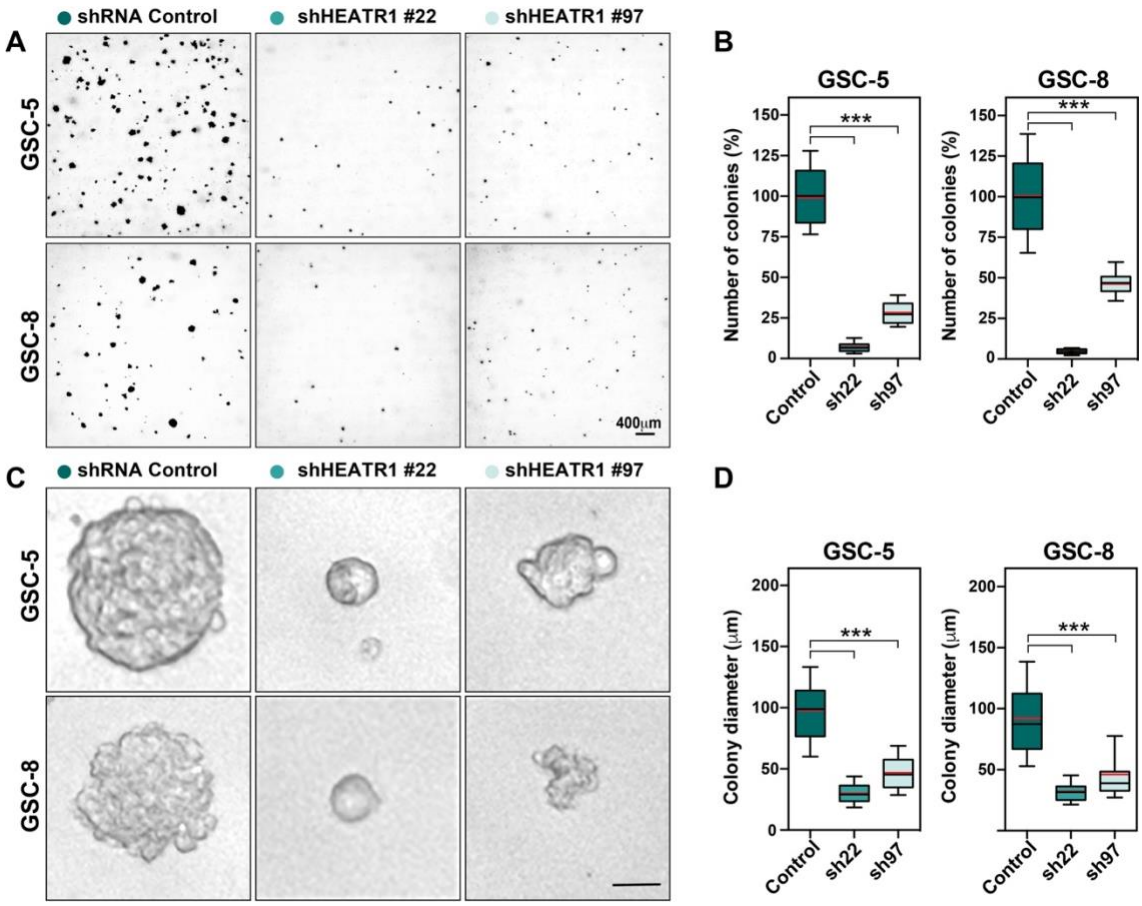

Figure 2.10 HEATR1 inhibition impairs GSC stemness potential. (A) Representative images of whole culture wells and **(B)** quantification of the number of colonies formed on soft agar assay showing a strong reduction upon *HEATR1* knockdown. **(C)** Single colonies growing in soft agar and **(D)** quantification of colony size showing a decrease upon *HEATR1* inhibition (n=3, independent assays). Median is represented by a black line and mean by a red line. Student's t-test used for all comparisons; ***p<0.001. Scale bar 50µm.

2.8 HEATR1 localises predominantly to the nucleolus of GBM cells

HEATR1 has been previously linked to rDNA transcription and pre-rRNA processing, events that take place in the nucleolus[149,151]. I first investigated the localization of HEATR1 in GSCs and GBM cell lines by performing a co-immunocytofluorescent (co-ICF) staining with antibodies against HEATR1 and the nucleolar protein Fibrillarin (FBL), a well-known nucleolar marker. In GSC-5, HEATR1 signal appears very strong in the nucleolus in most cells, overlapping to a large extent with FBL, and a weaker signal can be detected in the nucleoplasm and cytoplasm **(Figure *2.11* A)**. The nucleolar localization of HEATR1 is also observed in GBM cell lines, as shown for U87MG and U251MG,

where the highest intensity of the signal is also found overlapping with FBL, with signal also detected in the nucleoplasm and cytoplasm **(Figure *2.11* B, C)**. Immunohistochemistry staining against HEATR1 of formalin-fixed paraffin embedded (FFPE) tissue sections of control non-tumorous brain samples from white matter regions **(Figure *2.11* F)** grey matter regions **(Figure *2.11* G)**, DAs **(Figure *2.11* H)** and GBMs **(Figure *2.11* I)** was performed by Dr. Hilton's team in the Department of Cellular and Anatomical Pathology at University Hospitals Plymouth (UK). Consistent with the observation in GBM cells and GSCs, HEATR1 is predominantly detected in the nucleoli of both tumour types and controls. In control grey matter regions, enriched in neurons, HEATR1 staining is stronger due to the bigger size of neuronal nucleoli, whereas in control white matter regions, enriched in glia, HEATR1 signal is very weak **(Figure *2.11* F, G)**. Overall, the signal appears more intense in GBMs, consistently with the quantification of HEATR1 levels performed by WB analysis represented in **Figure 2.5**. These results show that HEATR1 is localised to nucleoli and may have a ribogenesis-related function in brain cancer cells.

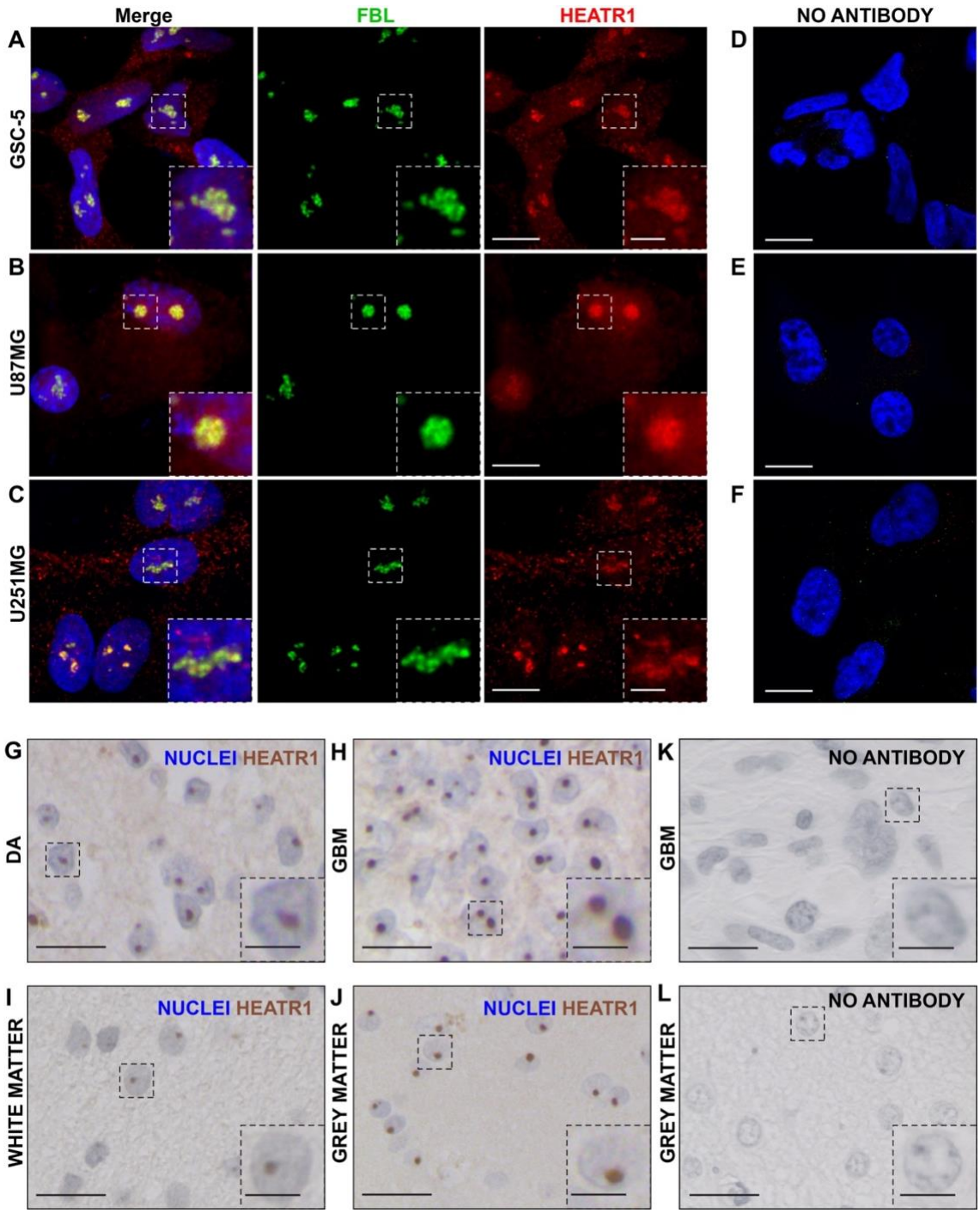

Figure 2.11 HEATR1 is mainly localised in the nucleolus. (A) GSC-5, **(B)** U87MG, and **(C)** U251MG cells labelled with antibodies against FBL (green) and HEATR1 (red), counterstained with DAPI (blue) and **(D-E)** secondary antibodies controls performed using the exact same specifications but omitting primary antibodies. Images D-F were kindly provided by N. Nsek, Barros laboratory. HEATR1 Immunohistochemistry in **(G)** DA, **(H)** GBM tissue **(I)** white matter and **(J)** grey matter from control brain. Negative controls using no primary antibody in **(K)** grey matter and **(L)** GBM tissue sections. Nuclei are counterstained with haematoxylin. Scale bar 10μm.

2.9 HEATR1 is required for ribosome biogenesis of GBM cell lines

The nucleolus is a dynamic organelle formed by three different structural and functional compartments; the fibrillar centre (FC), where rDNA transcription occurs, the dense fibrillar component (DFC), where rRNA processing takes place, and the granular component (GC), dedicated to late rRNA processing and pre-ribosomal particles assembly[143,148,167]. The reorganization and modification of these spatial structures are indicative of alteration in nucleolar function, and therefore, can be studied by labelling with specific markers[143,167].

HEATR1 has been linked to rDNA transcription and pre-rRNA processing[149,151], processes that take place in the FC and the DFC of the nucleolus respectively[148] However, HEATR1's role in ribosome biogenesis is not fully understood and it has not been studied in the context of brain tumours. We hypothesised that if HEATR1 is involved in ribogenesis, its knockdown will affect the expression and functional localization of the nucleolar compartments and the proteins involved in their function. I analysed the expression and distribution upon *HEATR1* knockdown of UBF, a nucleolar-specific HMG-box protein that binds extensively across the rDNA as part of the Pol I complex, and is involved in rDNA transcription[149]. Similar analysis was performed for FBL, which is involved in the early processing and modification of the pre-rRNA[168], as well as for Nucleophosmin (NPM), that is required for ribosomal nuclear export. These three proteins are markers of the different compartments of the nucleolus (FC, DFC and GC, respectively) and provide a readout of the three main steps in ribogenesis[143,167].

HEATR1 was inhibited in U87MG cells using siRNA transfection and shRNA transduction. Western blot analysis of the nucleolar proteins upon *HEATR1* knockdown revealed decreased levels of UBF **(Figure 2.12 A)**, which consists of two bands of similar molecular sizes, which are the translational products of two different mRNAs[169]. However, it does not affect FBL level **(Figure 2.12 B).** Knockdown of *HEATR1* via shRNA achieved similar results. At 168 hpi, reduced UBF expression was observed but no effect on FBL nor NPM total levels could be detected **(Figure 2.12 C, D)**.

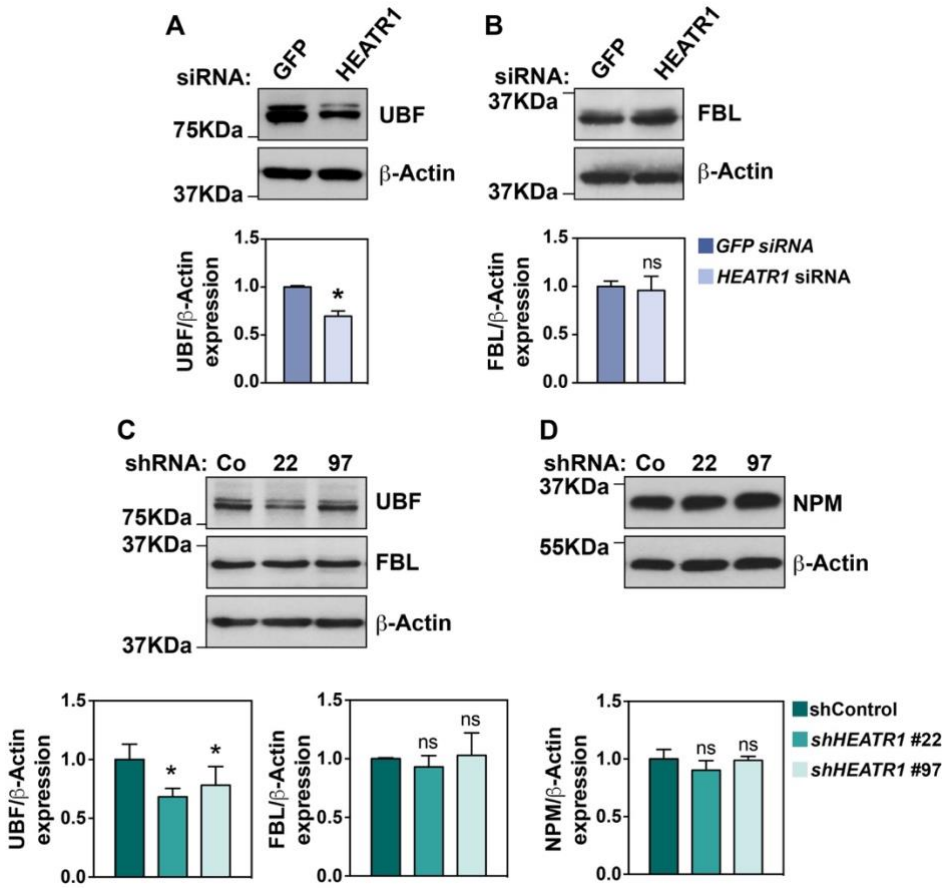

Figure 2.12 ***HEATR1* knockdown reduces UBF total expression levels but does not affect other nucleolar proteins in GBM U87MG cells.** Western blot showing effect of *HEATR1* knockdown using siRNAs 48 hpt on **(A)** UBF and **(B)** FBL, and respective densitometric quantifications of the bands**.** Western blots showing *HEATR1* knockdown effect using shRNAs 168 hpi on **(C)** UBF, FBL and **(D)** NPM and respective quantifications normalised to β-Actin acting as loading control. Error bars indicate SEM. Student's t-test used for all comparisons; n=3 biological repeats*, i.e., independent experiments*, ***p<0.001; *p<0.05; p>0.05, ns: non-significant.

Besides protein expression levels, the location and distribution of nucleolar proteins is essential for their appropriate functioning[143,167]. To further investigate ribosome biogenesis activity upon *HEATR1* knockdown, I performed ICF assays against UBF, FBL, and NPM, while inhibiting *HEATR1* via siRNAs and shRNAs. A significant decrease was observed in nucleolar FC and DFC area, labelled with UBF and FBL, respectively **(Figure 2.13 A-C, E-G, K)**, whereas GC area, labelled by NPM was only reduced by *shHEATR1* #22 **(Figure 2.13 H-J, M)**. Additionally, the pattern of these nucleolar proteins changed, becoming more dispersed in the centre and concentrating at the nucleolar

periphery in distinct but adjacent cap-like structures. These so-called “nucleolar caps” are recognized dynamic structures that consist of nucleolar proteins and rDNA, known to form under certain physiological conditions that induce transcription arrest[170,171]. Their formation is an energy-dependent process that has been suggested to serve as protection against rDNA damage[171]. UBF nucleolar cap-like structures can be found in 25.3% of the GBM cells in the control, whereas this number increases to 58.7% and 49.4% using *shHEATR1* #22 and #97, respectively. FBL nucleolar cap-like organization was found in 40.6% of the control GBM cells, and in 62.9% and 43.3% of the shHEATR1 #22 and #97 treated cells, respectively **(Figure 2.13 E-G, L)**. No nucleolar caps could be found in the case of NPM staining, although its localisation pattern appeared to also be mis-localised towards the periphery of nucleoli in 25.1% (#22) and 44.6% (#97) of the cells compared to 10.9% in the control **(Figure 2.13 H-J, N)**.

Taken together, these findings indicate a major dysfunction in all nucleolar processes when *HEATR1* is knocked down and suggest that HEATR1 has a role in all the steps of ribosome biogenesis in GBM cells.

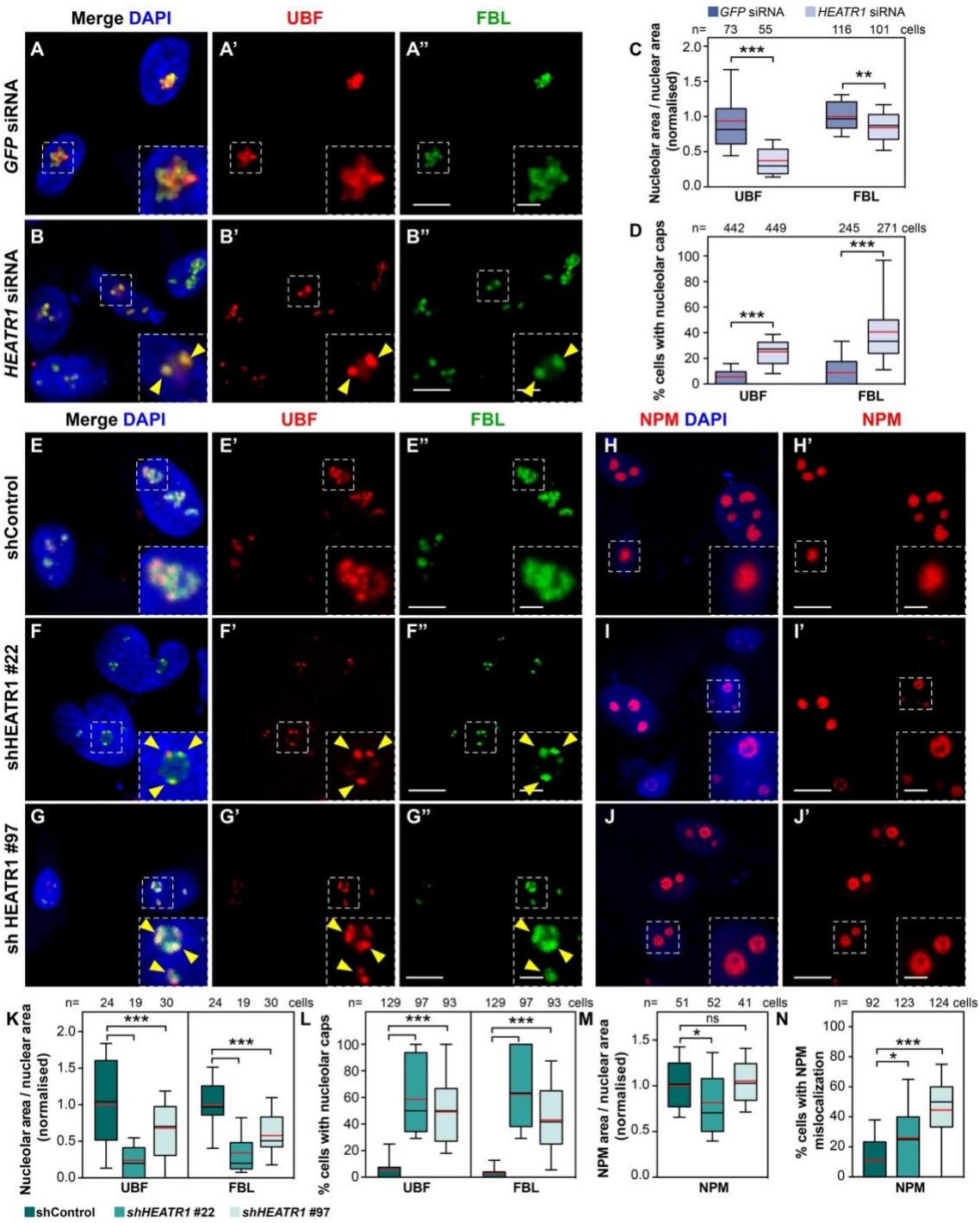

Figure 2.13 *HEATR1* knockdown disrupts nucleolar structure in GBM cell lines. U87MG cells transfected with **(A)** *GFP* siRNA as control and **(B)** *HEATR1* siRNA, immunostained with antibodies against UBF (red) and FBL (green) and nuclei labelled with DAPI (blue). **(C)** Ratio of nucleolar UBF or FBL area versus nuclear area shows a size reduction upon *HEATR1* knockdown. Mann-Whitney's test; ***p<0.001; **p<0.01. **(D)** Percentage of cells which have nucleolar UBF or FBL caps showing a strong increment after *HEATR1* knockdown. Mann-Whitney's test; ***p<0.001. U87MG cells infected with **(E-E'')** shControl and HEATR1 shRNAs **(F-F'')** #22 and **(G-G'')** #97, stained with UBF (red), FBL (green) and DAPI (blue). Nucleolar caps are indicated by yellow arrow heads. U87MG cells infected with **(H, H')** shControl and *HEATR1* shRNAs **(I, I')** #22 and **(J, J')** #97 stained with NPM (red) and DAPI (blue). **(K)** Ratio of nucleolar

UBF or FBL area versus nuclear area showing a reduction upon *HEATR1* loss. Mann-Whitney's test; ***p<0.001. **(L)** Percentage of cells which have UBF and FBL nucleolar caps showing an increase upon *HEATR1* downregulation. Mann-Whitney's test; ***p<0.001. **(M)** Ratio of nucleolar NPM area versus nuclear area showing a small reduction with #22. Mann-Whitney's test; *p<0.001; ns: non-significant. **(N)** Percentage of cells that have NPM mis-localization to the periphery showing an increase upon *HEATR1* downregulation. Student's t-test; ***p<0.001; *p<0.05. N=3, biological repeats*, i.e., independent experiments*. Median is represented by a black line and mean by a red line. Scale bar 10μm.

2.10 HEATR1 is necessary for RNA Polymerase I localisation in GBM cell lines

To provide further insight into the potential roles of HEATR1 in ribosome biogenesis, I analysed the expression of RPA194, the largest subunit of the RNA Polymerase I (RNA Pol I) complex, which catalyses the transcription of rDNA into rRNA[172,173]. In normal conditions, proteins associated with RNA Pol I co-localize in the FC[90].

RPA194 western blot revealed that total protein expression was not affected by *HEATR1* knockdown neither 48 hours after siRNA transfection **(Figure 2.14 A)**, nor seven days after shRNA transduction **(Figure 2.14 B)**. However, at the same timepoints, similarly to UBF, FBL, and NPM immunostainings for RPA194 in U87MG cells show that signal area was reduced by approximately 60% upon *HEATR1* knockdown and mis-localised into nucleolar caps in 34.3% (siRNA), 53.9% (sh22), and 65.6% (sh97) of cells **(Figure 2.14 C-K)**. These data suggest an impairment in RNA Pol I functioning dependent on HEATR1.

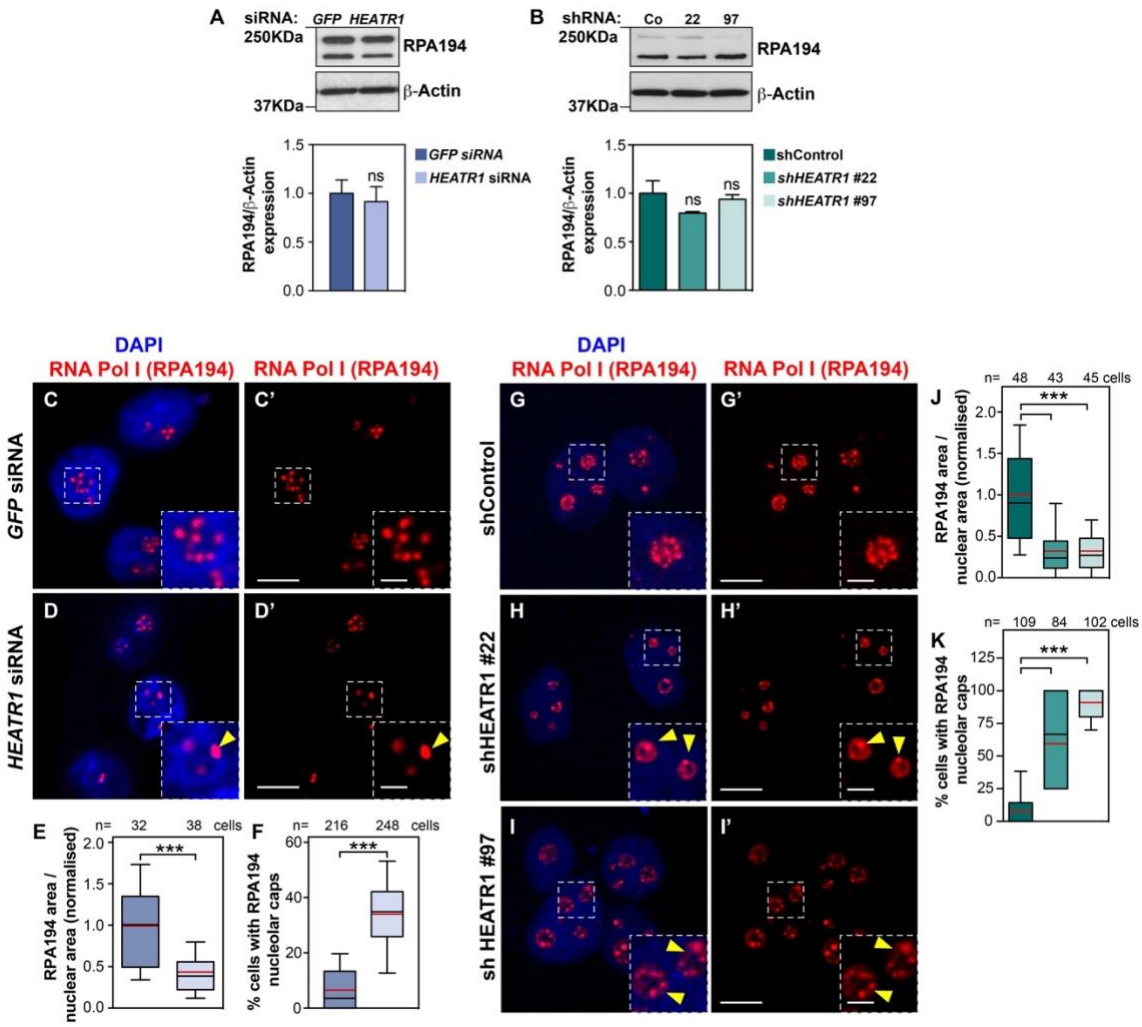

Figure 2.14 ***HEATR1*** **knockdown does not affect RNA Pol I total expression but it impairs its localisation. (A)** RPA194 (RNA Pol I) western blots and respective densitometric quantifications of U87MG cells transfected with *GFP* and *HEATR1* siRNAs or **(B)** transduced with shRNA control and *HEATR1* shRNAs #22 and #97 show no effect after *HEATR1* knockdown (n=3). Error bars indicate SEM. RPA194 (red) and DAPI (nuclei; blue) staining of U87MG cells transfected with **(C)** *GFP* and **(D)** *HEATR1* siRNAs reveals **(E)** a reduction in area, and **(F)** an increased number of cells presenting RPA194 nucleolar caps upon HEATR1 loss. Immunostaining with the same antibodies on U87MG cells infected with **(G)** shRNA control and *HEATR1* shRNAs **(H)** #22, and **(I)** #97 confirms the **(J)** reduction on area and **(K)** increase on number of caps. Yellow arrow heads indicate nucleolar caps. Median is represented by a black line and mean by a red line. Student's t-test used for all comparisons; ***p<0.001, ns: non-significant. N=3, biological repeats, *i.e., independent experiments*. Scale bar 10μm. Insets' scale bar 3μm.

2.11 HEATR1 is required for ribosome biogenesis in GSCs

To determine whether HEATR1 had a similar function as the described above in GSCs, *HEATR1* was knocked down in GSC-5 using shRNAs. Consistently with the

results obtained in U87MG cells, western blot analysis of *HEATR1* knockdown showed a depletion of UBF total expression in GSCs **(Figure 2.15 A)**. Yet, no effect could be seen on FBL **(Figure 2.15 B)**, NPM, which consists of two bands in these cells possibly due to alternative splicing isoforms **(Figure 2.15 C)**, or RPA194 **(Figure 2.15 D)** expression levels.

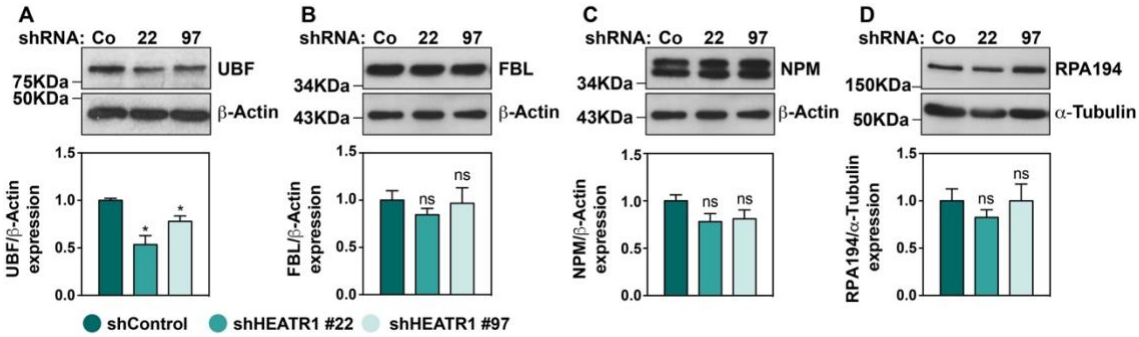

Figure 2.15 HEATR1 affects total expression levels of UBF but not of other nucleolar proteins in GSCs. Western blots showing effect of *HEATR1* knockdown in GSC-5 on **(A)** UBF, **(B)** FBL**, (C)** NPM and (**D**) RPA194. Error bars indicate SEM. Student's t-test used for all comparisons; n=3 biological repeats*, i.e., independent experiments*, *p<0.05; p>0.05, ns: non-significant.

Localisation analysis of the above mentioned proteins via ICF assays on GSCs cells, shows that similar to findings using U87MG cells, nucleolar areas labelled by UBF and FBL antibodies are extremely reduced upon *HEATR1* loss **(Figure 2.16 A-C, J)**. Additionally, UBF reorganises in nucleolar caps in 49.77% (#22) and 57.12% (#97) of *HEATR1*-depleted cells, compared to only 1.79% in the control. FBL nucleolar caps were found in 83.36% (#22) and 88.5% (#97) of *HEATR1* knockdown cells compared to 1.71% in controls **(Figure 2.16 A-C, K)**. Upon HEATR1 loss, NPM overall area is reduced only in cells transduced with the #22 shRNA **(Figure 2.16 D-F, L)** and no cells with NPM nucleolar caps can be found. However, the distribution of the NPM protein is also mis-localised towards the periphery, forming a ring-like shape in 63.4% (#22) and 83.0% (#97) of the cells compared to 11.6% in the control **(Figure 2.16 D-F, M)**.

Moreover, RPA194 (RNA Pol I) immunostaining analysis revealed similar defects to those observed in U87MG cells consequent to *HEATR1* knockdown: a strong reduction in RPA194 nucleolar area and a re-localization of the protein in nucleolar caps in 42.2%

(#22) and 40.0% (#97) of the cells compared to 7.6% in the control. This result indicates that RNA Pol I machinery is also affected in these cells and dependent on HEATR1 **(Figure 2.16 G-I, N, O)**.

Taken together, given that size and organisation of nucleolar compartments reflect their function[143,167], the above findings suggest a role for HEATR1 in ribosome biogenesis in U87MG cells and GSCs. Loss of HEATR1 may directly affect all main ribogenesis steps, i.e., rDNA transcription, rRNA processing, and assembly. Yet, it is also possible that its loss affects initial stages, and the subsequent steps as a consequence. Interestingly, HEATR1 in yeast and zebrafish has been implicated in more than one ribogenesis step; UTP10 in yeast has been shown to regulate rRNA transcription levels and processing[149], while BAP28 in zebrafish was reported to regulate rRNA processing[151].

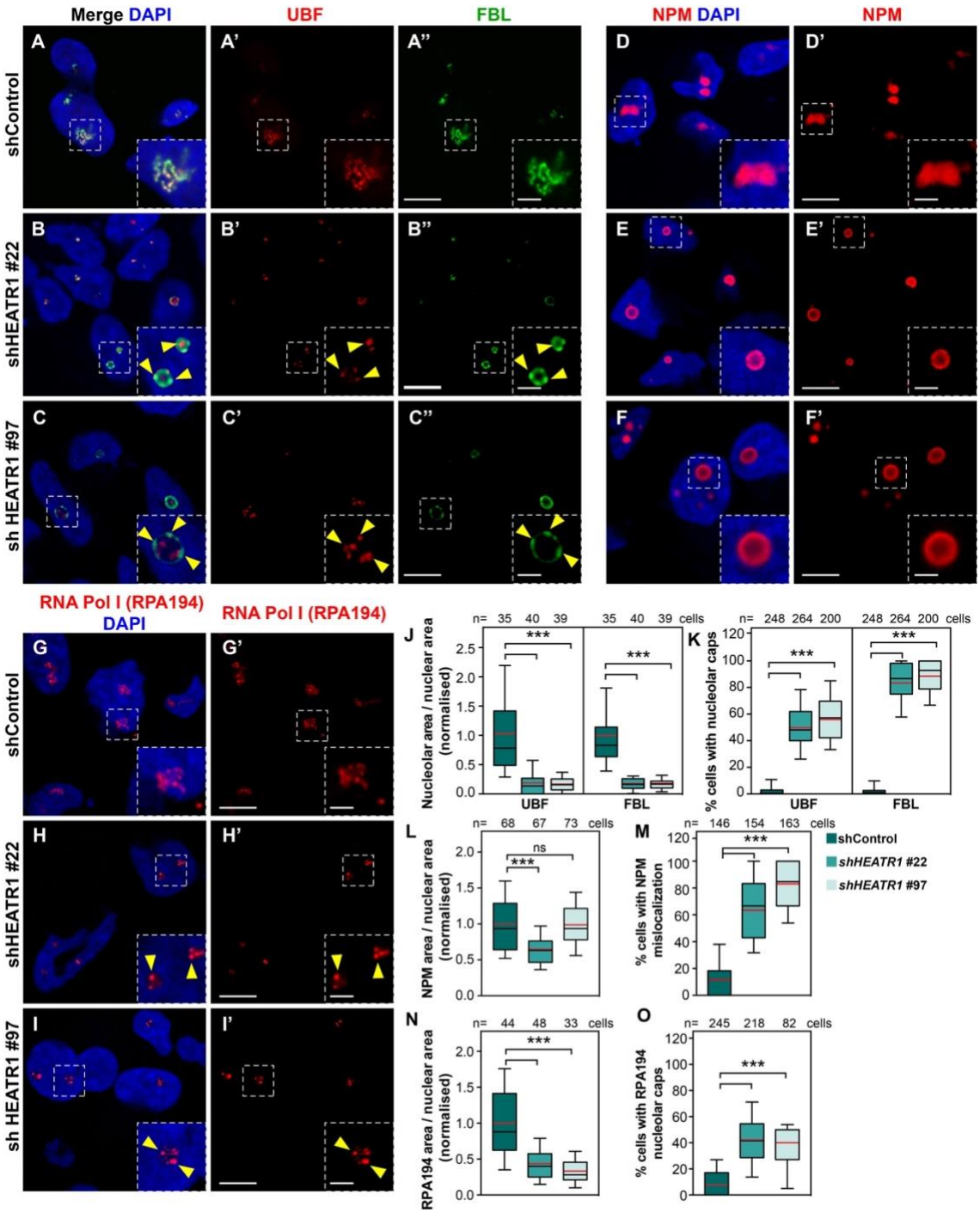

Figure 2.16 *HEATR1* knockdown disrupts nucleolar structure in GSCs. GSC-5 infected with shControl and *HEATR1* shRNAs, #22 and #97. **(A, B, C)** Immunostaining with antibodies against UBF (red) and FBL (green), and DAPI nuclei counterstain (blue). **(D, E, F)** Immunostaining with NPM (red) and DAPI (blue). **(G, H, I)** Immunostaining with RPA194 (red) and DAPI (blue)**.** **(J)** Ratio of nucleolar UBF or FBL area versus nuclear area shows a strong area reduction upon *HEATR1* knockdown. Mann-Whitney's test; ***p<0.001. **(K)** Quantification of the percentage of cells which have nucleolar UBF or FBL caps shows an increase upon *HEATR1* downregulation. Mann-Whitney's test; ***p<0.001. **(L)** Ratio of nucleolar NPM area versus nuclear area is reduced when knocking down *HEATR1* with #22. Mann-Whitney's test; ***p<0.001; ns: non-significant. **(M)** Percentage of cells that present NPM mis-localization to the periphery showing an increase

upon *HEATR1* downregulation. Mann-Whitney's test; ***p<0.001. **(N)** Ratio of nucleolar RPA194 area versus nuclear area is strongly decreased upon *HEATR1* knockdown. Mann-Whitney's test; ***p<0.001. **(O)** Quantification of the percentage of cells that present RPA194 nucleolar caps shows an increase upon HEATR1 loss. Student's t-test; ***p<0.001. N=3, biological repeats*, i.e., independent experiments*. Nucleolar caps are indicated by yellow arrow heads. Median is represented by a black line and mean by a red line. Scale bar 10μm.

2.12 dHEATR1 is required for enhanced ribosome biogenesis in brat tumour initiating cells

Drosophila NSCs are characterized by having larger nucleoli than their progeny due to a higher rate of ribosome biogenesis needed in these cells. In type II NSC lineages of *brat* mutants, however, all cells have enlarged nucleoli, probably on account of an increased metabolic activity of brain tumour cells[98].This enlargement can also be found in human cancer cells, which frequently present larger nucleoli[174]. *dHEATR1* is enriched in *brat* brain tumour initiating cells. As the data in GBM cell lines and GSCs indicates that HEATR1 is required for nucleolar organisation, I next tested whether it could also contribute to nucleolar size increase in *brat* tumour cells. *Drosophila* nucleoli do not display the characteristic vertebrate tripartite organisation[175], instead, only a homogeneous region with a regular surface can be observed, which can be measured using FBL[98].

Using FBL as a nucleolar marker, I analysed the size of nucleoli of cells in the type II NSC lineages of control, *dHEATR1* knockdown, *brat* knockdown, and *dHEATR1, brat* double knockdown. Nucleolar size was calculated as the ratio between the maximum diameters of nucleoli and respective whole cells, the latter marked with membrane tagged GFP. *dHEATR1* knockdown in a control background induces a small reduction in nucleolar size **(Figure *2.17* A, B, E)**. As previously described[98], in *brat* tumour initiating cells nucleoli are significantly bigger **(Figure *2.17* C, E)**. Interestingly, knockdown of *dHEATR1* in the *brat* background is able to rescue the phenotype, and reduced nucleolar sizes are observed, even smaller than those in controls **(Figure *2.17* D, E)**.

This finding mirrors the results obtained using GBM cells and GSCs, and suggest that dHEATR1 is also necessary for brain tumour ribosome biogenesis *in vivo* as seen in brain tumour initiating cells of the *brat* model.

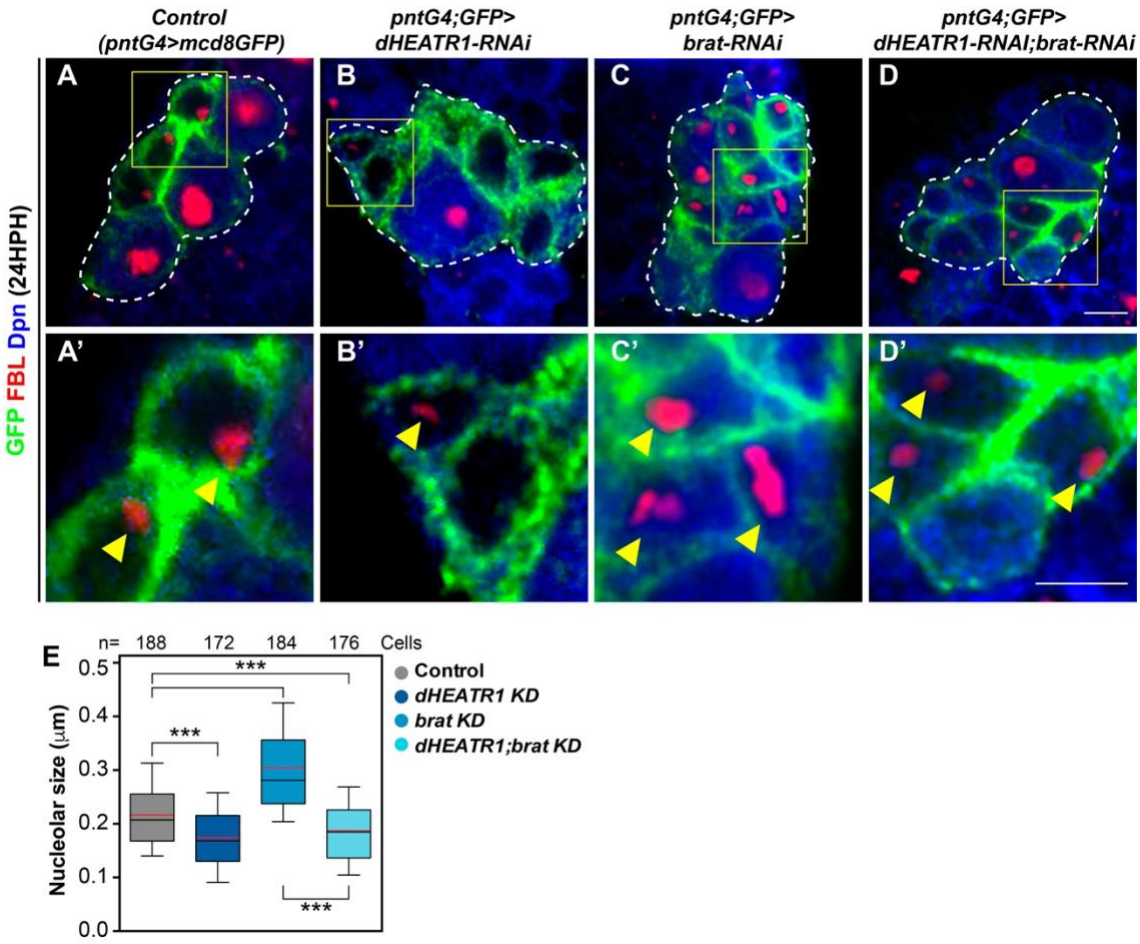

Figure 2.17 *dHEATR1* knockdown rescues nucleolar overgrowth of *brat* tumour initiating cells. Type II NSC lineages at 24HPH immunostained with antibodies against GFP (green), FBL (red) and Dpn (blue) from **(A)** control (pntG4>mcd8GFP), **(B)** dHEATR1 knockdown (pntG4>mcd8GFP,dHEATR1-RNAi), **(C)** brat knockdown (pntG4>mcd8GFP,brat-RNAi*),* and **(D)** *d*HEATR1*,* brat double knockdown (pntG4>mcd8GFP,dHEATR1-RNAi;brat-RNAi). **(A'-D')** Insets of yellow squares. Yellow arrowheads indicate nucleoli. **(E)** Quantification of the maximum diameter of nucleoli normalised to cellular maximum diameter, showing rescue of size in *dHEATR1;brat*-RNAi lineages. Number (n) of cells indicated in figure corresponds to 5 brain lobes in each condition. Median is represented by a black line and mean by a red line. Student's t-test used for control vs dHEATR1 knockdown comparison and Mann-Whitney for all other comparisons; ***p<0.001. Scale bar 5μm.

2.13 HEATR1 is required for rRNA synthesis and processing in GBM cell lines

The defects in nucleolar organization caused by *HEATR1* knockdown, suggest an impairment on rDNA transcription and processing, which are limiting steps in ribosome biogenesis[176].

To examine rRNA synthesis defects, I used two different strategies. First, as transcription from active rDNA loci into rRNA in the nucleoli constitutes the majority of cellular transcription[177], I measured incorporation of the nucleotide analogue 5-ethynyl uridine (EU) into nascent RNA after a one-hour pulse in the nucleus **(Figure 2.18 A, B)**. Second, RT-qPCR quantification of the *47S pre-rRNA* using primers against the 5' external transcribed spacer (ETS) end, which is spliced out upon its maturation and rapidly degraded[148,178] **(Figure 2.18 C, D)**. Both assays demonstrate that *HEATR1* depleted GBM cells display downregulation of rRNA transcription.

After rDNA transcription, the *47S pre-rRNA* is rapidly subjected to cleavage and base modifications to yield the mature *18S, 5.8S* and *28S* rRNAs[143–145] **(Figure 2.18 C)**. To determine whether HEATR1 is also involved in rRNA processing, I measured by qRT-PCR the abundance of the *18S, 5.8S* and *28S.* The results show a significant reduction in the levels of all of the subunits upon *HEATR1* inhibition **(Figure 2.18 E)**, indicating an impairment in the processing of the transcribed *47S pre-rRNA*.

I next evaluated the effect of *HEATR1* upregulation on levels of *47S pre-rRNA* using again primers against the *5'ETS* end. *HEATR1* is a large gene with a coding sequence of ~13000 base-pairs. Due to its size, despite multiple strategies attempted, I was unable to successfully transfect its full-length cDNA into U87MG cells, a technical issue previously reported by Fang et al[179]. However, when using the more transfection-permissive human embryonic kidney 293T cells, *HEATR1* overexpression was readily obtained with approximately 9.5 fold change increase detected. Nevertheless, *HEATR1* overexpression did not trigger an effect in the expression of *47S pre-rRNA* **(Figure 2.18 F)**. However, this result must be carefully interpreted, as due to lack of time, the knockdown of HEATR1 was not tested in 293T cells, and therefore, it cannot be assumed

that the same mechanism is in place. In the future, members of the lab will be performing these experiments to confidently publish these results.

Together these results indicate that HEATR1 is necessary for normal rRNA synthesis and processing in brain tumour cells. However, as shown by the described gain of function assays, it seems it is not sufficient to induce rDNA synthesis.

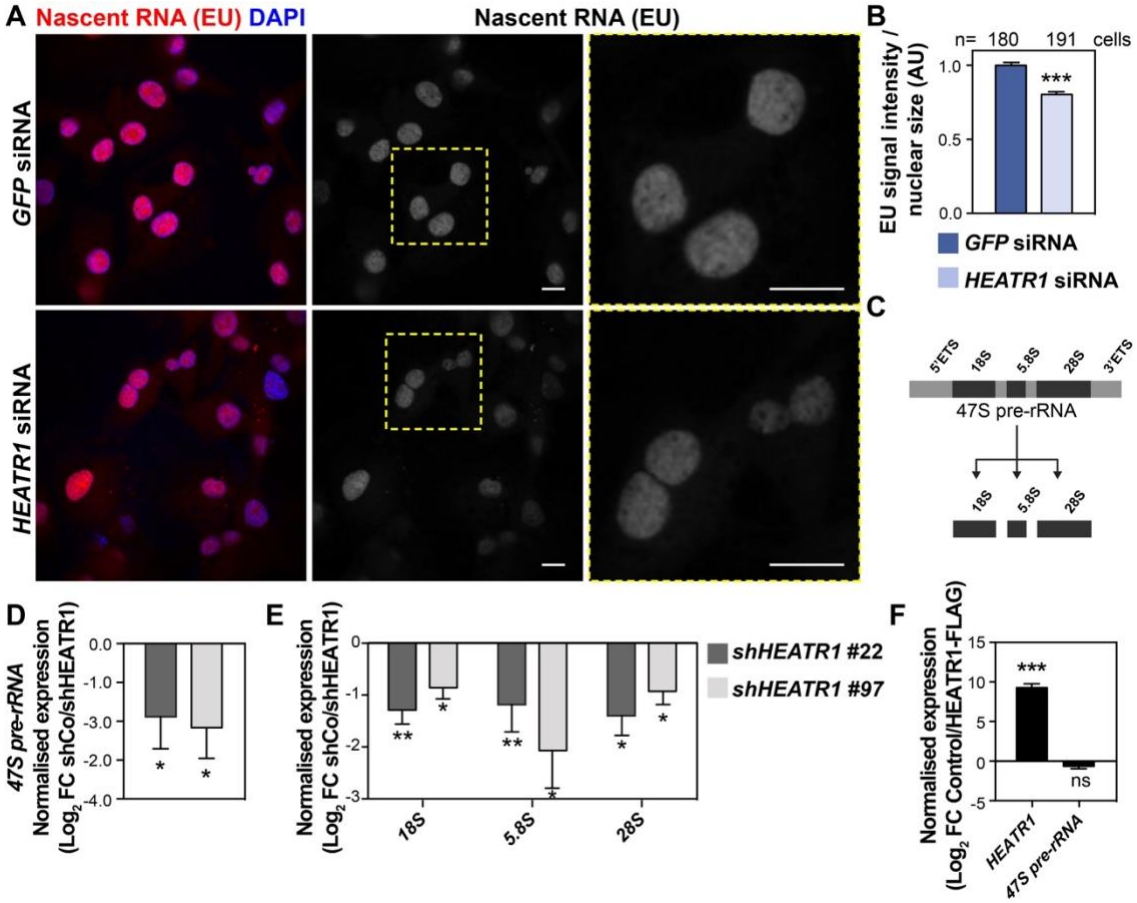

Figure 2.18 ***HEATR1*** **knockdown impairs rRNA synthesis and processing. (A)** Visualization of nascent RNA in U87MG cells transfected with *GFP* or *HEATR1* siRNAs following a 1h pulse of EU labelling (red and monochrome) and counterstained with DAPI to highlight nuclei (blue)**. (B)** Quantification of EU fluorescence intensity per nucleus area shows a reduction upon *HEATR1* knockdown. Number (N) of cells analysed are indicated on the figure, from 3 biological repeats*, i.e., independent experiments* **(C)** Diagram of *47S pre-rRNA* and respective rRNA products. **(D)** RT-qPCR showing fold change (Log_2FC) downregulation of *47S pre-rRNA* upon *HEATR1* knockdown in U87MG cells (n=3, biological repeats*, i.e., independent experiments*). **(E)** RT-qPCR showing effect of *HEATR1* knockdown on U87MG cells on 18S, 5.8S and 28S subunits arising from processing of *47S pre-rRNA* (n=3, biological repeats*, i.e., independent experiments*). **(F)** RT-qPCR showing upregulation of HEATR1 on 293T cells transfected with full length *HEATR1* FLAG tagged cDNA plasmid with no effect on *47S pre-rRNA* expression (n=3, biological repeats*, i.e., independent experiments*). Error bars indicate SEM. Student's t-test used for all comparisons; ***p<0.001; **p<0.01; *p<0.05; p>0.05, ns: non-significant. Scale bar 10μm.

2.14 HEATR1 is required for protein synthesis in GBM cell lines

rRNA synthesis is a limiting step for ribosome biogenesis and subsequent protein synthesis and cell growth[148]. As defects in ribogenesis were observed in *HEATR1* deficient tumour cells, I next examined if this could be reflected in their overall protein synthesis capacity. I incubated U87MG and U251MG GBM cells for one hour with a puromycin analogue (OP-Puro Kit) to label nascent proteins and measure the intensity of the fluorescent signal in every image, normalising it to the number of cells. This analysis revealed a reduction in protein synthesis of approximately 20% in U87MG **(Figure *2.19* A-C)** and 60% in U251MG cells **(Figure *2.19* D-F)** after 48 hours of *HEATR1* knockdown. The stronger effect observed in U251MG highlights the differences with U87MG and may be related to the GBMs from which they were derived, that may have had different characteristics. Nevertheless, ribogenesis defects triggered by *HEATR1* knockdown lead to reduced protein synthesis in both human GBM cell lines.

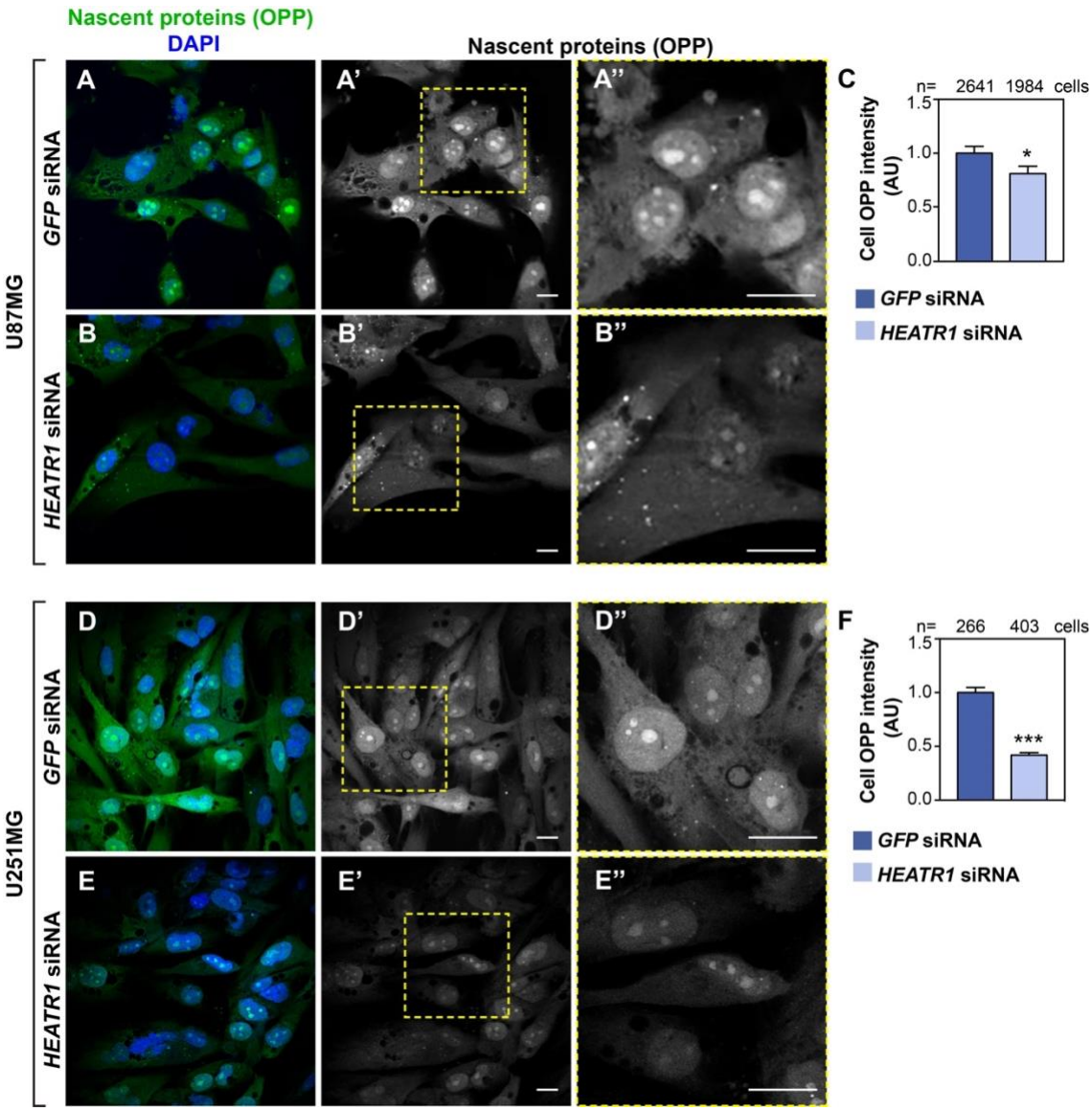

Figure 2.19 *HEATR1* knockdown impairs protein synthesis in human GBM cell lines. U87MG cells transfected with **(A)** *GFP* or **(B)** *HEATR1* siRNA, incubated for 1 hour with OPP (green, monochrome) and counterstained with DAPI (blue). **(C)** Quantification of the intensity of OPP signal in U87MG cells showing a decrease upon *HEATR1* knockdown. Mann Whitney's test; **p*<0.05. U251MG cells transfected with **(D)** *GFP* or **(E)** *HEATR1* siRNA incubated for 1 hour with OPP (green/monochrome) and counterstained with DAPI (blue). **(F)** Quantification of OPP signal intensity in U251MG cells shows a decrease upon *HEATR1* knockdown. Student's t-test; ****p*<0.001. N numbers indicated in the graphs represent number of cells from three biological repeats, i.e., independent experiments. Error bars represent SEM. Scale bar 10μm.

2.15 HEATR1 inhibition does not affect p53 levels in GBM cells and GSCs

The data so far indicates that HEATR1 has an important role in the regulation of brain tumour cell ribosome biogenesis, growth and proliferation. I next sought to examine in more depth the molecular mechanism underlying this function.

Previous studies conducted in an osteosarcoma cell line have reported that *HEATR1* loss or downregulation results in the upregulation and stabilization of the tumour suppressor p53, suggesting that HEATR1 suppresses p53 action[152]. Further, the authors show that suppression of p53 is able to rescue cell cycle arrest following *HEATR1* knockdown[152]. Similarly, *bap28* (HEATR1's orthologue) knockdown in zebrafish resulted in increased apoptosis, which was rescued upon *p53* knockdown[151], and another study reported that *HEATR1* knockdown lead to the activation of the p53/PUMA apoptotic pathway in non-small cell lung carcinoma[153]. Although as previously mentioned I did not detect an effect on cell death, I explored the possible effect of *HEATR1* knockdown in p53 expression. Western blot analysis demonstrates that transfection of U87MG cells with *HEATR1* siRNA at 48 hpt does not affect p53 levels **(Figure 2.20A)**. I also repeated the assay at 72 hpt, the timepoint when p53 upregulation was reported by Turi *et al*. in osteosarcoma cells subjected to *HEATR1* siRNA knockdown[152], yet no effect on p53 expression was observed **(Figure 2.20 B)**. Interestingly, in U251MG cells that are known to have a mutation in codon 273 of the *p53* gene[180], which has no transcriptional activity, p53 expression is strongly reduced at 48 hpt upon *HEATR1* siRNA knockdown. However, as this p53 is not functional it was not explored any further **(Figure 2.20 C)**. As inhibition of HEATR1 was more severe when using shRNAs, I have also used this approach. Transduction in GBM cell lines at 168 hpi shows also no significant differences in total p53 protein levels **(Figure 2.20 D)**. Finally, *HEATR1* was also knocked-down using shRNAs in GSC-5 showing no effect in p53 **(Figure 2.20 E)**.

Taken together, these findings indicate that in GBM cell lines and GSCs HEATR1 seems not to affect p53, and must be implicated in a different mechanism contributing to ribosome biogenesis and cell proliferation.

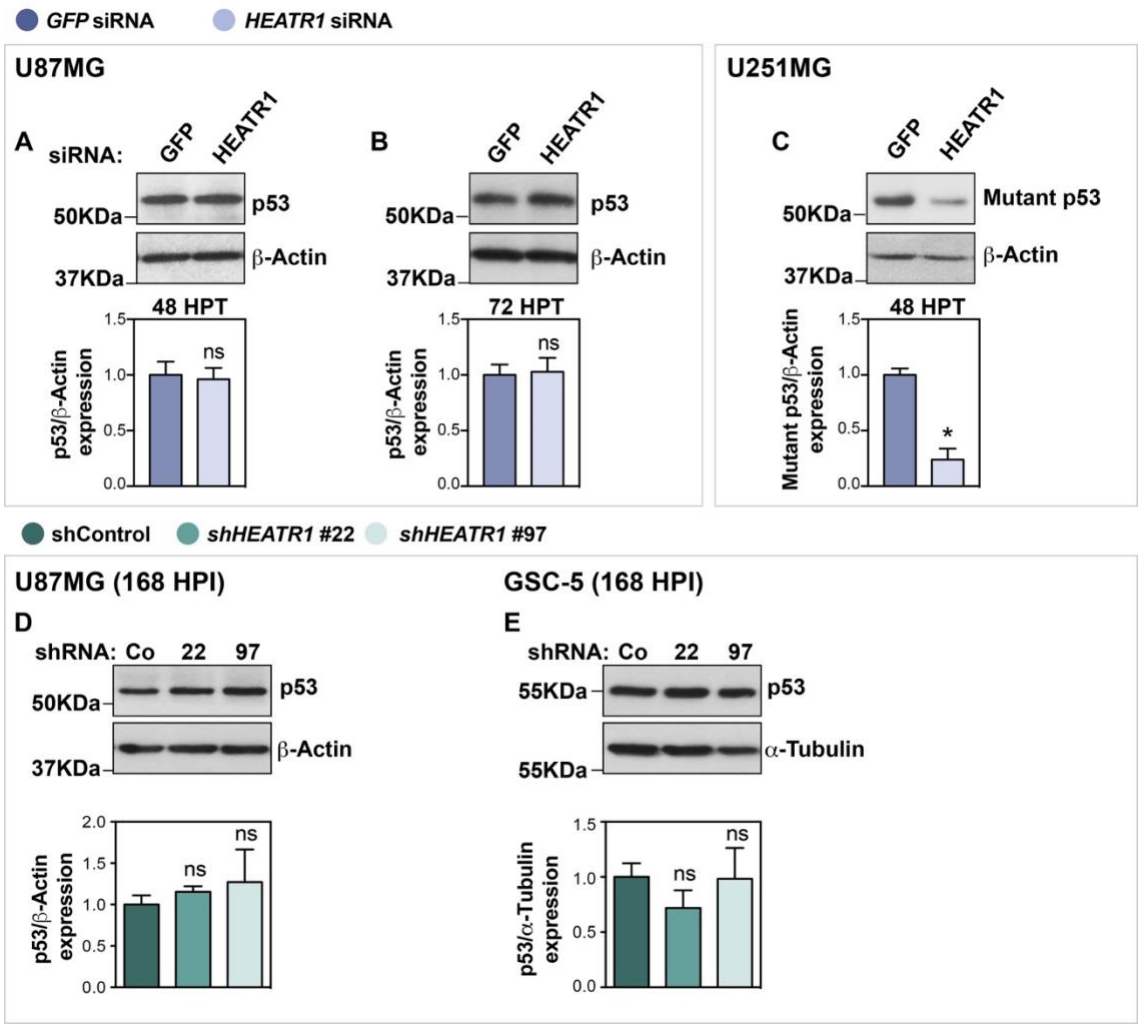

Figure 2.20 HEATR1 does not affect p53 levels in GBM cell lines and GSCs. U87MG western blots showing that *HEATR1* knockdown does not affect p53 expression levels at **(A)** 48 hours post transfection (hpt) **(B)** or 72 hpt. **(C)** *HEATR1* knockdown results in reduced mutant p53 expression in U251MG 48 hpt. Knockdown of *HEATR1* via shRNA transduction 168 hours post infection (hpi) does not affect p53 expression in **(D)** U87MG or **(E)** GSC-5. Error bars indicate SEM. Student's t-test used for all comparisons; n=3 biological repeats, *i.e., independent experiments*, ***p<0.001; **p<0.01; *p<0.05; p>0.05, ns: non-significant.

2.16 *HEATR1* inhibition does not affect total c-Myc protein expression levels in GBM cells and GSCs.

The oncogene c-Myc is a transcription factor which acts as a major regulator of cell-cycle progression, ribogenesis and cell growth[129,181]. An analysis across 33 cancers using the cancer genome atlas (TCGA) database revealed that 28% of all samples have at least one of the Myc paralogs amplified, indicating that Myc is a leading driver of

tumourigenesis[130]. Moreover, both *Drosophila* Brat and its human orthologue TRIM3 have been shown to suppress Myc expression and activity[98,131]. Thus, it was next explored whether HEATR1's mechanism of action could involve the regulation of c-Myc.

Inhibition of *HEATR1* in U87MG and GBM stem cells, GSC-5 and GSC-8, did not affect total expression levels of c-Myc **(Figure 2.21)**.

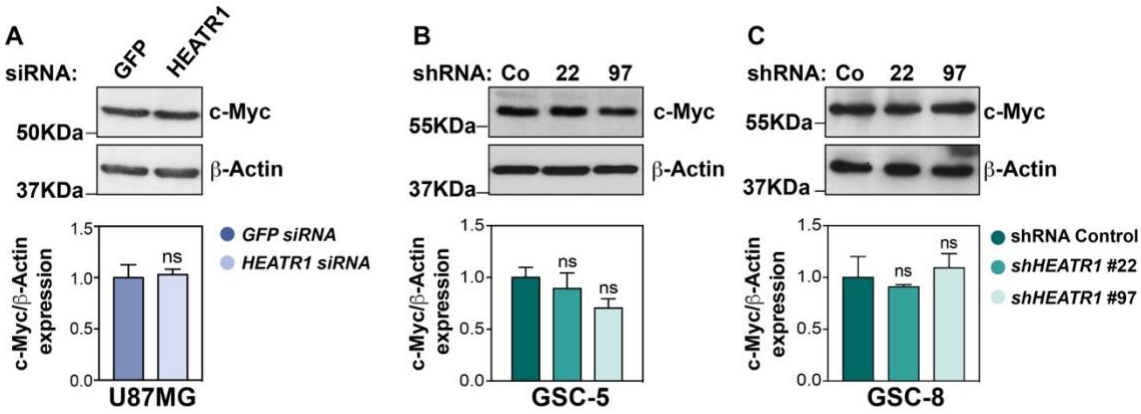

Figure 2.21 c-Myc total expression level is not affected by *HEATR1* knockdown. Western blots and respective densitometric quantifications of **(A)** U87MG, **(B)** GSC-5 and **(C)** GSC-8 show no effect on c-Myc expression when *HEATR1* is knocked down. Error bars indicate SEM. (Student's t-test used for all comparisons; n=3 biological repeats, *i.e., independent experiments*, p>0.05, ns: non-significant).

2.17 HEATR1 is required for c-Myc nucleolar localization

In GMB cells, the majority of endogenous c-Myc is evenly distributed in the nucleoplasm and continuously shuttles between nucleoli, nucleus and cytoplasm[182]. To perform its role in ribosome biogenesis and transcription, c-Myc localises to nucleoli, however, the dynamic nature of this process and the rapid turnover of Myc by the proteasome system, makes it very difficult to observe it in this site[182,183]. An established method to detect it, is to overexpress c-Myc and temporarily inhibit protein degradation with proteasome inhibitors such as MG132[182,183].

While total levels of c-Myc remain unchanged upon *HEATR1* inhibition, the cell's localisation of overexpressed c-Myc upon *HEATR1* knockdown was next investigated in U87MG cells treated with MG132. Cells were infected with *HEATR1* shRNAs and cultured for a week. These were then transfected with 1μg of full length Myc tagged with

human influenza hemagglutinin (HA) for six hours and treated with 5μM MG132 for three hours, as described in Materials and Methods section[184]. Transfected cells were classified into three groups based on the c-Myc-HA expression pattern as follows: cells with nuclear c-Myc, cells with nucleolar c-Myc and cells with c-Myc forming so-called aggresomes. These are aggregations of misfolded protein that result from an overwhelmed protein-degradation system and are not functionally active, they have been previously reported upon c-Myc overexpression and MG132 treatment[182,185].

The majority of cells present exogenous c-Myc evenly distributed through the nucleoplasm (~42% of the cells) **(Figure *2.22* A, D)**. Nucleolar c-Myc is detected in a smaller proportion of cells, 19.9%, similar to published reports[182] and is mingled within the nucleolar compartment with FBL **(Figure *2.22* B, E).** However, upon *HEATR1* knockdown this nucleolar localisation is reduced to 12.1% (#22) and 16.5% (#97). In addition, c-Myc is clearly segregated around FBL caps, not entering the interior of the nucleolus **(Figure *2.22* B, F)**. This indicates that upon *HEATR1* knockdown, c-Myc is unable to enter the nucleoli. In the remaining cells (30 to 38%), c-Myc formed aggressomes within the nucleus or cytoplasm **(Figure *2.22* C, G)**. These findings suggest that HEATR1 is essential for c-Myc nucleolar localization in GBM cells, and without it, c-Myc is unable to perform its nucleolar function in ribosome biogenesis.

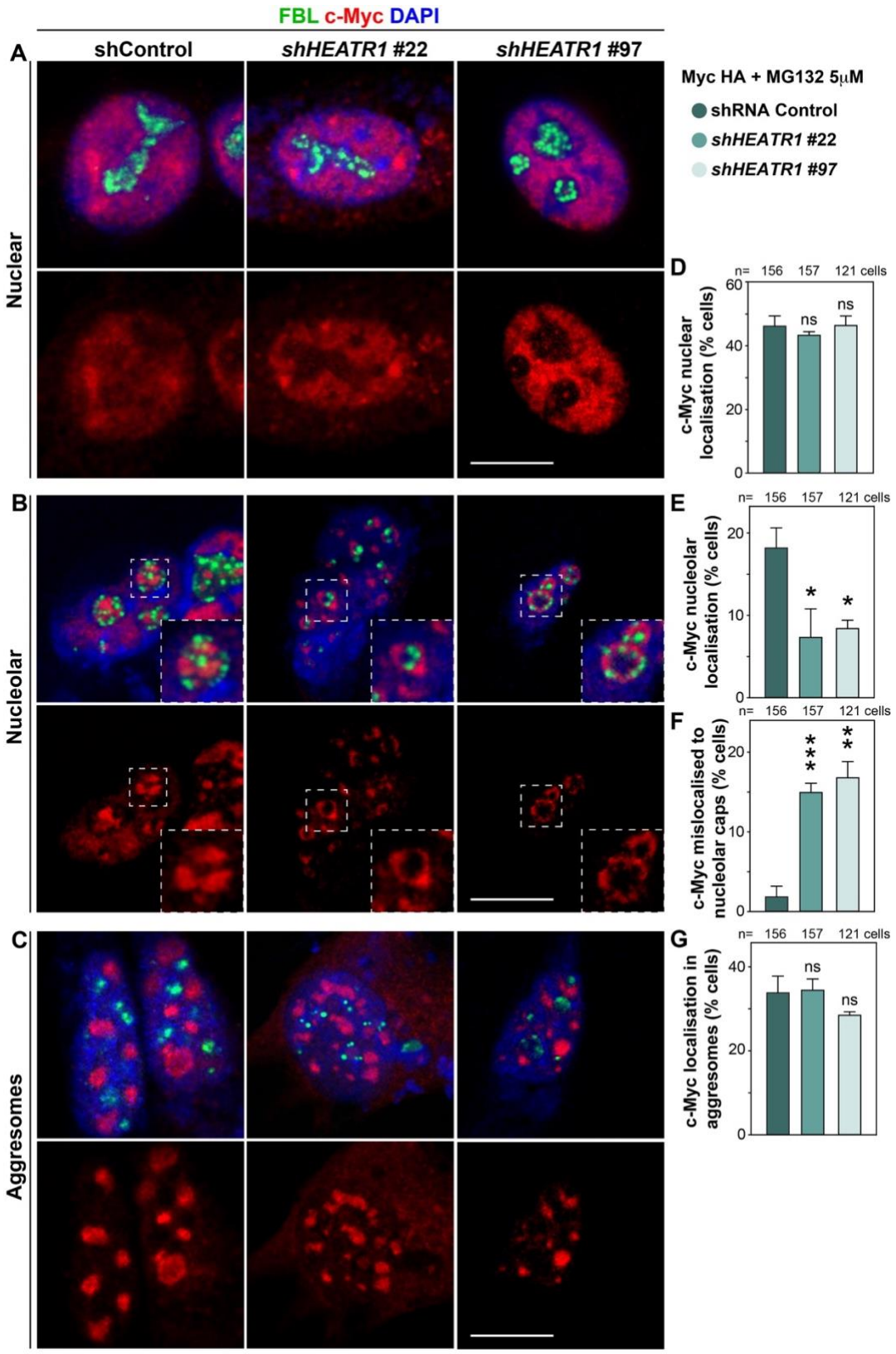

Figure 2.22 *HEATR1* knockdown prevents the nucleolar accumulation of c-Myc. U87MG cells transfected with Myc-HA (6 h) and treated with 5 μM MG132 (3 h) and *HEATR1* shRNAs (168 hpi) display three different c-Myc patterns, as shown by immunostaining against FBL (green), c-Myc (red), and DAPI (blue). **(A)** nuclear c-Myc, **(B)** nucleolar c-Myc, and **(C)** c-Myc aggresomes. **(D-F)** Quantification of these localisation patterns shows that upon *HEATR1* knockdown only nucleolar c-Myc is affected, redistributing around the nucleoli rather than inside.

Error bars indicate SEM. Student's t-test, n=4, ***p<0.001; *p<0.05; p>0.05, ns: non-significant. N numbers indicated in the graphs represent number of cells from three biological repeats, i.e., independent experiments. Scale bar 10μm.

2.18 dHEATR1 is necessary for the nucleolar localisation of dMYC in *brat* brain tumour initiating cells

In *Drosophila melanogaster*, c-Myc's orthologue, dMyc is both necessary and sufficient to regulate rRNA synthesis and ribosome biogenesis during larval development[128]. In *Drosophila* control larval brains, dMyc, is expressed in NSCs but not in the differentiating daughter cells due to Brat's post-transcriptional inhibition of the protein[98]. In absence of *brat*, dMyc is found in all cells in the lineage[98]. It is believed that Brat regulates growth and proliferation of NSCs and their progeny partially through the regulation of dMyc[98]. As *dHEATR1* knockdown impairs size growth and division of *brat* tumour initiating cells, and its human orthologue is necessary for the nucleolar localization of c-Myc in GBM cells, we hypothesized that it could be involved in the regulation of dMyc in *in vivo* in *brat* brain tumours.

I analysed the expression of dMyc upon *dHEATR1* knockdown by staining 24 HPH larval brains with dMyc and Dpn, confirming that dMyc can only be found in the NSCs of the type II NSC lineages in control brains, as reported[98] **(Figure *2.23* A)**. *dHEATR1* knockdown did not affect dMyc expression in NSCs **(Figure *2.23* B)**. As previously published[98], in *brat-RNAi* brains dMyc is expressed in all the cells in the type II clones throughout the cyto- and nucleoplasm, overlapping with Dpn **(Figure *2.23* C)**. Inhibition of *dHEATR1* in *brat-RNAi* type II lineages does not affect dMyc overall expression levels, measured as signal intensity normalised to the respective brain tumour initiating cells' areas, compared to that in *brat-RNAi* lineages **(Figure *2.23* D, G)**. However, a more detailed analysis measuring dMyc intensity only in areas overlapping with the nucleolar protein FBL, and normalised to nucleolar area, shows a relative higher accumulation of dMyc in *brat-RNAi* tumour initiating INP cells compared to that in double *dHEATR1-RNAi, brat-RNAi* **(Figure *2.23* E, F, H)**. These results demonstrate that dHEATR1

contributes to the nucleolar localisation of dMyc, and suggest an impairment on dMyc nucleolar function upon *dHEATR1* knockdown that may at least partially explain why tumour initiating cells cannot proliferate and grow as their *brat* counterparts.

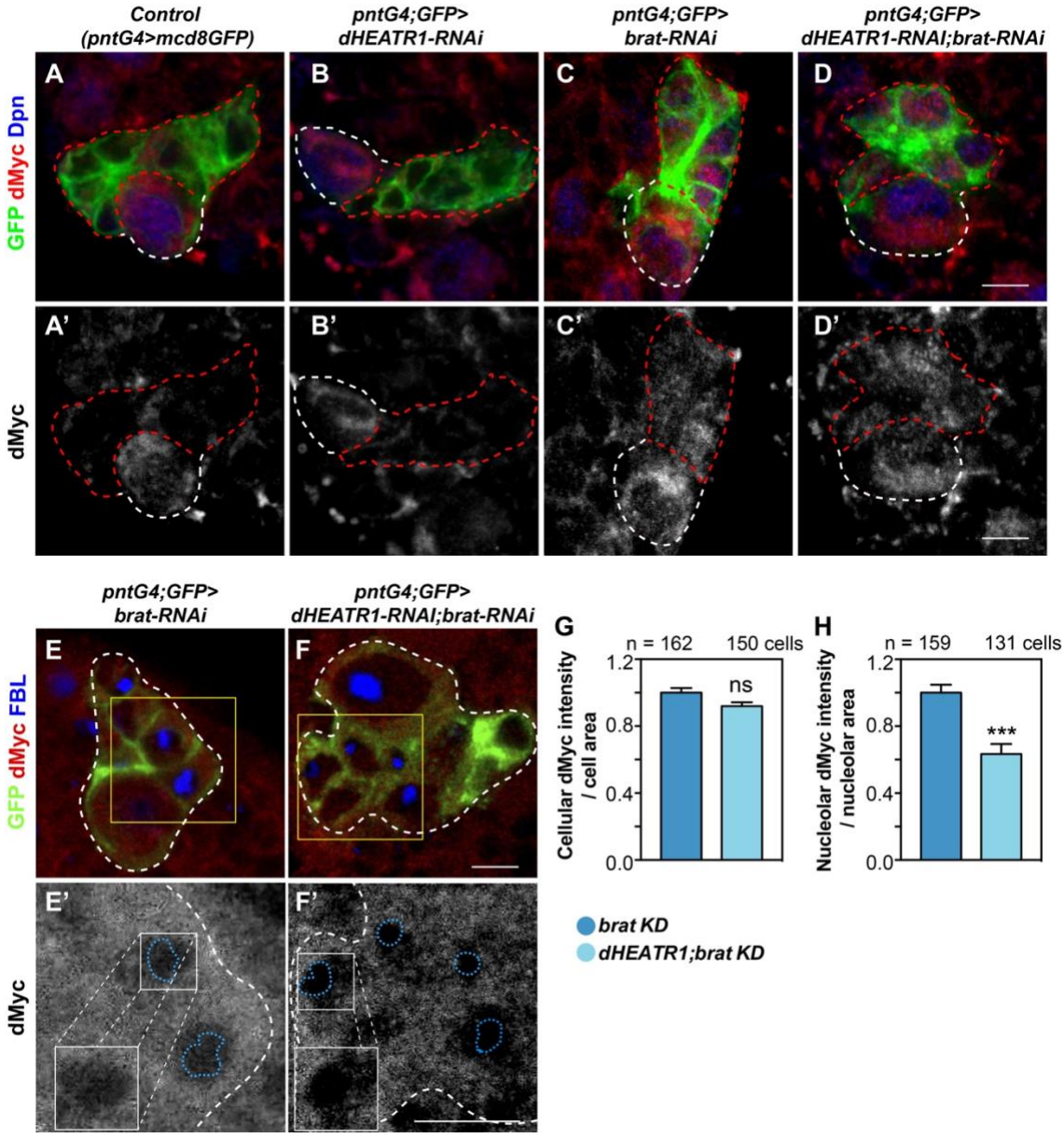

Figure 2.23 *dHEATR1* knockdown impairs dMyc nucleolar accumulation in *brat* brain tumour initiating cells. Immunostaining of type II NSC lineages from **(A)** control (*pntG4>mcd8GFP*), **(B)** *dHEATR1* knockdown (*pntG4;GFP>dHEATR1-RNAi*), **(C)** *brat* knockdown (*pntG4;GFP>brat-RNAi),* and **(D)** *dHEATR1,brat* double knockdown (*pntG4;GFP>dHEATR1-RNAi, brat*-RNAi) at 24 HPH with antibodies against GFP (green), dMyc (red/monochrome) and Dpn (blue) reveals overexpression of dMyc in brain tumour initiating cells of *brat* and *dHEATR1, brat* knockdown brains. White dotted line delineates NSCs, red dotted line delineates lineage daughter cells. Type II 24 HPH NSC lineages from **(E)** *brat* knockdown and **(F)**

dHEATR1, brat knockdown brains, immunostained with GFP (green), dMyc (red/monochrome) and FBL (blue). White dotted lines delineate type II lineages, blue dotted lines delineate nucleoli of yellow square insets. **(C)** Quantification of dMyc intensity of the whole cell normalised against cell area is not affected by *dHEATR1* knockdown. **(D)** Quantification of dMyc nucleolar intensity against nucleolar area shows a higher accumulation of the protein in *brat-RNAi* lineage cells' nucleoli than in *dHEATR1;brat-RNAi*. Error bars represent SEM. Mann-Whitney test used for all comparisons; ***$p<0.001$; **$p<0.01$; *$p<0.05$; $p>0.05$, ns: non-significant. N numbers indicated in the graphs represent number of cells from five biological repeats, i.e., independent fly brains. Scale bar 10μm.

2.19 HEATR1 is required for c-Myc driven rRNA synthesis

Both HEATR1 and c-Myc have a nucleolar function. c-Myc binds ribosomal DNA and activates RNA Pol I-mediated transcription in both in mammals[186,187] and *Drosophila melanogaster*[128]. I have shown that HEATR1 loss impairs rDNA transcription in GBM cell lines and prevents nucleolar localization of c-Myc **(Figure 2.)**. To further investigate whether c-Myc function may be dependent on HEATR1, I overexpressed c-Myc and simultaneously knocked down *HEATR1* in U87MG cells. RT-qPCR analysis revealed that Myc upregulation induces a strong overexpression of rRNA synthesis, as detected by levels of *47S pre-rRNA* transcript, and as extensively described in the literature[186,187]. However, when HEATR1 is knocked-down at the same time, this upregulation is reduced by almost 5.5 fold change, indicating that HEATR1 is required for this function of c-Myc **(Figure 2. A)**.

Moreover, although HEATR1 overexpression on its own did not affect levels of *47S pre-rRNA* synthesis in 293T cells **(Figure 2.18 F)**, simultaneous overexpression of HEATR1 and c-Myc significantly enhanced the increase observed upon c-Myc overexpression **(Figure 2. B)**, demonstrating that HEATR1 controls at least in part c-Myc-mediated rRNA synthesis.

On the basis of the findings described in this thesis, a model is proposed whereby increased HEATR1 expression enhances RNA Pol I-mediated c-Myc-induced rRNA synthesis, promoting ribosome biogenesis, protein synthesis and brain tumour growth (See Discussion).

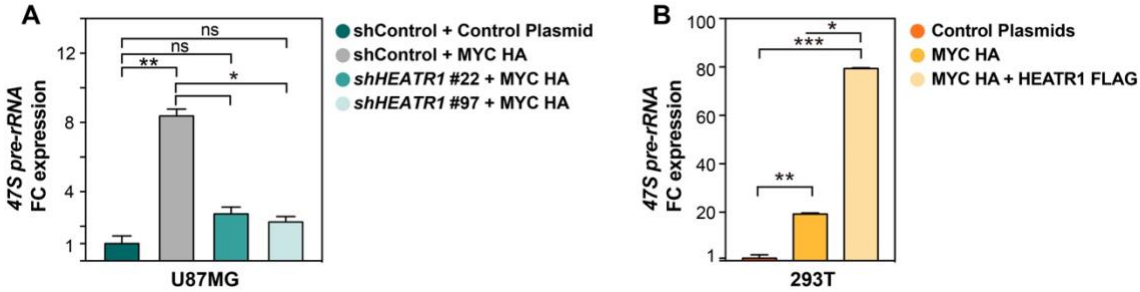

Figure 2.24 c-Myc mediated rDNA transcription is dependent on HEATR1 in GBM cell lines. (A) Upregulation of *c-Myc-HA* on its own in U87MG cells results in the overexpression of *47S pre-rRNA* mRNA whereas overexpression of *c-Myc-HA* and simultaneous *HEATR1* knockdown using shRNAs (168 hpi) prevents upregulation of *47S pre-rRNA*. **(B)** Upregulation of *c-Myc-HA* in 293T cells results in increased *47S pre-rRNA* expression, and simultaneous upregulation of *HEATR1-FLAG* induces a further enhances this increase. FC, fold change. Student's t-test used for all comparisons; n=3 biological repeats*, i.e., independent experiments*; ***p<0.001; **p<0.01; *p<0.05; p>0.05, ns: non-significant.

3 DISCUSSION

3.1 Preface

Many human tumours, and particularly GBMs, are characterised by high cellular heterogeneity[85], which poses a major challenge to diagnosis and treatment[188]. Single-cell resolution analysis have emerged as a useful tool to profile tumour heterogeneity and study concrete populations. My studies described in this thesis are based on a single-cell resolution transcriptome screen performed in Dr Barros laboratory to gain insights into the transcriptional alterations associated with brain tumour initiation. Single *Drosophila brat* iINPs were collected at the time of their transformation into brain tumour initiating cells and compared to their control counterparts. *L(2)k09022*, named here *dHEATR1*, was identified as highly upregulated in *brat* brain tumour initiating cells, and was selected for further investigation. *dHEATR1* is highly conserved to its human orthologue *HEATR1* (DIOPT score 13.8 out of 14)[189], with an identity of 28% and similarity of 47% at the amino-acid level. In my studies, I aimed to identify the role of HEATR1 in brain tumour initiation and growth and unravel its molecular mechanism of action using a combination of different model systems.

3.2 Advantages and limitations of models used in this study

Among CSCs, those of GBM have been extensively investigated by numerous groups across the world, demonstrating that they are responsible for the re-formation of these tumours[10,27,33]. However, despite all the advances in the field, GBMs remain untreatable, and there is an urgent need for research towards the development of models and therapies[66,86].

Classic GBM immortalised cell lines such as U87MG or U251MG are of undeniable historic value and have shaped our knowledge about GBMs and cancer in general. However, evidence suggests that the maintenance of these cell lines *in vitro* for extensive periods of time with serum-containing medium and extensive passaging, resulted in genetic aberrations and clonal selection processes to adapt to non-physiological

conditions, which lead to the progressive diversion of genotypes and phenotypes, bearing now little resemblance to their tumour of origin[191,192]. However, immortalised cell lines have many advantages too, they are easy and inexpensive to culture, can rapidly multiply, provide a pure population of cells, which is important for reproducibility, and can usually be subjected to complex genetic manipulations that are unachievable with other models[193]. The results obtained using these cells can serve as indicators and basis before moving on to superior models, that are often more expensive and complicated to use[193]. For these reasons, I used GBM immortalised cell lines for part of my studies. Although these cell lines are still useful to study certain aspects of gliomas, they fail to model accurately essential processes such as stemness and tumourigenicity[191,192], which can at least partly explain why cancer cell line-based preclinical models have been often found to poorly predict therapeutic outcomes[192].

To study CSCs of GBM (GSCs), protocols have been established allowing the isolation of these cells from GBM tumours and their maintenance *in vitro*[81,194]. GSC culture conditions have been adapted from those originally established to derive and expand NSC lines[81,194]. GSCs retain cancer initiating stem cell properties, which can be tested both *in vitro* and *in vivo,* via for example soft agar assays and xenotransplants in immunocompromised mice, providing a more accurate system to study these characteristics[82,192]. I have used two different patient-derived GSCs, GSC-5 and GSC-8, which were obtained from GBM specimens and previously characterized by Dr. Gil-Ranedo[83]. Briefly, both cell lines grow exponentially forming neurospheres in cell culture media supplemented with EGF and FGF-2 and express different neural stem cell markers like CD133, Nestin and Sox2 in 70-90% of cultured cells[83]. They effectively initiate tumours that recapitulate the cellular heterogeneity present in the parental GBM upon orthotopic xenografts in immunocompromised mice, and are able to differentiate into neurons, astrocytes and oligodendrocytes[83]. Nonetheless, it is worth noting again that the process of evaluating any population of cells, including CSCs, demands significant *ex vivo* manipulation, which may affect their intrinsic nature and compromise the relevance of the results in question compared to their functions in the patient[19,27].

Therefore, models in which CSCs can be identified and studied *in vivo* are extremely valuable.

This is one of the advantages of the *Drosophila brat* model, in which the brain tumour initiating cells, the immature INPs of type II NSC lineages, are relatively well characterised[6,98,99] (see Introduction). Additionally, Brat's human orthologue, TRIM3, has been well investigated in GBMs, where it was shown to have a similar function to that of Brat in *Drosophila*[7,127]. TRIM3 has been shown to be downregulated in many cancer types such as liver cancer[135], colorectal cancer[136], and importantly for my studies, GBM tumours[7,127,132,137], and GSCs[131]. This is also the case in the GBM samples I have used in my studies, in which previous members of our group confirmed TRIM3 downregulation (Diaz *et al*., *in preparation*). Moreover, TRIM3 expression is inversely correlated to stemness in GSCs, where $CD133^+$ cells express low levels of TRIM3 and viceversa[127], and its reconstitution in GSCs impairs neurosphere formation, switching from predominantly symmetric to asymmetric cell division, and inhibiting the expression of stem cell markers such as CD133, Nestin, and Nanog[131]. Given the proven analogous modes of action of Brat and its orthologue tumour suppressor TRIM3, new findings using the Brat model may also be relevant for aspects of human brain tumourigenesis.

By simultaneously knocking down *brat* and labelling type II NSC lineages using the UAS/GAL4 system, I could follow brain tumourigenesis from cell transformation, at a resolution and precision level that is still not possible in mouse models. This system allowed me to perform loss of function assays in a control and brain tumour background to address the potential role of dHEATR1 in the native environment of the cells, under physiological conditions.

Overall, in my studies I have used a combination of several models, *in vivo and in vitro*, taking advantage of their respective strengths to examine aspects of brain tumour initiation and development.

3.3 HEATR1 is overexpressed in brain tumours and tumour initiating cells

A few studies have previously linked HEATR1 to cancer. It was first shown to be upregulated in GBM in a study by Wu *et al*., who also reported its upregulation in the stem cell marker-expressing (A2B5^{+}) population of GBM U87MG cells[155], and more recently it was found overexpressed in non-small cell lung carcinoma cell lines[153]. These findings are consistent with preliminary data of this study, in which previous members of the Barros group found *dHEATR1* upregulated in *brat* brain tumour initiating cells, and with my own data, which show that HEATR1 is upregulated in GBMs and DAs, compared to control non-tumorous brain samples. The higher expression in GBMs compared to DAs could indicated an increase in HEATR1 expression with the progression of the glioma tumour grade, however, further evidence would be needed to confirm this. Interestingly, using the TCGA database to investigate the correlation between HEATR1 expression and patient survival in GBM and lower grade gliomas, we observed that high HEATR1 expression correlates with lower survival, although this is more evident in the case of lower grade gliomas (Diaz *et al. in preparation*).

Additionally, I also found that HEATR1 was overexpressed in GSCs compared to an NSC line derived from human foetal brain. Although this is not the ideal control, as foetal NSCs have more proliferative potential than adult NSCs, the fact that HEATR1 is overexpressed in GSCs suggests nevertheless a specific role in GBM CSCs and aligns with the findings using *brat* brain tumour initiating cells. In contrast, and interestingly, two different publications have shown the opposite result in pancreatic cancer, where HEATR1 was found downregulated in this type of tumour, compared to pancreatic control tissue[156,157], suggesting that HEATR1 could have different functions depending on tissue context.

In summary, my expression studies of HEATR1 together with published data, indicate it plays a role in brain tumour initiation and/or development.

3.4 HEATR1 is necessary for brain tumour development

Regulation of growth-promoting signals that coordinate entry and progression through the cell cycle is essential for maintenance of tissue homeostasis, architecture and function[195], and uncontrolled proliferation is one of the hallmarks of malignant transformation in cancer[195,196]. Cell proliferation was, therefore, one of the first characteristics to be analysed in my studies of HEATR1.

dHEATR1 knockdown at early developmental stages (24 or 48 HPH) does not have a significant effect in proliferation in a control background. However, when *brat* tumour initiating cells have escaped the non-proliferating stage and tumour overproliferation formation can already be detected, *dHEATR1* knockdown prevents the excess in cell divisions: in double *dHEATR1,brat-RNAi* brains the average number of dividing cells reverts back to that observed in control brains. The same assays at later stages before larvae pupation (93 HPH) showed that *dHEATR1* knockdown in a control background significantly reduces cell proliferation. A possible explanation for these findings is that once the RNAi is activated, there is still some dHEATR1 protein left in the early brains that is sufficient to perform its function in a control background, but not in the tumour background **(Figure *3.1* A, B)**. In addition, this result confirms the findings of a genome-wide RNAi screen performed by the Knoblich group (IMBA, Vienna) that identified *dHEATR1* among a large number of potential NSC proliferation regulators in *Drosophila*[154]. At late developmental time-points, the brain lobes of *brat* knock-down brains are severely enlarged due to the size of the tumours and simultaneous *dHEATR1* knockdown impairs proliferation and reduces tumour size **(Figure *3.1* A,B)**. These data indicate that dHEATR1 is required for tumour growth. Consistently, I observed that cell proliferation is also affected in human GBM cell lines (U87MG and U251MG) upon *HEATR1* knockdown, suggesting a potential similar function in human GBM.

Another well-known characteristic of the *brat* model is the acquisition of cell self-renewal markers like Dpn of the iINPs, which revert to an NSC-like state, becoming brain tumour initiating cells[98,99,101]. In other words, the transformation of iINPs into CSCs. I have found that d*HEATR1* knockdown does not stop the transformation of these cells.

All *dHEATR1;brat* depleted iINPs acquire expression of Dpn and do not express the maturation marker Ase, similar to *brat*-only depleted iINPs. However, during this transformation stage, *brat* tumour initiating cells also grow in size, and have been reported to be larger than control INPs[119], which is also common in human tumour cells[197]. Interestingly, upon *dHEATR1* knockdown, cell size growth of the transformed cells was prevented and remained at control levels **(Figure *3.1* A, B)**. Therefore, dHEATR1 seems to not be implicated in the transformation of tumour cells but it is required for their enlargement and subsequent overproliferation, contributing to brain tumour development and growth.

Similar results were found when examining the role of HEATR1 in human GSCs. The soft agar assays showed an extreme impairment on tumourigenic potential upon *HEATR1* knockdown on both GSC lines analysed: the cells were unable to grow in an anchorage-independent manner, which is considered a hallmark of carcinogenesis and indicating that HEATR1 affects the cancer stem cell properties of these cells **(Figure *3.1* C, D)**. Similarly, He *et al*. reported that *HEATR1* inhibition in the immortalised A549 and NCI-H460 lung cancer cell lines stopped colony formation in culture media and xenograft tumour growth in mice transplanted with these cells[153]. In contrast, *HEATR1* knockdown in pancreatic cells induces xenograft tumour growth[156], highlighting again the differences of actions in these tumour types.

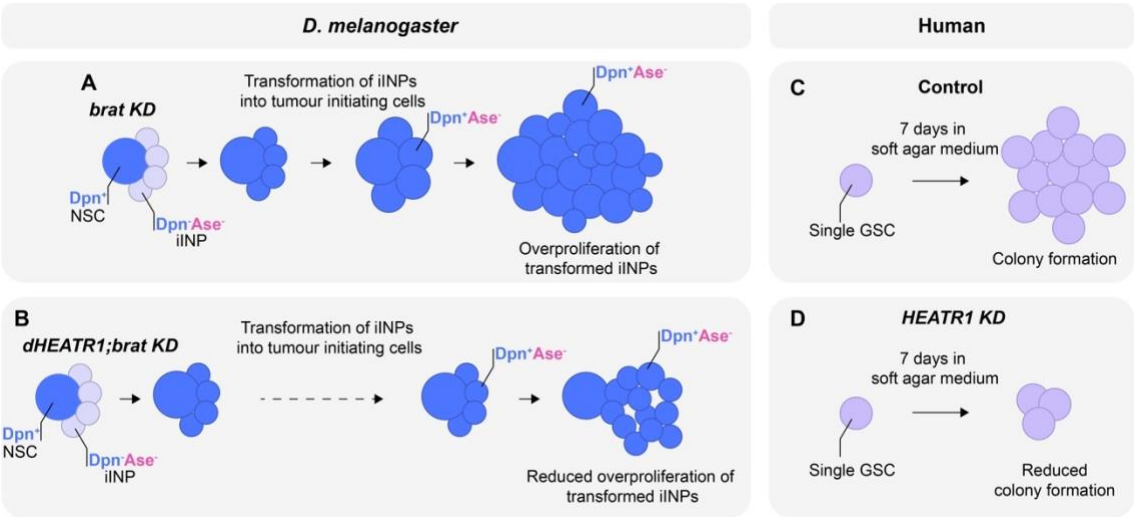

Figure 3.1 HEATR1 promotes brain tumour growth. (A) Schematic drawing depicting the development of brain tumours in the *brat* model. Dpn^+ NSCs give rise to immature intermediate progenitors (iINPs) that during a short non-proliferative period go through neoplastic transformation, acquiring NSC-like characteristics such as expressing the self-renewal marker Dpn, growing in size and never maturing (remain Ase^-). These brain tumour initiating INPs next start to overproliferate forming a massive brain tumour[98,99,101]. **(B)** Simultaneous knockdown of *dHEATR*1 and *brat* results in smaller and reduced numbers of tumour initiating INPs. Consequently, although tumours still form, their growth is severely impaired. **(C)** Similarly, single control GSCs grow in soft agar medium forming colonies. **(D)** Upon *HEATR1* knockdown, colony formation capability of GSCs is severely impaired, and after seven days in soft agar medium colony formation is extremely reduced.

3.5 HEATR1 is a nucleolar protein required for ribosome biogenesis of brain tumour cells

Ribosome biogenesis links various signalling pathways that coordinate protein synthesis with cellular growth and proliferation, core processes affected in cancer cells[173,198]. In fact, enlarged nucleoli, often correlate with increased proliferation[199], and nucleolar morphology visualized by nucleolar organizer regions (NORs) silver staining has been long used by tumour histopathologists to diagnose cancer patients[173]. Aberrant increase in nucleolar size and number reflects increased rates of ribogenesis[199], which has been recognized for more than a century as a hallmark of many cancers, and has been associated with poor prognosis[173]. However, the concept that increased ribosomal activity is not only required but sufficient to enhance malignant transformation has emerged only in the past few years[200]. Indeed, hyperactivation of ribosome biogenesis can be triggered by oncogenes or the loss of tumour suppressors, and has therefore been proposed to have a critical role in cancer initiation and progression[148,173]. Additionally, not only quantity is important, qualitative modifications in ribosomes can also promote oncogenesis. This is suggested by the elevated incidence of colon carcinoma and myeloid leukaemia in patients with inherited ribosomopathies, which are disorders caused by mutations in genes encoding ribosome components or other ribosome biogenesis factors, leading to impaired ribogenesis and/or function[201].

I have shown that HEATR1 localises mainly to the nucleoli, in GBM cell lines and GSCs, where it co-localises with the nucleolar protein FBL. Similar results were obtained when analysing GBM and control brain tissue samples (IHC performed by D. Hilton, Derriford Hospital, NHS), yet levels in the later were markedly reduced as expected. In all cases, a weaker HEATR1 signal could also be seen throughout the nucleus and cytoplasm of the cells. In previous studies, different groups have reported similar findings in other cell types and contexts: Prieto *et al*., (2007) have shown that UTP10, HEATR1's yeast orthologue, localises to the nucleoli, where it overlaps with other nucleolar proteins[149], and Wu *et al*., (2014) found HEATR1 both in the cytoplasm and nucleoli of GBM tumour cells in histological sections[155]. Interestingly, the distribution pattern in pancreatic tumours is different. In these tumours HEATR1 seems to be expressed in the cytoplasm and sometimes in the cell membranes, where it co-localises with Akt to inhibit it[156]. It is clear that HEATR1 has a different role in pancreatic cancer to that I have identified in brain tumours, however, as I did not explore Akt signalling nor a cytoplasmatic role of HEATR1, I cannot rule out that it may act with this pathway. Yet, if this is the case, HEATR1 must perform a different role than in pancreatic cells, where it inhibits Akt signalling leading to tumour development.

The nucleolus is a dynamic, non-membranous organelle that forms around a NOR comprising rDNA arrays[148]. In mammals, it is composed by three different structural and functional compartments; the fibrillar components (FCs), the dense fibrillar compartments (DFCs), that surround the FCs, and the granular compartments (GCs) that surround the DFCs[143,148,167]. Ribosomal genes are kept in the FCs where transcription rDNA takes place. Newly synthesized pre-rRNA molecules locate to the DFC where they begin to be processed by the small nucleolar RNAs (snoRNAs), and next transfer to the GC as they mature[143,148,167]. Of high relevance to my studies, the size, reorganization and modification of these spatial structures are indicative of alterations in nucleolar function, and therefore, can be studied by labelling them with specific markers[143,167]. Furthermore, knockdown of several nucleolar proteins has been shown to result in the formation of nucleolar caps[171]. These structures are believed to form as a

protection mechanism against rDNA damage, as studies inducing DNA breaks into the rDNA repeats in human and mouse cells consistently show RNA Pol I-dependent transcription inhibition and formation of nucleolar caps[202]. Additionally, treatment of cells with actinomycin D, an RNA Pol I inhibitor, results in the rapid reorganization of the nucleolus and formation of nucleolar caps[202]. Interestingly, a previous study reported that Actinomycin D treatment lead to HEATR1 nucleolar redistribution into caps, meaning that when RNA Pol I activity is impaired, HEATR1 is also affected and possibly non-functional[152].

As mentioned in the Results section, UBF, FBL and NPM were chosen to identify and examine each nucleolar compartment and associated ribogenesis step, as they have been widely studied and used for similar purposes[142,171,203]. The UBF protein is associated to the FCs and plays a critical role in rRNA transcription by mediating the recruitment of RNA Pol I to rDNA promoting regions, being a key component of the transcription pre-initiation complex[149,176]. FBL is located in the DFCs and is a methyltransferase involved in pre-rRNA processing[168]. NPM labels the GCs and is required for ribosomal nuclear export. Western blot analyses of the expression levels of these nucleolar proteins upon *HEATR1* knockdown in either GSCs or GBM immortalised cells showed that only UBF total expression was affected, whereas no significant effects could be seen in FBL or NPM. However, *HEATR1* knockdown does affect the morphology of all three nucleolar compartments, which become smaller in size. In addition, FCs and DFCs distribute towards the periphery of the nucleoli, resembling the formation of the so-called nucleolar caps, and although GCs do not relocate into caps, their pattern in most cases also changes, acquiring a doughnut-like shape with NPM protein accumulating in the periphery **(Figure *3.2*)**. The higher intensity of the signal in these reduced size areas might explain why total protein levels in the case of FBL and NPM are not significantly affected. These data suggest that HEATR1 might have a main role in the first step of ribosome biogenesis, rDNA transcription, as it regulates the production of UBF, while affecting to a lesser extent the subsequent steps, rRNA processing and assembly.

Interestingly, Turi *et al*. (2018) reported that *HEATR1* knockdown in osteosarcoma cells resulted in the release of NPM to the nucleoplasm[152], a different phenotype to what I observed in GBM cell lines and GSCs, suggesting potentially different actions of HEATR1 in ribogenesis processes possibly dependent on tumour cell types.

Strikingly, similar effects were observed *in vivo*, in our *Drosophila brat* model. *Drosophila brat* tumour initiating cells have enlarged nucleoli, consistently with the phenotype seen in a wide range of human cancer cells, and as mentioned above[98,199]. I observed that knockdown of *dHEATR1* in these cells results in the reduction of nucleolar area to levels comparable to those of control brains, suggesting that ribogenesis is also back to levels found in normal cell counterparts. The findings indicate a similar mechanism to that of human GBM cells, and strongly suggest that HEATR1 is essential for several steps of ribosome biogenesis in brain tumour cells.

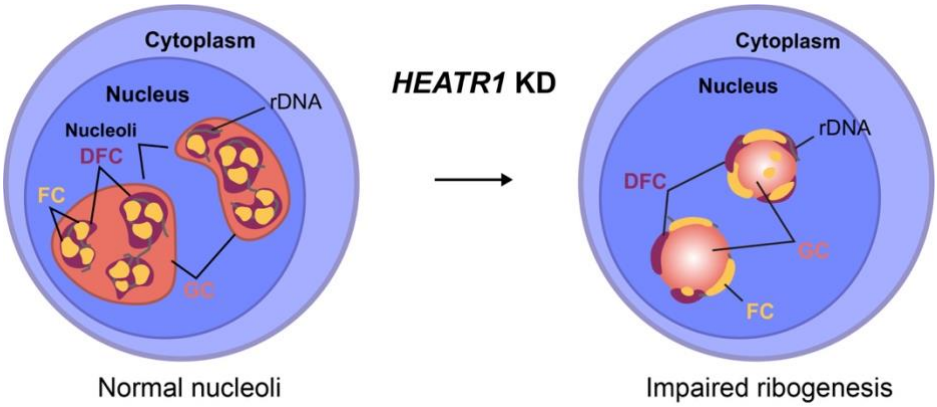

Figure 3.2 Nucleolar reorganization in response to *HEATR1* knockdown in GBM and GSC cells. Schematic representation of the structure of normal nucleoli within the nucleoplasm in which the fibrillar centres (FCs) form around the rDNA within the dense fibrillar compartments (DFCs) and the granular compartments (GCs). Upon *HEATR* knockdown the areas of the three compartments are reduced, the FCs and DFCs relocate to the periphery of the nucleoli forming compact structures, and the GCs become acquire a doughnut-like shape.

Synthesis of rRNA by RNA Pol I is a rate-limiting step of ribosome biogenesis[148]. Previous studies have reported the co-localization of HEATR1 with RPA194, the biggest subunit of RNA Pol I, in an osteosarcoma cell line[152]. Consistently, my results demonstrate that *HEATR1* knockdown impairs RPA194 localisation, suggesting that

RNA Pol I function might be affected. Further experiments analysing the rate and expression of rRNA synthesis in GBM cells by measuring 47S pre-rRNA synthesis confirmed its downregulation upon *HEATR1* knockdown, clearly demonstrating that RNA Pol I function is affected. After being transcribed by the RNA Pol I, the 47S pre-rRNA is heavily modified to yield the mature 28S, 18S and 5.8S rRNA subunits, which will then form the small and large subunits of the ribosomes in combination with ribosomal proteins[148,173]. Previous studies had reported that HEATR1 depletion resulted in the reduction of 18S rRNA levels, suggesting defects in rRNA processing of this specific subunit[151]. However, I have found that in GBM cells, *HEATR1* knockdown affected all the mature rRNAs at a similar level. Interestingly, *HEATR1* overexpression was not enough to increase 47S pre-rRNA synthesis levels. Collectively, the data indicate that although HEATR1 is required for several steps of ribosome biogenesis, it is not sufficient to stimulate it.

As ribosome biogenesis is directly responsible for protein synthesis, it is not surprising that the knockdown of *HEATR1* results in lower rates of protein synthesis in GBM cells. Given that cell size growth depends on ribogenesis and production of proteins[148,198], a role of HEATR1 in these processes is also consistent with the observations in the *in vivo brat* brain tumour model, in which upon *dHEATR1* knockdown, tumour initiating cell size growth is prevented. These findings suggest that hyperactive ribosome biogenesis (as seen by enlarged nucleoli) and consequent protein synthesis in *brat* tumour initiating cells depends on dHEATR1.

In conclusion, before a cell divides, protein synthesis needs to increase greatly so as to duplicate the cell structural and functional components, and to ensure the cell has a certain size to produced viable progeny[148,204]. This is achieved by up-regulation of ribosome biogenesis[204], which in brain tumour initiating cells results in the upregulation of HEATR1, which is needed to maintain increased levels of rDNA transcription, processing and assembly.

3.6 HEATR1 seems to play no major role in brain tumour cell survival

Regulation of apoptotic signals is another essential process that is known to affect cancer cells. In fact, many clinical approaches have focused on developing therapies promoting the elimination of cancer cells by inducing apoptosis[205]. HEATR1 has been previously implicated in cell survival as its knockdown was suggested to induce p53-mediated apoptosis in two independent studies. The knockdown of its zebrafish homologue, *bap28*, was claimed to trigger p53-dependent apoptosis during development[151], and in human non-small lung cancer cell lines, *HEATR1* downregulation induced a minor increase in cell death, that was linked to the activation of the p53/PUMA/BAX/BCL pathway[153]. However, during my studies I was not able to detect differences in levels of apoptosis in either the *Drosophila brat* model or in GBM immortalised cell lines upon *HEATR1* knockdown. Experiments performed by another member of our laboratory using GSCs subjected to *HEATR1* inhibition revealed only a small (5-10%) yet significant increase, in cell death (Diaz *et al*., *in preparation*). However, this increase was not accompanied by significant changes in the levels of BAX and Casp3 as measured by western-blot assays on GSCs that I performed. Additionally, I extensively investigated p53 expression in our human models and was unable to detect any upregulation of the protein upon *HEATR1* knockdown, including in GSCs. Moreover, BAX is regulated by p53 and an activator involved in p53-mediated apoptosis, therefore, the fact that BAX levels are not affected suggests that the p53/PUMA/BAX/BCL pathway may not be regulated by HEATR1 in GBMs.

Additionally, HEATR1 was shown to regulate p53-dependent cell cycle arrest in osteosarcoma cells through triggering the impaired ribosome biogenesis checkpoint (IRBC)[152]. Upon impaired ribosome biogenesis, a protein complex containing newly synthesised 60S Ribosomal Protein 5 (RPL5), 60S Ribosomal Protein 11 (RPL11) and the 5S rRNA is redirected from assembly into 60S ribosomes to the E3 ubiquitin-protein ligase human double minute 2 (HDM2; MDM2 in mice), which leads to p53 stabilization by preventing its ubiquitylation and degradation[173]. This process is known as the IRBC[173]. In *HEATR1* depleted osteosarcoma cells, HDM2 formed a complex with RPL5, which led

to the accumulation of p53[152] and cell cycle arrest, while simultaneous knockdown of either RPL5 or RPL11 prevented p53 accumulation[152]. However, how HEATR1 would inhibit p53 in these particular tumour cells, contributing to their overproliferation would require further investigation.

Together these findings suggest that even if HEATR1 has some contribution to cell survival, it seems it is not a main process by which it promotes brain tumourigenesis, in contrast to its striking effects on tumour cell size growth and proliferation. Moreover, unlike reports in other systems, my findings do not support an effect of HEATR1 on levels of the tumour suppressor P53 and therefore other mechanisms of possible mode of action were explored.

3.7 HEATR1 regulates dMyc nucleolar localisation and function

The underlying molecular mechanism by which HEATR1 affects cell cycle and ribosome biogenesis still remains an open question. Vast literature demonstrates that the oncogene c-Myc functions as a sequence-specific transcription factor that regulates cell-cycle progression, ribogenesis, and cell growth, and its deregulation has been implicated in a wide range of cancers[130]. Indeed, c-Myc regulates multiple steps of ribosome biogenesis[129]. It binds to upstream and downstream sequences of the coding regions of rDNA clusters, remodelling their chromatin structure, and directly regulates RNA Pol I transcription of the 47S pre-rRNA[182,186]. It also enhances expression and recruitment of the RNA Pol I cofactors like UBF and SL1, indirectly promoting rDNA transcription[186]. It also enhances expression and recruitment of the RNA Pol I cofactors like UBF and selective factor 1 (SL1), indirectly promoting rDNA transcription[186].Outside nucleoli, transcription of the 5S rRNA by RNA Pol III is also mediated by c-Myc through its interaction with TFIIIB[129], and transcription of ribosomal proteins is regulated by c-Myc as well through RNA Pol II[129]. In this way, c-Myc controls ribosome biogenesis through all three RNA polymerases and at different levels. I, therefore, decided to investigate whether HEATR1 action in ribogenesis is linked to that of c-Myc.

Drosophila Myc and vertebrate c-Myc share a sequence identity of 26% and the characterised domains are highly conserved[206]. dMyc is inhibited by Brat post-transcriptionally in the progeny of NSCs[98]. Therefore, in the *brat* tumour model dMyc is found overexpressed in tumour initiating INP cells[98], where our group detected *dHEATR1* also overexpressed. Moreover, using the TCGA database, *TRIM3* expression was shown to negatively correlate with that of *c-Myc* in GBM samples, and overexpression of TRIM3 in GBM immortalised cells results in reduced nuclear c-Myc expression[131]. These data suggest a conserved functional link between Myc and Brat/TRIM3.

During active rDNA transcription, c-Myc can be found at the nucleoli[186,187]. This is reportedly very difficult to detect possibly due to it being a transient and highly dynamic process[182]. To overcome the difficulties, researchers have used strategies such as inhibiting the proteasome machinery[182] which I have also utilised successfully in my work with cells in culture. It has been proposed that the recruitment of c-Myc to nucleoli is mediated at least partially by Nucleophosmin (NPM) in mouse embryonic fibroblasts (MEFs) as its overexpression leads to a higher accumulation of Myc in the nucleoli and its downregulation impairs this localization[184]. Additionally, the upregulation in rDNA transcription caused by Myc overexpression can be prevented by the simultaneous knockdown of NPM, which indicates that NPM controls c-Myc-mediated transcription[184]. In my studies, I have identified a similar relation between HEATR1 and c-Myc using both *in vivo* and *in vitro* models. I have shown that when *HEATR1* is knocked-down, less c-Myc can be detected in the nucleoli of GBM cells, and of *Drosophila brat* tumour initiating cells (in which c-Myc is found overexpressed). Moreover, HEATR1 depletion inhibits c-Myc-mediated rDNA transcription, and its overexpression enhances it. This is particularly interesting, as *HEATR1* upregulation on its own did not trigger a significant effect on rDNA transcription. Overall, these data indicate that c-Myc localisation in nucleoli of brain tumour cells is dependent on HEATR1, and HEATR1's nucleolar role is, at least in part, mediated by c-Myc.

3.8 Proposed model for HEATR1 function

Together with literature and contributions from other members of the Barros team (as indicated throughout this thesis), my findings using the *Drosophila brat* brain tumour model, GBM and GSC cells lead us to propose the following model of action of HEATR1 in brain tumour initiation and development.

Upon malignant transformation of neural cells, in which the tumour suppressor function of Brat/TRIM3 has been lost, HEATR1, a predominantly nucleolar protein, becomes upregulated. High HEATR1 levels lead to an increase in nucleoli size and function, namely in rDNA transcription and processing. I have further shown that this is in part mediated by recruitment of the oncogene and master regulator of rRNA synthesis, c-Myc[129,181], to nucleoli by HEATR1. Increased ribosome biogenesis raises the rate of protein synthesis, leading to cell size growth and contributing to tumour proliferation and development **(Figure *3.3*)**.

A limitation of this study is the lack of HEATR1 overexpression assays both in the *Drosophila* model and *in vitro* in GSCs. However, as HEATR1 does not regulate transformation, and its overexpression in 293T cells did not trigger an upregulation on rDNA transcription, overexpression of *dHEATR1* in a control background, or in the *brat* background or in GSCs, where it is already enriched, might not have any effect. Another possibility is that the overexpression of *dHEATR1* in a tumour background exacerbates tumourigenesis.

As mentioned in the Introduction (Section 1.5.1), HEATR1 contains only one HEAT repeat on its C-terminal end, which is its only known domain[141]. HEAT repeat domains are believed to be involved in protein-protein interactions[207]. Indeed, Prieto *et al*., (2007) found that UTP10, HEATR1's yeast orthologue, regulates rDNA transcription via binding chromatin in the rDNA repeat in a sequence-independent manner, as consequence of protein-protein interactions[149]. Moreover, HEATR1 was reported to have a cytoplasmic role in pancreatic cells, working as a scaffold protein between Akt and PP2A, further suggesting its role in protein-protein interactions[156]. Members of our group are still currently investigating whether HEATR1 and Myc interact physically, through co-

immunoprecipitation assays, but to date this has not been successful. As it is known that c-Myc forms a complex with NPM in mouse embryonic fibroblast cells, and this complex has a similar function to that observed for HEATR1 and Myc in GBM cells, it would be interesting to know whether HEATR1 belongs to the NPM/c-Myc complex, or if it is an independent interaction.

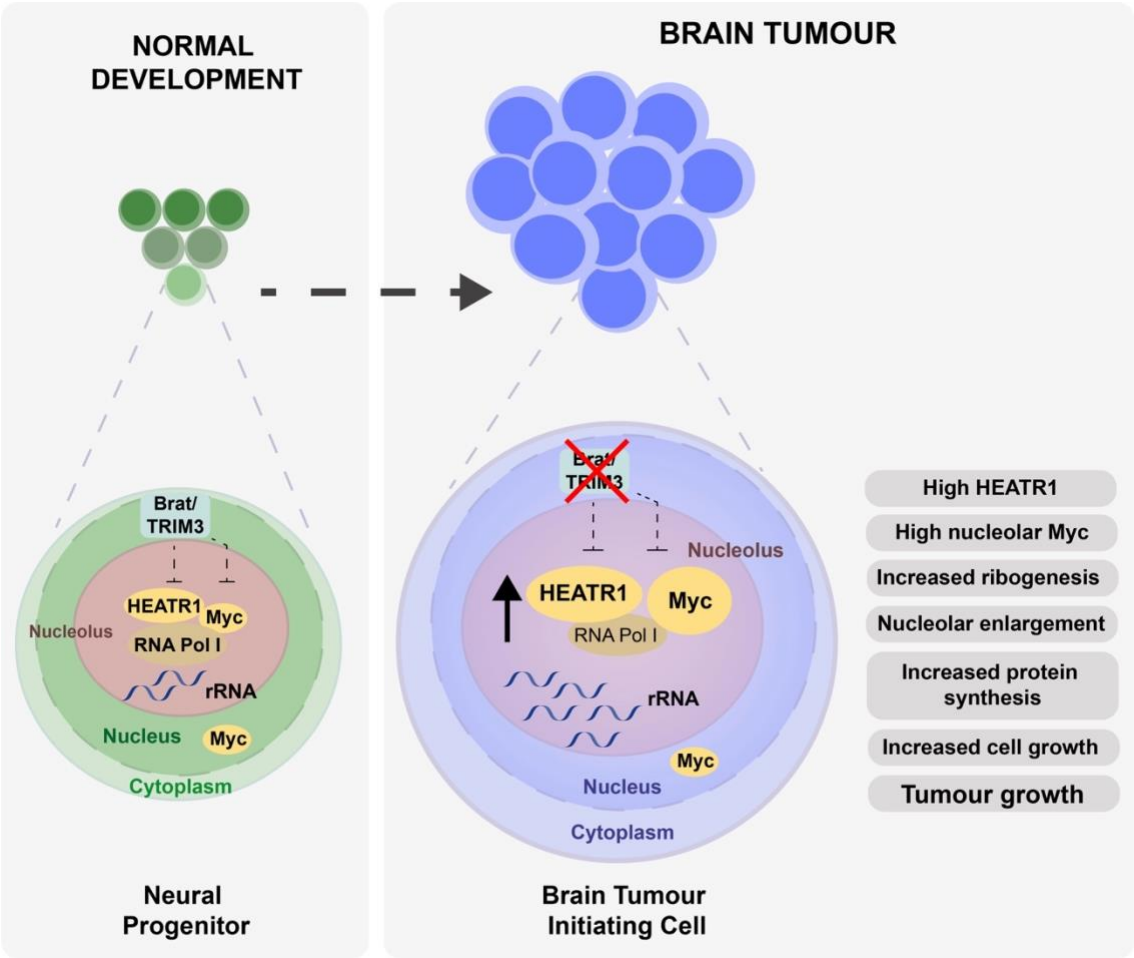

Figure 3.3 Proposed HEATR1 mechanism of action in brain tumour development. During normal development Brat/TRIM3 may inhibit both HEATR1 and c-Myc expression (directly or indirectly) maintaining their levels low. HEATR1 recruits c-Myc to the nucleoli, where they regulate RNA Pol I transcription of rDNA clusters into rRNA regulating ribosome biogenesis. In tumour cells, Brat/TRIM3 is lost and HEATR1 and c-Myc[7,98] are overexpressed. HEATR1 recruits higher levels c-Myc to nucleoli, enhancing RNA Pol I transcription of rDNA into rRNA and subsequent ribogenesis steps, which results in nucleolar enlargement and upregulated protein synthesis, which leads to increased cell growth and tumour growth.

3.9 Ribosome biogenesis and HEATR1 as a potential therapeutic target

It is now recognised that the hyperactivation of ribosome biogenesis is essential to promote cancer development, and therefore, it has been in the spotlight of cancer treatment for a while[143,173,204]. Moreover, it is known that expression of rRNAs and ribosome biogenesis factors directly control stem cell homeostasis and identity, and their deregulation, for example due to mutations in the respective genes, can lead to uncontrolled stem cell proliferation and tumour formation[198,208]. Loss-of-function mutations in tumour suppressors or activating mutations in some oncogenes lead to de-regulated signalling that stimulates Pol I transcription, resulting in upregulated ribosome biogenesis, protein synthesis, cell growth and proliferation[209].

In the past years, drugs targeting RNA Pol I transcription have been developed, showing promising therapeutic effects. Examples of these are CX-5461 and CX-3543, both small molecule fluoroquinolone derivates that selectively bind to G-quadruplex DNA structures, that are particularly enriched in rDNA[209]. These inhibit rDNA transcription by blocking binding of RNA Polymerase I complex components, such as nucleolin or SL1, to the promoter regions of rDNA, eventually leading to apoptosis of cancer cells[209]. Several phase I clinical trials of the CX-3543 compound in patients with carcinoid and neuroendocrine tumours have been successful, and a phase II clinical trial for the treatment of these malignancies was completed with preliminary evidence of clinical benefit[173,209]. Another compound recently described, which has been shown to specifically target RNA Pol I transcription, is metarrestin. This drug has been shown to inhibit metastatic development in three mouse models of human cancer, and extends survival of mice in a metastatic pancreatic cancer xenograft model with no organ toxicity[210].

The data presented in this thesis contributes to our knowledge on ribosome biogenesis in brain tumour initiation and development, including regulation of a major oncogene, c-Myc, by HEATR1. One could speculate that specifically targeting HEATR1 in brain tumours may be sufficient to modulate c-Myc activity in c-Myc-driven cancers, hampering tumour growth and leading to clinical benefits.

4 CONCLUSION

The overall aim of this candidate PhD thesis project was to characterise the role in brain tumour initiation and development of HEATR1, a candidate gene that arose from a single-cell transcriptome analysis of brain tumour initiating cells from the *Drosophila brat* model.

Using *Drosophila brat* as an *in vivo* brain tumour model[98,99,101], and GBM cell lines and patient-derived GSCs as human *in vitro* models, I investigated HEATR1 expression and function and identified a possible mechanism by which it acts in brain tumourigenesis, accomplishing the main goal of the study.

HEATR1 was found by our team upregulated in *Drosophila brat* tumour initiating cells, and I have contributed to show it is also overexpressed in high (GBM) and low grade (DA) glioma samples, and GSCs compared to controls. I have shown that HEATR1 is not required for the transformation of brain tumour initiating cells, but it is necessary for tumour initiation cell size growth and proliferation, and tumour growth development. I have further identified that HEATR1 acts by promoting ribosome biogenesis of tumour cells, which at least in part is mediated via recruiting the oncogene c-Myc to nucleoli, the cell's sites of ribogenesis. c-Myc is a master regulator of rDNA transcription and overall ribogenesis[129,181]. Increased ribogenesis results in upregulated protein synthesis and increased cell growth and proliferation, contributing to tumour cell growth. In summary, I have identified HEATR1 as a novel brain tumourigenesis player. These findings add to current knowledge in cancer research and may contribute to the development of future ribosome biogenesis-targeted therapies.

5 MATERIALS AND METHODS

5.1 *Drosophila* maintenance

All fruit fly stocks were maintained in vials or bottles for long-term storage at 18ºC and at 25ºC for on-going experiments. Stocks were kept in standard *Drosophila* food.

5.1.1 *Drosophila* standard food

Materials: 100g sugar, 50g dry yeast, 80g organic flour, 2g $(NH_4)_2SO_4$, 5g tartaric acid, 1.5g KH_2PO_4, 22g agar, 300ml grape juice, 10ml propionic acid and 1g nipagin (all chemicals were purchased from Sigma Aldrich). dH_2O to 1l.

For the preparation of 1l of standard fly food, sugar and dry yeast were dissolved completely in 500ml of boiling water. Organic flour was mixed into 200ml of water until a smooth paste was formed, and then added to the boiling water to dissolve. Two g of ammonium sulphate, 5g of tartaric acid and 1.5g of potassium phosphate monobasic were added to the water and boiled for 10 minutes. Agar was mixed with the grape juice in two separate batches (11g:150ml), slowly added to the mixture and boiled for another 10 minutes. The mixture was left at room temperature to cool down, and 1g of nipagin diluted in 10ml of propionic acid was added at 70ºC. Approximately 2cm high of food was added to each vial or bottle.

5.1.2 *Drosophila* agar plates

Materials: 800ml dH_2O, 21g agar, 200ml grape juice.

For the preparation of 1.2l of plate food, 21g of agar were mixed with 200ml of grape juice and slowly added to 1l of boiling water. The mixture was poured into small petri dish plates.

5.1.3 *Drosophila* genetic crosses and staging of embryos and larvae

Fly stocks were maintained in vials or bottles with standard *Drosophila* food at 18ºC for long-term maintenance and at 25ºC for ongoing experiments. Fly strains needed for experiments were grown in multiple bottles to yield maximum female virgin collections. Female virgins were collected every 3 hours (maximum) and stored with a similar number of the appropriate males at 18ºC[211]. The resulting crosses were transferred to egg-lay chambers assembled on top of agar juice plates supplemented with yeast paste and maintained at 25ºC. The plates were changed at least twice a day for two days. By the second day the flies were placed on a fresh agar plate and allowed to lay for one hour. Eggs laid during this time were transferred onto a fresh plate and left at 25ºC, allowing them to develop till the appropriate stage. Larvae were transferred every day to fresh plates in order to monitor their development.

5.1.4 *Drosophila* strains

Drosophila stocks were obtained from different sources. The *Drosophila* line pointed-Gal4 (Gal4$^{14-94}$) on chromosome III[158] was a gift to Dr. Barros laboratory by Dr. Jan laboratory (Howard Hughes Medical Institute, University of California, USA). *Drosophila* UAS line expressing mcd8-GFP (UAS-mcd8-GFP)[159] (BL5137) and UAS-brat-RNAi[126] (BL34646) were obtained from the Bloomington *Drosophila* Stock Centre (BSDC). The UAS-dHEATR1-RNAi[154] strain (V17000) is from the Vienna *Drosophila* Resource Centre. *Drosophila* stocks were obtained from different sources. The *Drosophila* line pointed-Gal4 (Gal4$^{14-94}$) on chromosome III[158] was a gift to Dr. Barros laboratory by Dr. Jan laboratory (Howard Hughes Medical Institute, University of California, USA).

The lines UAS-mcd8-GFP;pointed-Gal4 (used as control) and UAS-dHEATR1-RNAi;UAS-brat-RNAi (referred to as dHEATR1;brat-RNAi in the results section) were engineered in Dr. Barros laboratory by previous members of the group. For type II NSC lineage-RNAi knockdown assays UAS-mcd8-GFP;pointed-Gal4 flies were crossed with the appropriate RNAi line and assays were performed in the progeny.

5.2 Cells, media and culture conditions

5.2.1 Immortalised GBM and human Neural Stem cell lines

Cell lines used in this project included the immortalised glioma cell lines U87MG (American Type Culture Collection (ATCC) HTB-14) and U251MG (ATCC CRL-1690), and the human embryonic kidney HEK 293T line (ATCC CRL-11268). Cells were cultured in Advanced DMEM (Dulbecco's Modified Eagle Media) (Gibco) supplemented with 10% Foetal Bovine Serum (FBS) (Sigma), 2mM L-Glutamine (Gibco), 1x non-essential amino acids solution (Gibco 100X) and 100U/ml penicillin/streptomycin (Gibco). In all cases, cells were maintained at 37ºC in a 97% humidity atmosphere containing 5% CO_2, following standard procedures.

Cell lines were grown up to 70-80% confluency (from 2 to 4 days depending on the cell line and initial density) and then passaged. Cells were washed with Phosphate-Buffered Saline (PBS) (Gibco) and Trypsin- Ethylenediaminetetraacetic acid (EDTA) (0.05%) (Gibco) was added and incubated at 37ºC for approximately 3 minutes until cells detached. Trypsin was neutralised with complete media and the cell suspension was spun at 1200rpm for 5 minutes. The supernatant was then removed, the cell pellets resuspended in media, and plated in a 1:5 dilution.

A Neural Stem Cell (NSC) line derived from six weeks old foetal forebrain was obtained from the Glioma Cellular Genetics Resource (MRC Institute of Genetics and Molecular Medicine, The University of Edinburgh, Cancer Research, UK). NSCs were cultured in DMEM:F12 supplemented with 1.45g/l Glucose (Sigma), 1X non-essential amino acids solution (Gibco 100X), 100U/ml penicillin/streptomycin (Gibco), 0.012% BSA (Gibco), 0.1mM 2-Mercaptoethanol (Gibco), 0.5% B27 supplement (Gibco) and 0.5% N2 supplement (Gibco). Mouse Epidermal Growth Factor (EGF) (10ng/ml, Peprotech), human Fibroblast Growth Factor (FGF) (10ng/ml, Peprotech) and laminin (1μg/ml, Sigma) were added fresh to the media immediately before using it. When cells reached 70-80% confluency they were passaged as previously described for immortalised cell lines.

5.2.2 Patient derived GBM stem cell lines

Patient-derived GBM CSCs (GSCs), GSC-5 and GSC-8, were kindly provided by Dr. Izquierdo (Molecular Biology Department, Autonomous University of Madrid, Spain). The lines were isolated from GBMs of two different specimens from the Hospital Universitario Ramón y Cajal in Madrid, Spain[83]. None of the patients were treated with radiotherapy before the extraction of the samples. The lines are described in Gil-Ranedo *et al.,* (2011)[83]. Briefly, they grow exponentially forming floating neurospheres even when seeded at low density, indicating a strong self-renewal capacity, and were largely positive for several stem cell markers such as CD133 (76%), nestin (over 95%), Sox2 (over 95%), vimentin (over 95%) and nucleostemin (88%). When the cells were cultured in differentiation-inducing media they displayed the typical neural lineage phenotype, which was confirmed by immunostaining with β-III-tubulin and MAP2 (neurons), NG2 (oligodendrocytes) and GFAP (astrocytes). The karyotypic analysis showed alterations reflecting transforming activity and clonogenicity assays in soft agar and rat xenografts indicated a high tumourigenic potential. The lines formed large highly infiltrative tumours in 100% of the cases in xenografted rats and explants of these tumours were serially transplanted into the brains of other nude rat hosts generating lethal tumours that were equally enriched for CSCs, demonstrating high self-renewal capacity. Histopathological analysis of the xenografts revealed the typical GBM characteristics, pseudopalisades and focal necrosis, high cellularity, high epidermal growth factor receptor (EGFR) and high proliferative index (MIB-1). Their analysis shows that the transplanted tumours were phenocopies of the original patient's tumour[83].

GSCs were cultured using DMEM:F12 (1:1) supplemented with GlutaMax (Gibco), 0.5% AlbuMax I (Gibco), 5mM HEPES (Gibco), 0.6% glucose (Sigma), 10μg/ml N2 (Invitrogen), 2μg/ml Heparin (Sigma), 20ng/ml of both EGF and FGF-2 (Peprotech) and 1X non-essential amino acids solution (Gibco 100X). Cultures were grown at 37ºC in a 97% humidity atmosphere containing 5% CO_2 and fed twice a week with 20% volume of

fresh medium[83]. In these conditions, neurospheres developed in one to two weeks. When their size reached 200–300 mm, neurospheres were spun at 1000rpm for 5 minutes and dissociated with Trypsin-EDTA (0.05%) (Gibco) and manual pipetting once the supernatant was discarded. Trypsin was then blocked with the same volume of FBS containing DMEM and cells were spun at 1200rpm for 5 minutes. The supernatant was then removed, the cell pellets resuspended in GSC medium, and plated in a 1:5 dilution for normal passage or at the desired density for each assay.

5.2.2.1 Differentiation of GCSs

GSCs were differentiated as described in Gil-Ranedo et., al[83] (2011). Briefly, the cells were cultured at a density of $2.5x10^4$ on glass coverslips treated with a layer of Matrigel (Becton Dickinson) diluted 1/50 in DMEM:F12. The cells were maintained for 12 days in GSC media described above but deprived from FGF-2 and EGF and supplemented with 0.5 % FBS, and 10 μM all-trans retinoic acid (Sigma). The FBS complement system was previously inactivated by incubation at 56ºC for 30 minutes. This media was replaced once after 6 days with fresh media. Differentiation of the cells was verified by immunostaining against neural markers: β-III-tubulin (neurons), Olig2 (oligodendrocytes) and GFAP (astrocytes).

5.3 Growing plasmid DNAs

Luria-Bertani (LB) broth with Lennox L agar (ThermoFisher) was prepared from powder, autoclaved, and cooled down to around 50ºC to add the antibiotic carbenicillin 100μg/ml (Sigma). The medium was then poured into bacterial culture petri dishes and let solidify at room temperature. Bacterial glycerol stocks were kept at -80ºC and taken right before inoculating the plates with a pipette tip dipped in the bacterial tube. The plates were incubated upside down overnight at 37ºC. The next morning a swab of the colonies was taken with a pipette tip, inoculated into 5ml of liquid LB broth supplemented with carbenicillin 100μg/ml in a bacterial culture tube, incubated for at least 6 hours at

37ºC with shaking and then transferred to a bigger flask containing at least 250ml LB broth and incubated overnight. DNA plasmids were extracted from the bacterial cultures using GeneJet Plasmid Midiprep Kit (ThermoFisher) following the manufacturer's instructions. Concentration of the obtained cDNA was measured using a NanoDrop 2000 (Thermo Scientific).

5.4 Transfection of cells in culture

For small interfering RNA (siRNA) experiments, 200.000 cells per well were seeded in 6-well plates in DMEM supplemented with 10 % FBS and allowed to attach overnight. Transfections were performed with 15 ng of MISSION esiRNA (Sigma), which is an endoribonuclease-prepared siRNA pool comprised of a heterogeneous mixture of siRNAs that target the same mRNA sequence[212], using Lipofectamine 2000 (Invitrogen) in OptiMEM (Gibco) medium following the manufacturer's protocol. [212], using Lipofectamine 2000 (Invitrogen) in OptiMEM (Gibco) medium following the manufacturer's protocol. Cells were incubated overnight and medium changed to DMEM supplemented with 10 % FBS. All assays were performed at 48 and 72 hours post-transfection.

For plasmid transfection experiments, cells were transfected as described above but using 0.5μg (qPCR assays) or 1μg (localization assays) of pCMV-HA (control) or the human c-Myc full length cDNA cloned into the pCMV-HA-N vector[213] (pCMV-HA-h-c-Myc), both kindly provided by Dr. Murai (The Jikei University School of Medicine, Japan) and/or 1μg of pIRES-FLAG or pIRES-FLAG-HEATR1[156], a gift from Prof. Lou (Mayo Clinic, USA). Cells were processed 6, 18, and 24 hours after transfection.

5.5 Lentiviral infection of cultured cells

5.5.1 Lentiviral particle generation

For the packaging of lentiviral vectors enabling knockdown of *HEATR1,* five validated *HEATR1* MISSION short hairpin RNAs (shRNAs) cloned into the pLKO.1 lentiviral vector

were purchased from Sigma Aldrich as bacterial glycerol stocks (SHCLNG-NM_018072; **Table 2**) and grown as described above (section 5.3). The base vector pLKO.1 contains a puromycin resistance sequence. In all cases the empty vector MISSION pLKO.1-Puro (Sigma Aldrich) was used as a control.

HEK 293T were transfected using Lipofectamine 2000 (Invitrogen) and Opti-MEM (Gibco) following manufacturer´s guidance. For the transfection of each shRNA vector $5.5x10^6$ 293T cells were seeded in 100mm tissue culture dishes (Thermo Scientific). The following were used: 10μg of the HEATR1 MISSION shRNA, 5μg of the packaging plasmid psPAX2 (created by Didier Trono, Addgene plasmid #12260) and 5μg of the packaging plasmid pMD2.G (also created by Didier Trono, Addgene plasmid #12259). After 24 hours, OptiMEM was replaced for CSC media, as described above, and incubated 54-56 hours, allowing the cells to produce lentiviral particles. Supernatant containing the virus was then collected, filtered (0.45μm pore), aliquoted and stored at -80ºC or used immediately.

Name	Reference	Sequence
Sh22	TRCN0000137322	CCGGGCAGAGTTGATGGAAGATGAACTCGAGTTCATCTTC CATCAACTCTGCTTTTTTG
Sh39	TRCN0000133839	CCGGCCCAGAACATTAGATGTTGTACTCGAGTACAACATC TAATGTTCTGGGTTTTTTG
Sh50	TRCN0000137850	CCGGGCACAGATGGTTCTGGTTGTTCTCGAGAACAACCA GAACCATCTGTGCTTTTTTG
Sh62	TRCN0000137162	CCGGGCTACCAGAATCCATTCCTTTCTCGAGAAAGGAATG GATTCTGGTAGCTTTTTTG
Sh97	TRCN0000136697	CCGGGCTGAACAAGTCCGAATAGAACTCGAGTTCTATTCG GACTTGTTCAGCTTTTTTG

Table 2. HEATR1 shRNAs tested.

5.5.2 Lentiviral transduction

Transduction of lentiviral vectors in GSCs was performed as described in Gil-Ranedo *et al*.,[83] (2011). Briefly, GSCs were seeded at a concentration of $6x10^4$ per cm^2 in Opti-MEM and incubated for 6 hours. Once cells were adhered to the well, OptiMEM was replaced with CSC media and lentiviral-containing supernatant (1ml supernatant with

viral particles: 5ml CSC media) supplemented with 4μg/ml polybrene (Sigma). After 12 hours incubation, cells were detached from the substrate by manual pipetting and cultured in CSC proliferating media. Puromycin (0.8μg/ml; Gibco) was added 8 hours after the media was changed and the cells were maintained 7 days at 37ºC in a 97% humidity atmosphere containing 5% CO_2 before being harvested.

For transduction in U87MG cells, the above protocol was used with minor modifications. $2x10^4$ cells were seeded per M6 well in 1.4ml of DMEM supplemented with 10 % FBS and allowed to attach overnight. The following morning, 0.6ml of lentiviral-containing supernatant (as described above) and 4μg/ml polybrene (Sigma) were added to the cells. After overnight incubation, the medium was replaced with DMEM supplemented with 10% FBS. As for the procedure using GSCs, puromycin 0.8μg/ml was added 8 hours after the medium was changed, and cells maintained for 7 days at 37ºC in a 97% humidity atmosphere with 5% CO_2 before being harvested.

In all cases, a negative control for efficient infections, comprising of non-infected cells was also used. The cells died a few days after the puromycin was added.

5.6 Soft agar GSC colony formation assay

Soft agar assays were conducted as described by Gil-Ranedo et., al (2011)[83]. GSCs were infected with lentiviral particles mediating expression of the chosen shRNAs and cultured under selection pressure in CSC proliferating medium containing puromycin (0.8μg/ml) for 7 days. A basal layer of agar was prepared mixing equal volumes of sterile agar (1%) and 2X CSC proliferating medium, obtaining a final solution of 0.5% agar in 1X media. For the top layer 0.7 % sterile agar was mixed with 2X CSC proliferating medium as the appropriate number of dissociated cells (5.000cells/ml CSC-5, 2.500cells/ml) was immediately added, obtaining a final concentration of 0.35% agar in 1X medium. Cells were cultured for 10 days and viable colonies were detected by applying 1ml/well of 0.6mg/ml of Thiazolyl Blue Tetrazolium Bromide, also known as MTT (Sigma Aldrich), in proliferating medium and photographed with a Leica DM1000

LED microscope coupled to a Leica MC170 HD camera. Regions of interest (ROIs) of the same size were determined for each condition and colony number was scored using the Nucleus Counter plugin included in Fiji/ImageJ[214] **(Figure *5.1*)**.

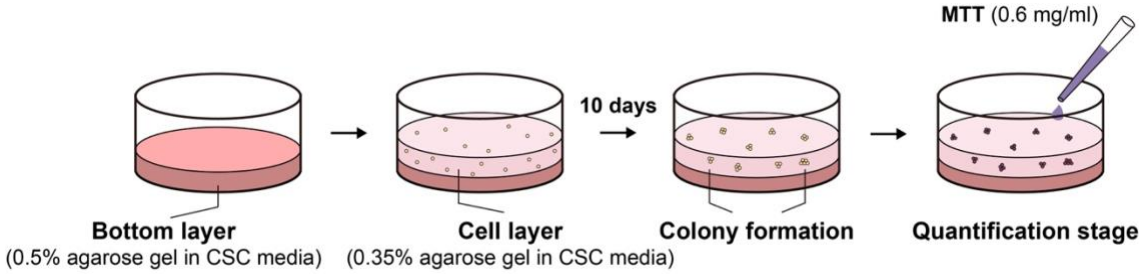

Figure 5.1 Schematic representation of the soft agar colony formation GSC assay protocol.

5.7 Immunostainings

5.7.1 Immunohistofluorescence (IHF) of *Drosophila* larval brains

Immunohistofluorescence (IHF) assays were performed as previously described[215] with minor modifications. Larval brains were dissected in PBS (8g NaCl, 0.2g KCl, 1.44g NA_2HPO_4, 0.24g KH_2PO_4, pH 7.4 in 1l H_2O) at the appropriate developmental stage and fixed for 20 minutes in 4% formaldehyde in PBS and supplemented with 0.5μM EGTA and 5μM $MgCl_2$ (1st instar larvae) or 1μM EGTA and 10μM $MgCl_2$ (2nd and 3rd instar larvae). All chemicals were purchased from Sigma Aldrich. Brains were then washed with PBS and incubated in blocking buffer (PBS-1% Triton X-100 (PBS-T), 1% FBS) for 1 hour at room temperature. Primary antibodies **(Table 3)** were diluted in PBS-T and incubated overnight at 4ºC. Larval brains were washed with PBS-T and incubated with appropriate secondary antibodies **(Table 4)** diluted 1:200 for 2 hours at room temperature. Secondary antibodies were washed in PBS-T and brains were successively embedded in 50% (>30 mins) and 70% (>3 hours) glycerol before being mounted on a microscope slide in a 1:1 mix of Vectashield media (Vector Laboratories) and 70% glycerol. All incubation steps were performed on continuous shaking except for overnight and glycerol incubations.

Primary Antibody	Species	Dilution; Purpose	Source
Ase	Rabbit	1:10000; IF	Gift from Y. Nung Yan
BAX	Mouse	1:500; WB	Santa Cruz (sc-7490)
c-Myc	Mouse	1:100; IF	Santa Cruz (sc-40)
c-Myc	Rabbit	1:500; WB	Cell Signalling Technologies (5605)
Casp3	Rabbit	1:1000; WB	Abcam (ab13847)
dMyc	Guinea Pig	1:100	Gift from G. Morata
Dpn	Guinea Pig	1:2000; IF	Gift from J. Knoblich
FBL	Rabbit	1:500; WB 1:200; IF	Abcam (ab5821)
GFP	Chicken	1:500; IF	Millipore (06-896)
GFP	Rabbit	1:1000; IF	Gift from U. Mayor
HA High affinity	Rat	1:1000; IF	Roche (11867423001)
HEATR1	Mouse	1:500; WB 1:100; IF	Santa Cruz (sc-390445)
Ki67	Mouse	1:75; IF	Dako (M7240)
Ki67	Rabbit	1:500; IF	Sigma Aldrich (10250)
NPM (b23)	Mouse	1:100; IF	Santa Cruz (sc-271737)
Olig-2	Rabbit	1:500; IF	Chemicon
P21 Waf1/Cip1	Rabbit	1:1000; WB	Cell Signalling Technologies (2947)
p53	Mouse	1:500; WB	Santa Cruz (sc-126)
PH3	Mouse	1:500; IF	Abcam (ab5176)
RPA194	Mouse	1:500; WB 1:50; IF	Santa Cruz (sc-48385)
UBF	Mouse	1:100; IF 1:500; WB	Santa Cruz (sc-13125)
α-Tubulin	Mouse	1:1000; WB	Sigma Aldrich (T5168)
β-Actin	Mouse	1:10000; WB	Cell Signalling Technologies (4967)
β-III-Tubulin	Rabbit	1:100; IF	Sigma Aldrich (ZRB1140)

Table 3: Primary antibodies used for immunofluorescence (IF) or western blot (WB).

Secondary Antibody	Dilution; Purpose	Source
Goat Anti-Mouse 488	1:200; IF	Thermo Fisher (A-10667)
Goat Anti-Mouse 568	1:200; IF	Thermo Fisher (A-11004)
Goat Anti-Mouse 633	1:200; IF	Thermo Fisher (A-21052)
Goat Anti-Guinea Pig 633	1:200; IF	Thermo Fisher (A-21105)
Goat Anti-Guinea Pig 568	1:200; IF	Thermo Fisher (A-11075)
Goat Anti-Chicken 488	1:200; IF	Thermo Fisher (A-11039)
Goat Anti-Rabbit 488	1:200; IF	Thermo Fisher (A-11008)
Goat Anti-Rabbit 568	1:200; IF	Thermo Fisher (A-11036)
Goat Anti-Rabbit Cy5	1:200; IF	Thermo Fisher (A-10523)
Goat Anti-Rabbit IgG – HRP	1:10000; WB	Cell Signalling Technologies (7074)
Goat Anti-Mouse IgG – HRP	1:10000; WB	Cell Signalling Technologies (7076)

Table 4: Secondary antibodies used for immunofluorescence (IF) or western blotting (WB). HRP, Horse Radish Peroxidase.

5.7.2 Immunocytofluorescence (ICF)

Cell lines were seeded at a concentration of $5x10^4$ on glass coverslips and fixed with 4% formaldehyde for 15 minutes. For GSCs' stainings[83], coverslips were pre-coated with a laminin (10μg/ml, Sigma) matrix for at least one hour at 37ºC and washed 3 times with PBS. GSCs neurospheres were dissociated, seeded at a density of $5x10^4$ on the treated coverslips, incubated overnight, and fixed. Washes were performed using PBST (PBS, 0.2% Triton X-100) and cells permeabilised for 15 minutes in this buffer, blocked 20 minutes with 0.1% Triton X-100 and 1% FBS in PBS and incubated with primary antibodies **(Table 3)** overnight at 4ºC. Primary antibodies were washed with PBST and appropriate secondary antibodies **(Table 4)** were diluted 1:200 in PBST and incubated for 1 hour at room temperature. In all cases nuclei were counterstained with DAPI (15 minutes, 1:1000) and mounted on microscope slides with ProLong Diamond (Invitrogen).

5.8 EdU, EU and OPP incorporation assays

Assays were performed using Click-iT kits (Invitrogen) and following manufacturer's instructions using $5x10^4$ cells seeded on glass coverslips. To detect mitotic activity using EdU incorporation, cells on coverslips were incubated for 1 hour in 10μM 5-ethynyl-2´-deoxyuridine (EdU)/MEM at 37ºC (Click-iT EdU Imaging Kit, Invitrogen) and fixed in 4% formaldehyde in PBS. In this assay the modified thymidine analogue, EdU, is incorporated into newly synthesised DNA and fluorescently labelled with a photostable Alexa Fluor dye. EdU incorporation was combined with Ki67 antibody labelling, which was performed after the Click-It reaction between the azide-containing dye and the EdU as described above. Slides were systematically imaged and all cells that showed any EdU staining were counted as EdU positive.

To detect rRNA synthesis, cells on coverslips were incubated for 1 hour at 37ºC in 1mM 5-ethynyl uridine (EU)/MEM (Click-IT EU RNA labelling Kit, Invitrogen). EU is an alkyne-modified nucleoside that is actively incorporated into nascent RNA, the small size

of the tag enables efficient incorporation into RNA but not into DNA. The modified nucleoside is then detected by the chemoselective reaction between an azyde-containing dye and the EU. Coverslips were mounted on microscope slides as specified above. EU intensity was quantified in FiJi from images acquired using the same laser power and gain settings throughout all the conditions by measuring the total signal intensity in the region occupied by a mask corresponding to DAPI staining and normalizing it to the DAPI area.

To detect protein synthesis, 20µM O-propargyl-puromycin (OPP) was added to the cells medium and incubated for 30 minutes at 37ºC (Click-iT Plus OPP Alexa Fluor 647 Protein Synthesis Assay Kit, Invitrogen). OPP is an alkyne analogue of puromycin, which is incorporated into newly synthesised proteins. After fixation, OPP was detected by adding a pycolil azide-containing dye according to the manufacturer's instructions. Coverslips were mounted on microscope slides as previously described and OPP intensity was measured in FiJi from images acquired using the same laser power and gain settings throughout the conditions by quantifying the total signal intensity in the whole image field and normalising it to the number of cells in the image.

5.9 Cell death (TUNEL) assays

Terminal deoxynucleotidyl transferase-mediated dUTP nick end labeling (TUNEL) technology (In situ Cell Death Detection Kit, Roche Applied Science) was used to detect apoptosis at a single-cell level by labelling DNA strand breaks. Following manufacturer's instructions cells were seeded at a density of $5x10^4$ on glass coverslips and fixed with 4% formaldehyde for 15 minutes. Coverslips were washed in freshly prepared 0.1% sodium citrate ($Na_3C_6H_5O_7$), 0.1% Triton diluted in PBS and incubated in this buffer for 5 minutes on ice for permeabilization. TUNEL enzyme solution was mixed with label solution (1:10), added to the cells and incubated for one hour at 37ºC in a humidified atmosphere in the dark. Cells were then rinsed three times with PBS and mounted on microscope slides with ProLong Diamond antifade mountant with DAPI (Invitrogen).

The same protocol was optimised for TUNEL detection in *Drosophila* CNS. Briefly, larval brains were dissected 93 HPH in PBS and fixed for 20 minutes in 4% formaldehyde in PBS supplemented with 1μM EGTA and 10μM $MgCl_2$. The brains were then washed in 0.1% sodium citrate, 0.1% Triton diluted in PBS and incubated in this buffer for 30 minutes at 4ºC. TUNEL reaction was prepared as above and incubated for one hour at 37ºC in a humidified atmosphere in the dark. The brains were washed in PBS and incubated in primary antibodies **(Table 3)** overnight at 4ºC, washed again, and incubated in secondary antibodies **(Table 4)** for 2 hours at room temperature. Secondary antibodies were washed, and the brains were mounted on microscope slides as previously described.

5.10 C-Myc localization assay

Inhibition of cells' proteolysis is widely used to enable the visualization of nucleolar c-Myc[182]. For this purpose, the proteasome inhibitor MG132 (Sigma) was used following published protocols[184]. U87MG cells per M6 well were seeded in DMEM supplemented with 10% FBS. Once they were attached this medium was replaced with 1.4ml of fresh DMEM supplemented with 10% FBS, 0.6ml of shRNA lentiviral particle containing media, and 4μg/ml polybrene (Sigma). The next day the medium was replaced by fresh DMEM supplemented with 10%FBS and 0.8μg/ml of puromycin (Gibco) was added 8 hours later. After 6 days, cells were passaged, seeded on glass coverslips at a concentration of $5x10^4$ and let to attach overnight. The next day, cells were transfected with 1μg of pCMV-HA-h-c-Myc or pCMV-HA (control) using Lipofectamine 2000 (Invitrogen) in OptiMEM following manufacturer's instructions and incubated for 6 hours. During this time the cells were treated with 5μM of MG132 for 3 hours. DMSO was used as vehicle control in cells cultured in parallel. Cells were fixed and immunostained as described above (section 5.7.2).

5.11 Brain tumour tissue and cell lysate preparation

Brain tumour and control tissue samples **(Table 5)** were obtained by Dr. Barros via the Brain UK biobank (licence 14004) and immediately processed into protein lysates by trained members of the Barros team in compliance with the Human Tissue Act and following established protocols (adapted from Sigma Aldrich). Tissues were manually homogenised in lysis buffer consisting of radioimmunoprecipitation assay (RIPA) buffer (50mM Tris-HCl pH 7.5; 300mM NaCl, 0.5% SDS, 1% Triton X-100 and 10mM PMSF) supplemented with protease inhibitor (cOmplete, EDTA-free; Sigma Aldrich) and phosphatase inhibitors (Cocktails B and C; Santa Cruz Biotechnology). Cells in culture were similarly lysed in 100μl of complete RIPA lysis buffer per $5x10^5$ cells and incubated for 30 minutes on ice. Both tissue and cell extracts were spun at 14,000rpm for 30 minutes at 4ºC and supernatants collected and transferred to fresh 1.5ml microcentrifuge tubes. Protein concentrations were determined using a Pierce BCA protein assay kit (Thermo Scientific) as specified by the manufacturer and measured in a multi-well microplate reader PHERAstar FS (BMG Labtech). Samples were used immediately or stored at -80ºC.

Study Number	Patient Age	Patient Sex	Location	Neuropathology Diagnosis	IDH status
9	33	Male	Frontal	Non-tumourous/ normal	-
10	22	Male	Frontal	Non-tumourous/ normal	-
20	57	Female	Frontal	Non-tumourous/ normal	-
77	77	Male	Frontal cortex	Non-tumourous/ normal	-
78	61	Male	Cerebellum	Non-tumourous/ normal	-
79	65	Male	Cerebellum	Non-tumourous/ normal	-
55	38	Female	Frontal	DA	IDH mutant
56	38	Male	Frontal	DA	IDH mutant
57	44	Male	Intra/periventricular	DA	IDH mutant
61	31	Male	Frontal	DA	IDH mutant
63	37	Female	-	DA	IDH mutant
15	55	Female	Cortex	GBM	-
22	73	Female	Temporal	GBM	-
29	68	Male	Parietal	GBM	-

35	65	Female	Frontal	GBM	-
42	73	Female	Frontal	GBM	-
43	69	Female	Frontal	GBM	-
44	41	Female	Frontal	GBM	-
45	54	Male	Frontal	GBM	-
46	61	Male	Frontal	GBM	-
65	23	Female	Frontal	GBM	IDH wt
68	77	Male	Frontal	GBM	IDH wt
70	61	Male	Temporal	GBM	IDH wt
71	55	Male	Frontotemporal	GBM	IDH mutant
73	51	Female	Temporoparietal	GBM	IDH wt

Table 5: Human tissue samples used for western blot analysis. DA, grade II diffuse astrocytoma. GBM, grade IV glioblastoma multiforme. All information was provided by Dr. David Hilton (Brain Bank Deputy director, Senior consultant neuropathologist Plymouth Derriford Hospital, NHS). Samples obtained via the Brain UK biobank under licence 14004. Isocitrate dehydrogenase (IDH) mutational status, wild type (wt) or mutant. Information not available for those in which it is not specified.

5.12 Western Blot

Western blot was performed following standard procedures. To each sample lysate, a dilution of 1:5 Laemmli loading buffer (2% SDS, 5% 2-mercaptoethanol, 10% glycerol, 0,02% bromophenol blue and 0.065M Tris, all chemicals purchased from Sigma Aldrich) plus RIPA buffer up to the desired volume was added for equal protein loading. Samples were boiled for 5 minutes, loaded on SDS-polyacrylamide gels and separated by electrophoresis (SDS-PAGE). The polyacrylamide percentage varied depending on the molecular weight of the protein of interest. Proteins were separated at 95V at room temperature in running buffer (3g Tris, 14.4g glycine, 1g SDS to 1l of dH_2O) until resolved and transferred to a polyvinylidene difluoride (PVDF) membrane (Amersham Hybond), previously activated in methanol for 3 minutes. Protein transfer was performed at 35mA overnight at 4ºC in transfer buffer (3g Tris, 14.4g glycine, 200ml MeOH to 800ml of dH_2O). For HEATR1 blotting, transfer buffer was supplemented with 0.1% SDS. Membranes were next blocked with 3% BSA in PBS-0.4% Tween for 1 hour at room temperature followed by overnight incubation with primary antibodies at 4ºC **(Table 3)**. β-Actin or α-Tubulin were used as loading controls in all cases. Membranes were washed

in 0.4% tween-20 in PBS and incubated for 2 hours at room temperature with the appropriate secondary antibodies **(Table 4)**. After incubation, membranes were again washed, and detection was achieved applying the enhanced chemiluminescence (ECL) or ECL plus western blotting substrate (Pierce) for 5 minutes in the dark. Membranes were exposed to CL-XPosure films (Thermo Scientific) to detect chemiluminescence signal and developed. Densitometric analyses of the bands were performed using FiJi v1.0.

5.13 RNA and complementary DNA (cDNA) synthesis generation

RNA was isolated from $2x10^5$ cultured cells using the RNAaqueus-Micro Kit (Invitrogen) following the manufacturer's instructions and treated with DNase I to remove traces of contaminating genomic DNA. RNA concentration was measured using a NanoDrop 2000 (Thermo Scientific). cDNA was produced via reverse transcription from 500 ng of RNA template following manufacturer's instructions. In a 0.2ml PCR microtube, the RNA was diluted in up to 20μl of 0.1 % diethylpyrocarbonate (DEPC) treated dH_20 and mixed with 2μl of PolyT-anchored primer and 2μl of Smart Primer **(Table 6)**. The mix was incubated for annealing at 65 ºC for 3 minutes in a thermocycler and then cooled down on a frozen rack. Next, 8μl of 5x First Strand buffer (250mM), 4μl of DTT (0.1M), 2μl of dNTPs (10mM each), 1μl of SUPERase-In and 1μl of SuperScript II (all from Invitrogen) were added to each sample and incubated at 42ºC for 90 minutes for reverse transcription. The reaction was then inactivated by heating the samples at 65ºC for 15 minutes. Digestion of the RNA strand of the RNA/cDNA hybrids was achieved by treating the samples with 1μl of RNase H (Invitrogen) and 4μl of 10x RNase H buffer (Invitrogen) and incubating at 37ºC for 20 minutes following by inactivation by heating at 65ºC for 15 minutes. cDNA concentration was measured by loading 1μl of the sample to a NanoDrop 2000 (Thermo Scientific).

5.14 Real-time quantitative PCR (RT-qPCR)

RT-qPCR was performed using Power SYBR Green PCR Master Mix (Thermo Scientific) on a StepOnePlus Real Time PCR system (Thermo Scientific) following the Applied Biosystems guide for RT-qPCR (2008). PCR reaction mixtures were prepared by adding 0.5µl of each primer (forward and reverse, 10µM) **(Table 6)**, 5µl of SYBR Green master mix, 3.5µl of dH_2O and 5ng of cDNA per sample. 60S Ribosomal Protein L32 (RPL32) was used as an internal calibrator in all reactions as it has been described as a suitable control to normalise gene expression in tumours[216]. The following RT-qPCR conditions were used: initial denaturation at 95ºC for 15 minutes, followed by 35 cycles of denaturation at 95ºC for 1 minute and annealing and extension at 60ºC for 1 minute. Data was analysed using the Livak ΔΔCT method[217].

Primer name	Sequence (5' to 3')
HEATR1-Fw	GGTCTGAACACTTCGCTCCA
HEATR1-Rv	TACTGGCCTGGAAGAGTTGC
47S pre-rRNA-Fw	CCTGCTGTTCTCTCGCGCGTCCGAG
47S pre-rRNA-Rv	AACGCCTGACACGCACGGCACGGAG
18S - Fw	AAACGGCTACCACATCCAAG
18S - Rv	CCTCCAATGGATCCTCGTTA
5.8S - Fw	CTCTTAGCGGTGGATCACTC
5.8S - Rv	GACGCTCAGACAGGCGTAG
28S - Fw	CAGGGGAATCCGACTGTTTA
28S - Rv	ATGACGAGGCATTTGGCTAC
c-Myc - Fw	CCTCTCAACGACAGCAGCT
c-Myc - Rv	CAGAAGGTGATCCAGACTCTG
RPL32 - Fw	CATCTCCTTCTCGGCATCA
RPL32 - Rv	AACCCTGTTGTCAATGCCTC
Poly-T anchored	AAGCAGTGGTATCAACGCAGAGTACT(26)VN
Smart	AAGCAGTGGTATCAACGCAGAGTACGCrGrGrG

Table 6: List of primers used in this study. *HEATR1, 47S pre-rRNA, 18S, 5.8S, 28S, c-Myc* and *RPL32* were used for RT-qPCR, being RPL32 the calibrator. *Poly-T anchored* and *Smart* primers were used for reverse transcription. Fw, forward; Rv, Reverse.

5.15 Image acquisition and processing

Confocal images were acquired on a Leica SP8 or a Leica SPE confocal laser-scanning microscope using LAS X software. Larval CNS immunohistochemistry quantifications were made using z-stacks comprising whole brain lobes using a 0.5μm step size for 1st instar larvae and 1.5μm step size for 2nd and 3rd instar. All representative images shown in the Results section are single optical sections. Images were processed and phenotypes quantified using FiJi v1.0 and/or Adobe Photoshop v21.0. Figures were assembled in Adobe Illustrator CC v22.0.1.

5.15.1 Data quantification

Drosophila larval brains: PH3 scorings, number of lineage specific cells per phenotype, cell size (maximum diameter), TUNEL scoring, FBL size (maximum FBL diameter/maximum cell diameter) and dMyc intensity (cellular pixel intensity/cell area, nucleolar pixel intensity/cell area) in larval NSC were performed using FiJi v1.0.

Immortalised cell lines and GSCs: Ki65, EdU, TUNEL and c-Myc scorings were done using FiJi v1.0. Nucleolar size *in vitro* was quantified by measuring the area occupied by a mask corresponding to the nucleolar protein stain and using the "Analyse Particles" function on FiJi with the following parameters: size (pixels^2) 0.5-Infinity, circularity 0.0-1.0. The ratio between nucleolus and nucleus, was calculated by dividing this number to the area labelled with DAPI. Details for RNA and OPP intensity quantifications are specified in section 5.8 of this chapter.

5.16 Statistical analysis

Statistical analysis was conducted using GraphPad Prism v7.0a. Parametric distribution of the data was analysed using the D'Angostino-Pearson normality test. Significant differences between two groups were calculated using unpaired two tailed Student's t-tests with Welch's correction for parametric samples, and Wilcoxon rank-sum test for non-parametric. Significant differences (p values) are indicated as: * for $p<0.05$;

** for $p<0.01$ and *** for $p<0.001$. Data from *Drosophila in vivo* assays was obtained from a minimum of two biological replica sets; sample numbers are indicated in figures or figure legends. Cell culture-derived results derive from a minimum of three independent assays. Histograms are presented as mean ±SEM unless indicated otherwise. Boxplots represent 25th and 75th percentiles, black line indicates median, red line specifies mean, whiskers indicate 10th and 90th percentiles.

6 REFERENCES

1. Aldape K, Brindle KM, Chesler L, et al. Challenges to curing primary brain tumours. *Nat Rev Clin Oncol*. 2019;16(8):509-520. doi:10.1038/s41571-019-0177-5

2. Lu QR, Qian L, Zhou X. Developmental origins and oncogenic pathways in malignant brain tumors. *Wiley Interdiscip Rev Dev Biol*. 2019;8(4):1-23. doi:10.1002/wdev.342

3. Lytle NK, Barber AG, Reya T. Stem cell fate in cancer growth, progression and therapy resistance. *Nat Rev Cancer*. 2018;18(11):669-680. doi:10.1038/s41568-018-0056-x

4. Saygin C, Matei D, Majeti R, Reizes O, Lathia JD. Targeting Cancer Stemness in the Clinic: From Hype to Hope. *Cell Stem Cell*. 2019;24(1):25-40. doi:10.1016/j.stem.2018.11.017

5. Singh SK, Hawkins C, Clarke ID, et al. Identification of human brain tumour initiating cells. *Nature*. 2004;432(November):396-401. doi:10.1038/nature03031.1.

6. Bowman SK, Rolland V, Betschinger J, Kinsey KA, Emery G, Knoblich JA. The Tumor Suppressors Brat and Numb Regulate Transit-Amplifying Neuroblast Lineages in Drosophila. *Dev Cell*. 2008;14(4):535-546. doi:10.1016/j.devcel.2008.03.004

7. Chen G, Kong J, Tucker-Burden C, et al. Human brat ortholog TRIM3 is a tumor suppressor that regulates asymmetric cell division in glioblastoma. *Cancer Res*. 2014;74(16):4536-4548. doi:10.1158/0008-5472.CAN-13-3703

8. Nowell P. C. The clonal evolution of tumor cell populations. *Science (80-)*. 1976;194:23-28.

9. Bray F, Ren JS, Masuyer E, Ferlay J. Global estimates of cancer prevalence for 27 sites in the adult population in 2008. *Int J Cancer*. 2013;132(5):1133-1145. doi:10.1002/ijc.27711

10. Ostrom QT, Gittleman H, Fulop J, et al. CBTRUS statistical Report: primary brain and central nervous system tumors diagnosed in the United States in 2008-2012. *Neuro Oncol*. 2015;17:iv1-iv62. doi:10.1093/neuonc/nov189

11. Philips A, Henshaw DL, Lamburn G, O'Carroll MJ. Brain tumours: Rise in glioblastoma multiforme incidence in England 1995-2015 Suggests an Adverse

Environmental or Lifestyle Factor. *J Environ Public Health*. 2018;2018. doi:10.1155/2018/7910754

12. Vescovi AL, Galli R, Reynolds BA. Brain tumour stem cells. *Nat Rev Cancer*. 2006;6(6):425-436. doi:10.1038/nrc1889

13. Nassar D, Blanpain C. Cancer stem cells: Concepts and therapeutic implications. *Annu Rev Pathol Mech Dis*. 2016;11(1):47-76. doi:10.3923/ajava.2015.509.517

14. Reya T, Morrison SJ, Clarke MF, Weissman IL. Stem Cells, Cancer, and Cancer Stem Cells. *Nature*. 2001;414(November):105-111. doi:10.1007/978-1-60327-933-8

15. Clarke MF, Dick JE, Dirks PB, et al. Cancer Stem Cells — Perspectives on Current Status and Future Directions : AACR Workshop on Cancer Stem Cells. *Cancer Res*. 2006;66(19):9339-9345. doi:10.1158/0008-5472.CAN-06-3126

16. Ishizawa K, Rasheed ZA, Karisch R, et al. Tumor-initiating cells are rare in many human tumors. *Cell Stem Cell*. 2010;7(3):279-282. doi:10.1016/j.stem.2010.08.009

17. Lathia JD, Mack SC, Mulkearns-hubert EE, Valentim CLL, Rich JN. Cancer stem cells in glioblastoma. *Genes Dev*. 2015;29:1203-1217. doi:10.1101/gad.261982.115.tumors

18. Chesler, David A, Berger MS, Quinones-Hinojosa A. The potential origin of glioblastoma initiating cells. *Front Biosci (School Ed)*. 2012;4(1):190-205. doi:10.2741/S261

19. Batlle E, Clevers H. Cancer stem cells revisited. *Nat Med*. 2017;23(10):1124-1134. doi:10.1038/nm.4409

20. Bonnet D, Dick JE. Human acute myeloid leukemia is organized as a hierarchy that originates from a primitive hematopoietic cell. *Nat Med*. 1997;3:730-7037. doi:10.1038/nm0798-822

21. Lapidot T, Sirard C, Vormoor J, et al. A cell initiating human acute myeloid leukaemia after transplantation into SCID mice. *Nature*. 1994;367(6464):645-648. doi:10.1038/367645a0

22. Al-Hajj M, Wicha MS, Benito-Hernandez A, Morrison SJ, Clarke MF. Prospective identification of tumorigenic breast cancer cells. *Proc Natl Acad Sci U S A*. 2003;100(7):3983-3988. doi:10.1073/pnas.0530291100

23. Collins AT, Berry PA, Hyde C, Stower MJ, Maitland NJ. Prospective identification of tumorigenic prostate cancer stem cells. *Cancer Res*. 2005;65(23):10946-

10951. doi:10.1158/0008-5472.CAN-05-2018

24. Florek M, Haase M, Marzesco AM, et al. Prominin-1/CD133, a neural and hematopoietic stem cell marker, is expressed in adult human differentiated cells and certain types of kidney cancer. *Cell Tissue Res*. 2005;319(1):15-26. doi:10.1007/s00441-004-1018-z

25. Fang D, Nguyen TK, Leishear K, et al. A tumorigenic subpopulation with stem cell properties in melanomas. *Cancer Res*. 2005;65(20):9328-9337. doi:10.1158/0008-5472.CAN-05-1343

26. Driessens G, Beck B, Caauwe A, Simons BD, Blanpain C. Defining the mode of tumour growth by clonal analysis. *Nature*. 2012;488(7412):527-530. doi:10.1038/nature11344

27. Clevers H. Modeling Development and Disease with Organoids. *Cell*. 2016;165(7):1586-1597. doi:10.1016/j.cell.2016.05.082

28. Lancaster MA, Knoblich JA. Organogenesisin a dish: Modeling development and disease using organoid technologies. *Science (80-)*. 2014;345(6194). doi:10.1126/science.1247125

29. Cortina C, Turon G, Stork D, et al. A genome editing approach to study cancer stem cells in human tumors. *EMBO Mol Med*. 2017;9(7):869-879. doi:10.15252/emmm.201707550

30. Shimokawa M, Ohta Y, Nishikori S, et al. Visualization and targeting of LGR5 + human colon cancer stem cells. *Nature*. 2017;545(7653):187-192. doi:10.1038/nature22081

31. Desai A, Yan Y, Gerson SL. Concise Reviews: Cancer Stem Cell Targeted Therapies: Toward Clinical Success. *Stem Cells Transl Med*. 2019;8(1):75-81. doi:10.1002/sctm.18-0123

32. Annett S, Robson T. Targeting cancer stem cells in the clinic: Current status and perspectives. *Pharmacol Ther*. 2018;187:13-30. doi:10.1016/j.pharmthera.2018.02.001

33. Nduom E, Hadjipanayis CG, Meir EG Van. Glioblastoma Cancer Stem-like Cells–Implications for Pathogenesis and Treatment. *Cancer J*. 2012;18(1):100-106. doi:10.1097/PPO.0b013e3182452e0d.Glioblastoma

34. Diehn M, Cho RW, Clarke MF. Therapeutic Implications of the Cancer Stem Cell Hypothesis. *Semin Radiat Oncol*. 2009;19(2):78-86. doi:10.1016/j.semradonc.2008.11.002

35. Davis ME. Glioblastoma: Overview of disease and treatment. *Clin J Oncol Nurs*. 2016;20(5):1-8. doi:10.1188/16.CJON.S1.2-8

36. Das B, Tsuchida R, Malkin D, Koren G, Baruchel S, Yeger H. Hypoxia Enhances Tumor Stemness by Increasing the Invasive and Tumorigenic Side Population Fraction. *Stem Cells*. 2008;26(7):1818-1830. doi:10.1634/stemcells.2007-0724

37. Clarke L, Van Der Kooy D. Low oxygen enhances primitive and definitive neural stem cell colony formation by inhibiting distinct cell death pathways. *Stem Cells*. 2009;27(8):1879-1886. doi:10.1002/stem.96

38. Soeda A, Park M, Lee D, et al. Hypoxia promotes expansion of the CD133-positive glioma stem cells through activation of HIF-1α. *Oncogene*. 2009;28(45):3949-3959. doi:10.1038/onc.2009.252

39. Chen J, Li Y, Yu TS, et al. A restricted cell population propagates glioblastoma growth after chemotherapy. *Nature*. 2012;488(7412):522-526. doi:10.1038/nature11287

40. Dembinski JL, Krauss S. Characterization and functional analysis of a slow cycling stem cell-like subpopulation in pancreas adenocarcinoma. *Clin Exp Metastasis*. 2009;26(7):611-623. doi:10.1007/s10585-009-9260-0

41. Gao MQ, Choi YP, Kang S, Youn JH, Cho NH. CD24+ cells from hierarchically organized ovarian cancer are enriched in cancer stem cells. *Oncogene*. 2010;29(18):2672-2680. doi:10.1038/onc.2010.35

42. Kalluri R, Weinberg RA. The basics of epithelial-mesenchymal transition. *J Clin Invest*. 2009;119(6):1420-1428. doi:10.1172/JCI39104

43. Mani SA, Guo W, Liao MJ, et al. The Epithelial-Mesenchymal Transition Generates Cells with Properties of Stem Cells. *Cell*. 2008;133(4):704-715. doi:10.1016/j.cell.2008.03.027

44. Charafe-jauffret E, Ginestier C, Iovino F, et al. Breast cancer cell lines contain functional cancer stem cells with metastatic capacity and a distinct molecular signature. *Cancer Res*. 2009;69(4):1302-1313. doi:10.1158/0008-5472.CAN-08-2741.Breast

45. Ye X, Tam WL, Shibue T, et al. Distinct EMT programs control normal mammary stem cells and tumour-initiating cells. *Nature*. 2015;525(7568):256-260. doi:10.1038/nature14897

46. Malta TM, Sokolov A, Gentles AJ, et al. Machine Learning Identifies Stemness Features Associated with Oncogenic Dedifferentiation. *Cell*. 2018;173(2):338-354.e15. doi:10.1016/j.cell.2018.03.034

47. Spranger S, Bao R, Gajewski TF. Melanoma-intrinsic β-catenin signalling prevents anti-tumour immunity. *Nature*. 2015;523(7559):231-235. doi:10.1038/nature14404

48. Cheah MT, Chen JY, Sahoo D, et al. CD14-expressing cancer cells establish the inflammatory and proliferative tumor microenvironment in bladder cancer. *Proc Natl Acad Sci U S A*. 2015;112(15):4725-4730. doi:10.1073/pnas.1424795112

49. Ramos EK, Hoffmann AD, Gerson SL, Liu H. New Opportunities and Challenges to Defeat Cancer Stem Cells. *Trends in Cancer*. 2017;3(11):780-796. doi:10.1016/j.trecan.2017.08.007

50. Vey N, Delaunay J, Martinelli G, et al. Phase I clinical study of RG7356, an anti-CD44 humanized antibody, in patients with acute myeloid leukemia. *Oncotarget*. 2016;7(22):32532-32542. doi:10.18632/oncotarget.8687

51. Plaks V, Kong N, Werb Z. The cancer stem cell niche: How essential is the niche in regulating stemness of tumor cells? *Cell Stem Cell*. 2015;16(3):225-238. doi:10.1016/j.stem.2015.02.015

52. Sugiyama T, Kohara H, Noda M, Nagasawa T. Maintenance of the Hematopoietic Stem Cell Pool by CXCL12-CXCR4 Chemokine Signaling in Bone Marrow Stromal Cell Niches. *Immunity*. 2006;25(6):977-988. doi:10.1016/j.immuni.2006.10.016

53. Uy GL, Rettig MP, Motabi IH, et al. A phase 1/2 study of chemosensitization with the CXCR4 antagonist plerixafor in relapsed or refractory acute myeloid leukemia. *Blood*. 2012;119(17):3917-3924. doi:10.1182/blood-2011-10-383406

54. Ginestier C, Liu S, Diebel ME, et al. CXCR1 blockade selectively targets human breast cancer stem cells in vitro and in xenografts Christophe. *J Clin Invest*. 2010;120(2):485-497. doi:10.1172/JDI39397DS1

55. Schott AF, Goldstein LJ, Cristofanilli M, et al. Phase Ib pilot study to evaluate reparixin in combination with weekly paclitaxel in patients with HER-2–negative metastatic breast cancer. *Clin Cancer Res*. 2017;23(18):5358-5365. doi:10.1158/1078-0432.CCR-16-2748

56. Nüsslein-volhard C, Wieschaus E. Mutations affecting segment number and polarity in drosophila. *Nature*. 1980;287(5785):795-801. doi:10.1038/287795a0

57. Carballo GB, Honorato JR, De Lopes GPF, Spohr TCLDSE. A highlight on Sonic hedgehog pathway. *Cell Commun Signal*. 2018;16(1):1-15. doi:10.1186/s12964-018-0220-7

58. Machold R, Hayashi S, Rutlin M, et al. Sonic hedgehog is required for progenitor

cell maintenance in telencephalic stem cell niches. *Neuron*. 2003;39(6):937-950. doi:10.1016/S0896-6273(03)00561-0

59. Shin K, Lee J, Guo N, et al. Hedgehog/Wnt feedback supports regenerative proliferation of epithelial stem cells in bladder. *Nature*. 2011;472(7341):110-116. doi:10.1038/nature09851

60. Clement V, Sanchez P, de Tribolet N, Radovanovic I, Ruiz i Altaba A. HEDGEHOG-GLI1 Signaling Regulates Human Glioma Growth, Cancer Stem Cell Self-Renewal, and Tumorigenicity. *Curr Biol*. 2007;17(2):165-172. doi:10.1016/j.cub.2006.11.033

61. Sloan AE, Nock CJ, Ye X, et al. Targeting glioma-initiating cells in GBM: ABTC-0904, a randomized phase 0/II study targeting the Sonic Hedgehog-signaling pathway. *J Clin Oncol*. 2014;32(2026).

62. Nowell CS, Radtke F. Notch as a tumour suppressor. *Nat Rev Cancer*. 2017;17(3):145-159. doi:10.1038/nrc.2016.145

63. Gallahan D, Kozak C, Callahan R. A new common integration region (int-3) for mouse mammary tumor virus on mouse chromosome 17. *J Virol*. 1987;61(1):218-220. doi:10.1128/jvi.61.1.218-220.1987

64. Pisapia DJ. The updated world health organization glioma classification: Cellular and molecular origins of adult infiltrating gliomas. *Arch Pathol Lab Med*. 2017;141(12):1633-1645. doi:10.5858/arpa.2016-0493-RA

65. Louis DN, Perry A, Reifenberger G, et al. The 2016 World Health Organization Classification of Tumors of the Central Nervous System: a summary. *Acta Neuropathol*. 2016;131(6):803-820. doi:10.1007/s00401-016-1545-1

66. Von Neubeck C, Seidlitz A, Kitzler HH, Beuthien-Baumann B, Krause M. Glioblastoma multiforme: Emerging treatments and stratification markers beyond new drugs. *Br J Radiol*. 2015;88(1053). doi:10.1259/bjr.20150354

67. Cohen A, Holmen S, Colman H. IDH1 and IDH2 Mutations in Gliomas. *Curr Neurol Neurosci Rep*. 2013;13(5). doi:10.1038/jid.2014.371

68. Gage FH. Mammalian neural stem cells. *Science (80-)*. 2000;287(5457):1433-1438.

69. Gage FH, Temple S. Perspective Neural Stem Cells: Generating and Regenerating the Brain. *Neuron*. 2013;80(3):588-601. doi:10.1016/j.neuron.2013.10.037

70. Nunes MC, Roy NS, Keyoung HM, et al. Identification and isolation of

multipotential neural progenitor cells from the subcortical white matter of the adult human brain. *Nat Med*. 2003;9(4):439-447. doi:10.1038/nm837

71. Lee DA, Bedont JL, Pak T, et al. Tanycytes of the hypothalamic median eminence form a diet-responsive neurogenic niche. *Nat Neurosci*. 2012;15(5):700-702. doi:10.1038/nn.3079

72. Bond AM, Ming GL, Song H. Adult Mammalian Neural Stem Cells and Neurogenesis: Five Decades Later. *Cell Stem Cell*. 2015;17(4):385-395. doi:10.1016/j.stem.2015.09.003

73. Sorrells SF, Paredes MF, Cebrian-Silla A, et al. Human hippocampal neurogenesis drops sharply in children to undetectable levels in adults. *Nature*. 2018;555(7696):377-381. doi:10.1038/nature25975

74. Boldrini M, Fulmore CA, Tartt AN, et al. Human Hippocampal Neurogenesis Persists throughout Aging. *Cell Stem Cell*. 2018;22(4):589-599.e5. doi:10.1016/j.stem.2018.03.015

75. Eriksson PS, Perfilieva E, Björk-Eriksson T, et al. Neurogenesis in the adult human hippocampus. *Nat Med*. 1998;4(11):1313-1317. papers2://publication/uuid/23D025A2-F765-488E-B71D-EA85EF8842B1.

76. Spalding KL, Bergmann O, Alkass K, et al. Dynamics of hippocampal neurogenesis in adult humans. *Cell*. 2013;153(6):1219. doi:10.1016/j.cell.2013.05.002

77. Ernst A, Alkass K, Bernard S, et al. Neurogenesis in the striatum of the adult human brain. *Cell*. 2014;156(5):1072-1083. doi:10.1016/j.cell.2014.01.044

78. Holland EC, Celestino J, Dai C, Schaefer L, Sawaya RE, Fuller GN. Combined activation of Ras and Akt in neural progenitors induces glioblastoma formation in mice. *Nat Genet*. 2000;25(1):55-57. doi:10.1038/75596

79. Sanai N, Alvarez-Buylla A, Berger MS. Neural stem cells and the origin of gliomas. *N Engl J Med*. 2005;353(8):811-822. doi:10.1056/NEJMra043666

80. Copeland DD, Vogel SF, Bigner DD. The induction of intracranial neoplasms by the inoculation of avian sarcoma virus in peri- natal and adult rats. *J Neuropathol Exp Neu- rol*. 1975;(34):340-358. http://repositorio.unan.edu.ni/2986/1/5624.pdf.

81. Pollard SM, Yoshikawa K, Clarke ID, et al. Glioma Stem Cell Lines Expanded in Adherent Culture Have Tumor-Specific Phenotypes and Are Suitable for Chemical and Genetic Screens. *Cell Stem Cell*. 2009;4(6):568-580. doi:10.1016/j.stem.2009.03.014

82. Galli R, Binda E, Orfanelli U, et al. Isolation and Characterization of Tumorigenic , Stem-like Neural Precursors from Human Glioblastoma Isolation and Characterization of Tumorigenic , Stem-like Neural Precursors from Human Glioblastoma. *Cancer Res*. 2004;64:7011-7021. doi:10.1158/0008-5472.CAN-04-1364

83. Gil-ranedo J, Medina D, Mendiburu-elic M, Garcı M. An Off-Target Nucleostemin RNAi Inhibits Growth in Human Glioblastoma-Derived Cancer Stem Cells. *PLoS One*. 2011;6(12). doi:10.1371/journal.pone.0028753

84. Lan X, Jörg DJ, Cavalli FMG, et al. Fate mapping of human glioblastoma reveals an invariant stem cell hierarchy. *Nature*. 2017;549(7671):227-232. doi:10.1038/nature23666

85. Patel AP, Tirosh I, Trombetta JJ, et al. Single-cell RNA seq highlights intratumoral heterogeneity in primary glioblastoma. *Science (80-)*. 2014;344(6190):1396-1402.

86. Pearson JRD, Regad T. Targeting cellular pathways in glioblastoma multiforme. *Signal Transduct Target Ther*. 2017;2(May):1-11. doi:10.1038/sigtrans.2017.40

87. McLendon R, Friedman A, Bigner D, et al. Comprehensive genomic characterization defines human glioblastoma genes and core pathways. *Nature*. 2008;455(7216):1061-1068. doi:10.1038/nature07385

88. Villegas SN. One hundred years of Drosophila cancer research: No longer in solitude. *DMM Dis Model Mech*. 2019;12(4). doi:10.1242/dmm.039032

89. Reiter LT, Potocki L, Chien S, Gribskov M, Bier E. A systematic analysis of human disease-associated gene sequences in Drosophila melanogaster. *Genome Res*. 2001;11(6):1114-1125. doi:10.1101/gr.169101

90. Hales KG, Korey CA, Larracuente AM, Roberts DM. Genetics on the fly: A primer on the drosophila model system. *Genetics*. 2015;201(3):815-842. doi:10.1534/genetics.115.183392

91. Brand AH, Perrimon N. Targeted gene expression as a means of altering cell fates and generating dominant phenotypes. *Development*. 1993;118(2):401-415. doi:10.1101/lm.1331809

92. Caygill EE, Brand AH. The GAL4 system: A versatile system for the manipulation and analysis of gene expression. *Methods Mol Biol*. 2016;1478:4-6. doi:10.1007/978-1-4939-6371-3

93. Homem CCF, Knoblich JA. Drosophila neuroblasts: a model for stem cell biology. *Development*. 2012;139(23):4297-4310. doi:10.1242/dev.080515

94. Harding K, White K. Drosophila as a model for developmental biology: Stem cell-fate decisions in the developing nervous system. *J Dev Biol*. 2018;6(4). doi:10.3390/jdb6040025

95. Miyares RL, Lee T. Temporal control of Drosophila central nervous system development. *Curr Opin Neurobiol*. 2019;56:24-32. doi:10.1016/j.conb.2018.10.016

96. Knoblich JA. Asymmetric cell division: Recent developments and their implications for tumour biology. *Nat Rev Mol Cell Biol*. 2010;11(12):849-860. doi:10.1038/nrm3010

97. Choksi SP, Southall TD, Bossing T, et al. Prospero Acts as a Binary Switch between Self-Renewal and Differentiation in Drosophila Neural Stem Cells. *Dev Cell*. 2006;11(6):775-789. doi:10.1016/j.devcel.2006.09.015

98. Betschinger J, Mechtler K, Knoblich JA. Asymmetric Segregation of the Tumor Suppressor Brat Regulates Self-Renewal in Drosophila Neural Stem Cells. *Cell*. 2006;124:1241-1253. doi:10.1016/j.cell.2006.01.038

99. Lee C, Wilkinson BD, Siegrist SE, Wharton RP, Doe CQ. Brat Is a Miranda Cargo Protein that Promotes Neuronal Differentiation and Inhibits Neuroblast Self-Renewal. *Dev Cell*. 2006;10:441-449. doi:10.1016/j.devcel.2006.01.017

100. Boone JQ, Doe CQ. Identification of Drosophila type II neuroblast lineages containing transit amplifying ganglion mother cells. *Dev Neurobiol*. 2008;68(9):1185-1195. doi:10.1002/dneu.20648

101. Bello B, Reichert H, Hirth F. The brain tumor gene negatively regulates neural progenitor cell proliferation in the larval central brain of Drosophila. *Development*. 2006;2648:2639-2648. doi:10.1242/dev.02429

102. Izergina N, Balmer J, Bello B, Reichert H. Postembryonic development of transit amplifying neuroblast lineages in the Drosophila brain. *Neural Dev*. 2009;13:1-13. doi:10.1186/1749-8104-4-44

103. Bayraktar OA, Doe CQ. Combinatorial temporal patterning in progenitors expands neural diversity. *Nature*. 2013;498(7455):449-455. doi:10.1038/nature12266

104. Caussinus E, Gonzalez C. Induction of tumor growth by altered stem-cell asymmetric division in Drosophila melanogaster. *Nat Genet*. 2005;37(10):1125-1129. doi:10.1038/ng1632

105. Lee CY, Andersen RO, Cabernard C, et al. Drosophila Aurora-A kinase inhibits neuroblast self-renewal by regulating aPKC/Numb cortical polarity and spindle orientation. *Genes Dev*. 2006;20(24):3464-3474. doi:10.1101/gad.1489406

106. Hassan B, Ling LI, Bremer KA, Chang W, Pinsonneault J, Vaessin H. Prospero is a panneural transcription factor that modulates homeodomain protein activity. *Proc Natl Acad Sci U S A*. 1997;94(20):10991-10996. doi:10.1073/pnas.94.20.10991

107. Torii MA, Matsuzaki F, Osumi N, et al. Transcription factors Mash-1 and Prox-1 delineate early steps in differentiation of neural stem cells in the developing central nervous system. *Development*. 1999;126(3):443-456.

108. Elsir T, Smits A, Lindström MS, Nistér M. Transcription factor PROX1: Its role in development and cancer. *Cancer Metastasis Rev*. 2012;31(3-4):793-805. doi:10.1007/s10555-012-9390-8

109. Stockhausen M-T, Kritsoffersen K, Poulsen HS. The functional role of Notch signaling in human gliomas. *Neuro Oncol*. 2010;12(2):199-211. doi:10.1016/B978-0-12-416673-8.00013-7

110. Zhu S, Wildonger J, Barshow S, Younger S, Huang Y, Lee T. The bHLH Repressor Deadpan Regulates the Self-renewal and Specification of Drosophila Larval Neural Stem Cells Independently of Notch. *PLoS One*. 2012;7(10). doi:10.1371/journal.pone.0046724

111. Zacharioudaki E, Magadi SS, Delidakis C. bHLH-O proteins are crucial for Drosophila neuroblast self-renewal and mediate notch-induced overproliferation. *Development*. 2012;139(7):1258-1269. doi:10.1242/dev.071779

112. Weng M, Golden KL, Lee CY. dFezf/Earmuff Maintains the Restricted Developmental Potential of Intermediate Neural Progenitors in Drosophila. *Dev Cell*. 2010;18(1):126-135. doi:10.1016/j.devcel.2009.12.007

113. Southall TD, Davidson CM, Miller C, Carr A, Brand AH. Dedifferentiation of neurons precedes tumor formation in lola mutants. *Dev Cell*. 2014;28(6):685-696. doi:10.1016/j.devcel.2014.01.030

114. Kuzin A, Brody T, Moore AW, Odenwald WF. Nerfin-1 is required for early axon guidance decisions in the developing Drosophila CNS. *Dev Biol*. 2005;277(2):347-365. doi:10.1016/j.ydbio.2004.09.027

115. Froldi F, Szuperak M, Weng CF, Shi W, Papenfuss AT, Cheng LY. The transcription factor Nerfin-1 prevents reversion of neurons into neural stem cells. *Genes Dev*. 2015;29(2):129-143. doi:10.1101/gad.250282.114

116. Carney TD, Struck AJ, Doe CQ. Midlife crisis encodes a conserved zinc-finger protein required to maintain neuronal differentiation in Drosophila. *Dev*. 2013;140(20):4155-4164. doi:10.1242/dev.093781

117. Arama E, Dickman D, Kimchie Z, Shearn A, Lev Z. Mutations in the β-propeller domain of the Drosophila brain tumor (brat) protein induce neoplasm in the larval brain. *Oncogene*. 2000;19(33):3706-3716. doi:10.1038/sj.onc.1203706

118. Sonoda J, Wharton RP. Drosophila Brain Tumor is a translational repressor. *Genes Dev*. 2001;15:762-773. doi:10.1101/gad.870801.ements

119. Frank DJ, Edgar BA, Roth MB. The Drosophila melanogaster gene brain tumor negatively regulates cell growth and ribosomal RNA synthesis. *Development*. 2002;129:399-407.

120. Komori H, Xiao Q, Mccartney BM, Lee C. Brain tumor specifies intermediate progenitor cell identity by attenuating β -catenin / Armadillo activity. *Development*. 2014;141:51-62. doi:10.1242/dev.099382

121. Beaucher M, Goodliffe J, Hersperger E, Trunova S, Frydman H, Shearn A. Drosophila brain tumor metastases express both neuronal and glial cell type markers. *Dev Biol*. 2007;301(1):287-297. doi:10.1016/j.ydbio.2006.09.019

122. Komori H, Xiao Q, McCartney BM, Lee C-Y. Brain tumor specifies intermediate progenitor cell identity by attenuating -catenin/Armadillo activity. *Development*. 2014;141(1):51-62. doi:10.1242/dev.099382

123. Morin PJ. Beta-Catenin Signaling and Cancer. *Bioessays*. 1999;21(12):1021-1030. doi:10.1002/(SICI)1521-1878(199912)22:1<1021::AID-BIES6>3.0.CO;2-P

124. Zhang H, Qi Y, Geng D, et al. Expression profile and clinical significance of Wnt signaling in human gliomas. *Oncol Lett*. 2017;(9):610-617. doi:10.3892/ol.2017.7315

125. Lee Y, Lee JK, Ahn SH, Lee J, Nam DH. WNT signaling in glioblastoma and therapeutic opportunities. *Lab Investig*. 2016;96(2):137-150. doi:10.1038/labinvest.2015.140

126. Reichardt I, Bonnay F, Steinmann V, et al. The tumor suppressor Brat controls neuronal stem cell lineages by inhibiting Deadpan and Zelda. *EMBO Rep*. 2017;19(1):102-117. doi:10.15252/embr.201744188

127. Mukherjee S, Tucker-Burden C, Zhang C, et al. Drosophila brat and human ortholog TRIM3 maintain stem cell equilibrium and suppress brain tumorigenesis by attenuating notch nuclear transport. *Cancer Res*. 2016;76(8):2443-2452. doi:10.1158/0008-5472.CAN-15-2299

128. Grewal SS, Li L, Orian A, Eisenman RN, Edgar BA. Myc-dependent regulation of ribosomal RNA synthesis during Drosophila development. *Nat Cell Biol*. 2005;7(3):295-302. doi:10.1038/ncb1223

129. Van Riggelen J, Yetil A, Felsher DW. MYC as a regulator of ribosome biogenesis and protein synthesis. *Nat Rev Cancer*. 2010;10(4):301-309. doi:10.1038/nrc2819

130. Schaub FX, Dhankani V, Berger AC, et al. Pan-cancer Alterations of the MYC Oncogene and Its Proximal Network across the Cancer Genome Atlas. *Cell Syst*. 2018;6(3):282-300.e2. doi:10.1016/j.cels.2018.03.003

131. Chen G, Kong J, Tucker-Burden C, et al. Human brat ortholog TRIM3 is a tumor suppressor that regulates asymmetric cell division in glioblastoma. *Cancer Res*. 2014;74(16):4536-4548. doi:10.1158/0008-5472.CAN-13-3703

132. Liu Y, Raheja R, Yeh N, et al. TRIM3, a tumor suppressor linked to regulation of p21Waf1/Cip1 Yuhui. *Oncogen*. 2014;33(3):308-315. doi:10.1038/onc.2012.596.TRIM3

133. Schwamborn JC, Berezikov E, Knoblich JA. The TRIM-NHL Protein TRIM32 Activates MicroRNAs and Prevents Self-Renewal in Mouse Neural Progenitors. *Cell*. 2009;136(5):913-925. doi:10.1016/j.cell.2008.12.024

134. Hatakeyama S. TRIM proteins and cancer. *Nat Rev Cancer*. 2011;11(11):792-804. doi:10.1038/nrc3139

135. Huang X-Q, Zhang X-F, Xia J-H, et al. Tripartite motif-containing 3 (TRIM3) inhibits tumor growth and metastasis of liver cancer. *Chin J Cancer*. 2017;36(1):1-13. doi:10.1186/s40880-017-0240-5

136. Piao M, Cao H, He N, et al. Potential role of TRIM3 as a novel tumour suppressor in colorectal cancer (CRC) development development. *Scand J Gastroenterol*. 2015;5521(January):1502-7708. doi:10.3109/00365521.2015.1124285

137. Sonoda Y, Iizuka M, Yasuda J, et al. Loss of Heterozygosity at 11p15 in Malignant Glioma. *Cancer Res*. 1995;55(10):2166-2168.

138. Zhu S, Barshow S, Wildonger J, Jan LY, Jan YN. Ets transcription factor Pointed promotes the generation of intermediate neural progenitors in Drosophila larval brains. *Proc Natl Acad Sci*. 2011;108(51):20615-20620. doi:10.1073/pnas.1118595109

139. Bossing T, Barros CS, Fischer B, Russell S, Shepherd D. Disruption of Microtubule Integrity Initiates Mitosis during CNS Repair. *Dev Cell*. 2012;23(2):433-440. doi:10.1016/j.devcel.2012.06.002

140. Liu B, Bossing T. Single neuron transcriptomics identify SRSF/SR protein B52 as a regulator of axon growth and Choline acetyltransferase splicing. *Sci Rep*. 2016;6(April):1-13. doi:10.1038/srep34952

141. Bateman A. UniProt: A worldwide hub of protein knowledge. *Nucleic Acids Res*. 2019;47(D1):D506-D515. doi:10.1093/nar/gky1049

142. Yang K, Yang J, Yi J. Nucleolar Stress: hallmarks, sensing mechanism and diseases. *Cell Stress*. 2018;2(6):125-140. doi:10.15698/cst2018.06.139

143. Matos-Perdomo E, Machín F. Nucleolar and Ribosomal DNA Structure under Stress: Yeast Lessons for Aging and Cancer. *Cells*. 2019;8(8):779. doi:10.3390/cells8080779

144. Henras AK, Plisson-Chastang C, O'Donohue MF, Chakraborty A, Gleizes PE. An overview of pre-ribosomal RNA processing in eukaryotes. *Wiley Interdiscip Rev RNA*. 2015;6(2):225-242. doi:10.1002/wrna.1269

145. Turi Z, Lacey M, Mistrik M, Moudry P. Impaired ribosome biogenesis: mechanisms and relevance to cancer and aging. *Aging (Albany NY)*. 2019;11(8):2512-2540.

146. Boisvert FM, Van Koningsbruggen S, Navascués J, Lamond AI. The multifunctional nucleolus. *Nat Rev Mol Cell Biol*. 2007;8(7):574-585. doi:10.1038/nrm2184

147. Boulon S, Westman BJ, Hutten S, Boisvert FM, Lamond AI. The Nucleolus under Stress. *Mol Cell*. 2010. doi:10.1016/j.molcel.2010.09.024

148. Kressler D, Hurt E, Baßler J. A Puzzle of Life: Crafting Ribosomal Subunits. *Trends Biochem Sci*. 2017;42(8):640-654. doi:10.1016/j.tibs.2017.05.005

149. Prieto JL, McStay B. Recruitment of factors linking transcription and processing of pre-rRNA to NOR chromatin is UBF-dependent and occurs independent of transcription in human cells. *Genes Dev*. 2007;21(16):2041-2054. doi:10.1101/gad.436707

150. Dez C, Dlakić M, Tollervey D. Roles of the HEAT repeat proteins Utp10 and Utp20 in 40S ribosome maturation. *Rna*. 2007;13(9):1516-1527. doi:10.1261/rna.609807

151. Azuma M, Toyama R, Laver E, Dawid IB. Perturbation of rRNA Synthesis in the bap28 Mutation Leads to Apoptosis Mediated by p53 in the Zebrafish Central Nervous System. *J Biol Chem*. 2006;281(19):13309-13316. doi:10.1074/jbc.M601892200

152. Turi Z, Senkyrikova M, Mistrik M, Bartek J, Moudry P. Perturbation of RNA Polymerase I transcription machinery by ablation of HEATR1 triggers the RPL5/RPL11-MDM2-p53 ribosome biogenesis stress checkpoint pathway in human cells. *Cell Cycle*. 2018;17(1):92-101. doi:10.1080/15384101.2017.1403685

153. He S, Ma X, Ye Y, et al. HEATR1 modulates cell survival in non-small cell lung cancer via activation of the p53/PUMA signaling pathway. *Onco Targets Ther*. 2019;Volume 12:4001-4011. doi:10.2147/ott.s195826

154. Neumüller RA, Richter C, Fischer A, Novatchkova M, Neumüller KG, Knoblich JA. Resource Genome-Wide Analysis of Self-Renewal in Drosophila Neural Stem Cells by Transgenic RNAi. *Cell Stem Cell*. 2011;8:580-593. doi:10.1016/j.stem.2011.02.022

155. Wu ZB, Qiu C, Zhang AL, et al. Glioma-associated antigen HEATR1 induces functional cytotoxic T lymphocytes in patients with glioma. *J Immunol Res*. 2014;2014. doi:10.1155/2014/131494

156. Liu T, Fang Y, Zhang H, et al. HEATR1 Negatively Regulates Akt to Help Sensitize Pancreatic Cancer Cells to Chemotherapy. *Cancer Res*. 2016;1(22):572-581. doi:10.1158/0008-5472.CAN-15-0671

157. Zhou Y, Wang K, Zhou Y, et al. HEATR1 deficiency promotes pancreatic cancer proliferation and gemcitabine resistance by up-regulating Nrf2 signaling. *Redox Biol*. 2020;29(August 2019):101390. doi:10.1016/j.redox.2019.101390

158. Zhu S, Barshow S, Wildonger J, Jan LY, Jan Y-N. Ets transcription factor Pointed promotes the generation of intermediate neural progenitors in Drosophila larval brains. *Proc Natl Acad Sci*. 2011;108(51):20615-20620. doi:10.1073/pnas.1118595109

159. Lee T, Luo L. Mosaic Analysis with a Repressible Cell Marker for Studies of Gene Function in Neuronal Morphogenesis. *Neuron*. 1999;22:451-461.

160. Kros JM, Waarsenburg N, Hayes DP, Hop WCJ, Van Dekken H. Cytogenetic analysis of gemistocytic cells in gliomas. *J Neuropathol Exp Neurol*. 2000;59(8):679-686. doi:10.1093/jnen/59.8.679

161. Egger B, Chell JM, Brand AH. Insights into neural stem cell biology from flies. *Philos Trans R Soc B Biol Sci*. 2008;363(1489):39-56. doi:10.1098/rstb.2006.2011

162. Ding R, Weynans K, Bossing T, Barros CS, Berger C. The Hippo signalling pathway maintains quiescence in Drosophila neural stem cells. *Nat Commun*. 2016;7:1-12. doi:10.1038/ncomms10510

163. Gil-Ranedo J, Gonzaga E, Jaworek KJ, Berger C, Bossing T, Barros CS. STRIPAK Members Orchestrate Hippo and Insulin Receptor Signaling to Promote Neural Stem Cell Reactivation. *Cell Rep*. 2019;27(10):2921-2933.e5. doi:10.1016/j.celrep.2019.05.023

164. Harris RE, Pargett M, Sutcliffe C, Umulis D, Ashe HL. Brat Promotes Stem Cell Differentiation via Control of a Bistable Switch that Restricts BMP Signaling. *Dev Cell*. 2011;20(1):72-83. doi:10.1016/j.devcel.2010.11.019

165. Horibata S, Vo T V., Subramanian V, Thompson PR, Coonrod SA. Utilization of the soft agar colony formation assay to identify inhibitors of tumorigenicity in breast cancer cells. *J Vis Exp*. 2015;2015(99):1-7. doi:10.3791/52727

166. Xu XM, Yoo MH, Carlson BA, Gladyshev VN, Hatfield DL. Simultaneous knockdown of the expression of two genes using multiple shRNAs and subsequent knock-in of their expression. *Nat Protoc*. 2009;4(9):1338-1349. doi:10.1038/nprot.2009.145

167. Boulon S, Westman BJ, Hutten S, Boisvert FM, Lamond AI. The Nucleolus under Stress. *Mol Cell*. 2010;40(2):216-227. doi:10.1016/j.molcel.2010.09.024

168. Pollard KM, Hultman P. *Fibrillarin Autoantibodies*. Third Edit. Elsevier; 2013. doi:10.1016/B978-0-444-56378-1.00038-1

169. O'Mahony DJ, Rothblum LI. Identification of two forms of the RNA polymerase I transcription factor UBF. *Proc Natl Acad Sci U S A*. 1991;88(8):3180-3184. doi:10.1073/pnas.88.8.3180

170. McStay B. Nucleolar organizer regions: genomic 'dark matter' requiring illumination. *Genes Dev*. 2016:45-53. doi:10.1101/gad.283838.116.1598

171. Shav-Tal Y, Blechman J, Darzacq X, et al. Dynamic Sorting of Nuclear Components into Distinct Nucleolar Caps during Transcriptional Inhibition. *Mol Biol Cell*. 2005;16:2395-2413. doi:10.1091/mbc.E04

172. Peltonen K, Colis L, Liu H, et al. A Targeting Modality for Destruction of RNA Polymerase I that Possesses Anticancer Activity. *Cancer Cell*. 2015;25(1):77-90. doi:10.1016/j.ccr.2013.12.009.A

173. Pelletier J, Thomas G, Volarevic S. Ribosome biogenesis in cancer: new players and therapeutic avenues. *Nat Perspect*. 2017. doi:10.1038/nrc.2017.104

174. Zink D, Fischer AH, Nickerson JA. Nuclear structure in cancer cells. *Nat Rev Cancer*. 2004;4(9):677-687. doi:10.1038/nrc1430

175. Lu KL, Nelson JO, Watase GJ, Warsinger-Pepe N, Yamashita YM. Transgenerational dynamics of rDNA copy number in drosophila male germline stem cells. *Elife*. 2018;7:1-20. doi:10.7554/eLife.32421

176. Grummt I. Life on a planet of its own : regulation of RNA polymerase I transcription in the nucleolus. *Genes Dev*. 2003;17:1691-1702.

doi:10.1101/gad.1098503R.GENES

177. McStay B, Grummt I. The Epigenetics of rRNA Genes: From Molecular to Chromosome Biology. *Annu Rev Cell Dev Biol*. 2008;24(1):131-157. doi:10.1146/annurev.cellbio.24.110707.175259

178. Martins T, Eusebio N, Correia A, Marinho J, Casares F, Pereira PS. TGFβ/Activin signalling is required for ribosome biogenesis and cell growth in Drosophila salivary glands. *Open Biol*. 2017;7(1):160258. doi:10.1098/rsob.160258

179. Fang Y, Han X, Li J, Kuang T, Lou W. HEATR1 Deficiency Promotes Chemoresistance via Upregulating ZNF185 and Downregulating SMAD4 in Pancreatic Cancer. *J Oncol*. 2020;2020. doi:10.1155/2020/3181596

180. Van Meir EG, Kikuchi T, Tada M, et al. Analysis of the p53 Gene and Its Expression in Human Glioblastoma Cells. *Cancer Res*. 1994;54(3):649-652.

181. Oskarsson T, Trumpp A. The Myc trilogy : lord of RNA polymerases. *Nat Cell Biol*. 2005;7(3):215-217.

182. Arabi A, Rustum C, Hallberg E, Wright APH. Accumulation of c-Myc and proteasomes at the nucleoli of cells containing elevated c-Myc protein levels. *J Cell Sci*. 2003;116(9):1707-1717. doi:10.1242/jcs.00370

183. Li Z, Hann SR. Nucleophosmin is essential for c-Myc nucleolar localization and c-Myc-mediated rDNA transcription. *Oncogene*. 2013;32(15):1988-1994. doi:10.1038/onc.2012.227

184. Li Z, Boone D, Hann SR. Nucleophosmin interacts directly with c-Myc and controls c-Myc-induced hyperproliferation and transformation. *Proc Natl Acad Sci U S A*. 2008;105(48):18794-18799. doi:10.1073/pnas.0806879105

185. Johnston JA, Ward CL, Kopito RR. Aggresomes: A Cellular Response to Misfolded Proteins. *J Cell Biol*. 1998;143(7):1883-1898. http://www.jcb.org.

186. Grandori C, Gomez-Roman N, Felton-Edkins ZA, et al. c-Myc binds to human ribosomal DNA and stimulates transcription of rRNA genes by RNA polymerase I. *Nat Cell Biol*. 2005;7(3):311-318. doi:10.1038/ncb1224

187. Arabi A, Wu S, Ridderstråle K, et al. c-Myc associates with ribosomal DNA and activates RNA polymerase I transcription. *Nat Cell Biol*. 2005;7(3):303-310. doi:10.1038/ncb1225

188. Bedard PL, Hansen AR, Ratain MJ, Siu LL. Tumour heterogeneity in the clinic. *Nature*. 2013;501(7467):355-364. doi:10.1038/nature12627

189. Hu Y, Flockhart I, Vinayagam A, et al. An integrative approach to ortholog

prediction for disease-focused and other functional studies. *BMC Bioinformatics*. 2011;12:357. doi:10.1186/1471-2105-12-357

190. Galli R, Binda E, Orfanelli U, et al. Isolation and characterization of tumorigenic, stem-like neural precursors from human glioblastoma. *Cancer Res*. 2004;64:7011-7021.

191. Pan C, Kumar C, Bohl S, Klingmueller U, Mann M. Comparative proteomic phenotyping of cell lines and primary cells to assess preservation of cell type-specific functions. *Mol Cell Proteomics*. 2009;8(3):443-450. doi:10.1074/mcp.M800258-MCP200

192. Lee J, Kotliarova S, Kotliarov Y, et al. Tumor stem cells derived from glioblastomas cultured in bFGF and EGF more closely mirror the phenotype and genotype of primary tumors than do serum-cultured cell lines. *Cancer Cell*. 2006;9(5):391-403. doi:10.1016/j.ccr.2006.03.030

193. Kaur G, Dufour JM. Cell lines: Valuable tools or useless artifacts. *Spermatogenesis*. 2012;2(1):1-5. doi:10.4161/spmg.19885

194. Ignatova TN, Kukekov VG, Laywell ED, Suslov ON, Vrionis FD, Steindler DA. Human Cortical Glial Tumours Contain Neural Stem-Like Cells Expressing Astroglial and Neuronal Markers In Vitro. *Glia*. 2002;206(June):193-206. doi:10.1002/glia.10094

195. Hanahan D, Weinberg RA. Hallmarks of cancer: The next generation. *Cell*. 2011;144(5):646-674. doi:10.1016/j.cell.2011.02.013

196. Hanahan D, Weinberg RA. The Hallmarks of Cancer. *Cell*. 2000;100:57-70.

197. Shashni B, Ariyasu S, Takeda R, et al. Size-based differentiation of cancer and normal cells by a particle size analyzer assisted by a cell-recognition PC software. *Biol Pharm Bull*. 2018;41(4):487-503. doi:10.1248/bpb.b17-00776

198. Gabut M, Bourdelais F, Durand S. Ribosome and Translational Control in Stem Cells. *Cells*. 2020;9(2):497. doi:10.3390/cells9020497

199. Belin S, Beghin A, Solano-Gonzàlez E, et al. Dysregulation of ribosome biogenesis and translational capacity is associated with tumor progression of human breast cancer cells. *PLoS One*. 2009;4(9):1-13. doi:10.1371/journal.pone.0007147

200. Stępiński D. The nucleolus, an ally, and an enemy of cancer cells. *Histochem Cell Biol*. 2018;150(6):607-629. doi:10.1007/s00418-018-1706-5

201. Ajore R, Raiser D, McConkey M, et al. Deletion of ribosomal protein genes is a

common vulnerability in human cancer, especially in concert with TP 53 mutations . *EMBO Mol Med*. 2017;9(4):498-507. doi:10.15252/emmm.201606660

202. van Sluis M, McStay B. A localized nucleolar DNA damage response facilitates recruitment of the homology-directed repair machinery independent of cell cycle stage. *Genes Dev*. 2015;29(11):1151-1163. doi:10.1101/gad.260703.115

203. Buchwalter A, Hetzer MW. Nucleolar expansion and elevated protein translation in premature aging. *Nat Commun*. 2017;8(1). doi:10.1038/s41467-017-00322-z

204. Derenzini M, Montanaro L, Trerè D. Ribosome biogenesis and cancer. *Acta Histochem*. 2017:2-9. doi:10.1016/j.acthis.2017.01.009

205. Carneiro BA, El-Deiry WS. Targeting apoptosis in cancer therapy. *Nat Rev Clin Oncol*. 2020. doi:10.1038/s41571-020-0341-y

206. Bellosta P, Gallant P. Myc function in Drosophila. *Genes and Cancer*. 2010;1(6):542-546. doi:10.1177/1947601910377490

207. Yoshimura SH, Hirano T. HEAT repeats - versatile arrays of amphiphilic helices working in crowded environments? *J Cell Sci*. 2016;129(21):3963-3970. doi:10.1242/jcs.185710

208. Sanchez CG, Teixeira FK, Czech B, et al. Regulation of Ribosome Biogenesis and Protein Synthesis Controls Germline Stem Cell Differentiation. *Cell Stem Cell*. 2016;18(2):276-290. doi:10.1016/j.stem.2015.11.004

209. Drygin D, Siddiqui-Jain A, O'Brien S, et al. Anticancer activity of CX-3543: A direct inhibitor of rRNA biogenesis. *Cancer Res*. 2009;69(19):7653-7661. doi:10.1158/0008-5472.CAN-09-1304

210. Frankowski KJ, Wang C, Patnaik S, et al. Metarrestin, a perinucleolar compartment inhibitor, effectively suppresses metastasis. *Sci Transl Med*. 2018;10(441). doi:10.1126/scitranslmed.aap8307.Metarrestin

211. Greenspan RJ. *Fly Pushing: The Theory and Practice of Drosophila Genetics*. Second Edi.; 1996.

212. Roguev A, Talbot D, Negri GL, et al. Quantitative genetic-interaction mapping in mammalian cells. *Nat Methods*. 2013;10(5):432-437. doi:10.1038/nmeth.2398

213. Murai N, Murakami Y, Tajima A, Matsufuji S. Novel ubiquitin-independent nucleolar c-Myc degradation pathway mediated by antizyme 2. *Sci Rep*. 2018. doi:10.1038/s41598-018-21189-0

214. Schindelin J, Arganda-Carreras I, Frise E, et al. Fiji: An open-source platform for biological-image analysis. *Nat Methods*. 2012. doi:10.1038/nmeth.2019

215. Chell JM, Brand AH. Nutrition-responsive glia control exit of neural stem cells from quiescence. *Cell*. 2010. doi:10.1016/j.cell.2010.12.007

216. Kriegova E, Arakelyan A, Fillerova R, et al. PSMB2 and RPL32 are suitable denominators to normalize gene expression profiles in bronchoalveolar cells. *BMC Mol Biol*. 2008;9:1-14. doi:10.1186/1471-2199-9-69

217. Livak KJ, Schmittgen TD. Analysis of relative gene expression data using real-time quantitative PCR and the 2-ΔΔCT method. *Methods*. 2001;25(4):402-408. doi:10.1006/meth.2001.1262